UNIVERSIDAD DE CHILE
FACULTAD DE CIENCIAS FÍSICAS Y MATEMÁTICAS
DEPARTAMENTO DE INGENIERÍA MECÁNICA

THERMAL INSTABILITIES OF CHARGE CARRIER TRANSPORT IN SOLAR CELLS BASED ON GaAs PN JUNCTIONS

TESIS PARA OPTAR AL GRADO DE
MAGÍSTER EN CIENCIAS DE LA INGENIERÍA, MENCIÓN MECÁNICA

MEMORIA PARA OPTAR AL TÍTULO DE
INGENIERA CIVIL MECÁNICA

JOSEFA FERNANDA IBACETA JAÑA

PROFESOR GUÍA:
WILLIAMS CALDERÓN MUÑOZ

MIEMBROS DE LA COMISIÓN:
PATRICIO MENDOZA ARAYA
ÁLVARO VALENCIA MUSALEM

Este trabajo ha sido parcialmente financiado por
CONICYT-PCHA/Magíster Nacional/2016 - 22160729

SANTIAGO DE CHILE
2017

RESUMEN DE: Tesis para optar al grado de Magíster en Ciencias de la Ingeniería, Mención Mecánica y Memoria para optar al título de Ingeniera Civil Mecánica.
POR: Josefa Fernanda Ibaceta Jaña.
FECHA: 21 de Abril,2017
PROF. GUÍA: Williams Calderón Muñoz.

INESTABILIDADES TÉRMICAS DEL TRANSPORTE DE PORTADORES DE CARGA EN CELDAS SOLARES BASADAS EN JUNTURAS PN DE GaAs

Dentro de los factores que afectan negativamente una celda solar fotovoltaica se destaca la temperatura. Ya sea por imperfecciones del material o a condiciones de operación no uniformes, es posible que se concentre calor en una zona debido a la disminución de la resistencia local y su consecuente aumento de corriente eléctrica. Estas zonas de concentración de calor pueden estabilizarse, generando gradualmente degradación de la celda, disminución de su vida útil y eficiencia. En caso contrario, puede ocurrir un fenómeno de descontrol térmico que resulta catastrófico para la celda, inhabilitando su correcto funcionamiento. Estudios en módulos de película delgada revelan que esta condición ocurre incluso cuando la radiación está uniformemente distribuida y con ello, el perfil de temperatura inicial es constante. La evolución temporal, bajo radiación, induce zonas de calor que incrementan exponencialmente la temperatura, contrayendo su área; por otra parte, la temperatura de las zonas más alejadas disminuye simultáneamente mientras disipan pequeñas corrientes. Para evitar este fenómeno se pueden escalar propiedades del dispositivo, como aumentar la conductividad térmica y disminuir el espesor. Actualmente, estos análisis se realizan a partir de modelos numéricos y analíticos basados en el comportamiento de diodos y mediciones experimentales del perfil de temperatura en la capa superficial de la celda y en la juntura. El propósito de esta Tesis es determinar criterios de estabilidad electro-térmico que pueden ser utilizados para evitar el descontrol de temperatura a partir de aplicar un análisis a un modelo hidrodinámico de mayor complejidad que uno basado en diodos; más aún, considerar un estado fuera del equilibro entre la temperatura de la red y los portadores de carga. Se determinó que la inestabilidad ocurre en la juntura PN y depende fuertemente la temperatura de la juntura en los bordes. Además, aumentar la temperatura de los portadores, disminuir el largo y aumentar el voltaje aplicado pueden estabilizar el sistema, aumentando el tiempo en que el sistema duplica su temperatura.

ABSTRACT: Thesis to opt for Master degree in Engineering Sciences, Mechanical Mention, and Memory for the title of Mechanical Civil Engineering.
AUTHOR: Josefa Fernanda Ibaceta Jaña.
DATE: April 21, 2017
THESIS ADVISOR: Williams Calderón Muñoz.

THERMAL INSTABILITIES OF CHARGE CARRIER TRANSPORT IN SOLAR CELLS BASED ON GaAS PN JUNCTIONS

Among the factors that negatively affect a solar photovoltaic cell is the temperature. Either due to imperfections of the material or to non-uniform operating conditions, it is possible that heat is concentrated in an area due to the decrease in local resistance and its consequent increase of electric current. These areas of concentration of heat can stabilize, gradually generating cell degradation, shortening its lifespan and efficiency. Otherwise, a phenomenon of thermal runaway can occur and it is catastrophic for the cell, disabling its correct operation. Studies in thin film modules reveal that this condition occurs even when the radiation is uniformly distributed and therewith, the initial temperature profile is constant. The temporal evolution, under radiation, induces zones of heat that increase exponentially the temperature, contracting its area. On other hand, the temperature of the further zones decreases simultaneously while dissipating small currents. To avoid this phenomenon properties of the device, such as increase thermal conductivity and decrease the thickness, can be scaled. At present, these analysis are carried out from numerical and analytical models based on the behaviour of diodes and experimental measurements of the temperature profile in the surface layer of the cell and the junction. The purpose of this thesis is to determine electro-thermal stability criteria that can be used to avoid thermal runaway by applying an stability analysis to a hydrodynamic model of greater complexity than one based on diodes; Moreover, to consider a state outside the equilibrium between lattice and charge carrier temperature. It is determined that the instability occurs at the PN juncture and it strongly depends on the temperature of the junction at the edges. In addition, increasing the temperature of the carriers, decreasing the length and increasing the applied voltage can stabilize the system, increasing the time in which the system doubles its temperature.

"It's our choices that show what we truly are, far more than our abilities"
Albus Dumbledore

Agradecimientos

Quisiera dar las gracias a todos los que me apoyaron incondicionalmente, los que creyeron en mi desde un principio y estuvieron para escucharme cada vez que las cosas se volvían complicadas, trayendo desesperanza.

Realizar esta tesis como acto de finalización de este periodo de mi vida significó mucho para mi incluso antes de empezarla. Me hizo recurrir a todos los conocimientos que adquirí en clases, estudiando en mi casa o haciendo alguna tarea con algún amigo. Puedo recordar las veces en que mi familia me llevaba comida a la pieza o me invitaba a salir a relajarme, a todos los malos chistes sobre materia con mis amigos y a las infinitas horas de contestar pruebas para luego comentar cada mínimo detalle. Recuerdo con cariño a todos los que me apoyaron con cualquier pequeña meta personal o me preguntaban que tal me estaba yendo.

Y como todos somos los que las experiencias forman, quisiera agradecer en específico a mi mamá y a mi hermano por no asesinarme en mis estados de colapso;a mi abuelita por preguntarme cada vez si había terminado la tesis; a Rodrigo por siempre tratar de ordenar mi cabeza; a las procastinantes por siempre empatizar conmigo; al Alonso por compartirme toda su experiencia; a los chicos de la oficina por hacerme reir; a la Suu, la Karen, el Rub, el Rod y el Mirko por compartir el camino conmigo; al profesor Gerardo por darme la oportunidad de aplicar mi conocimiento en otras fronteras; a mis profesores del colegio que incentivaron mi gusto por aprender; por último, a mi comisión de profesores que con sus ideas y su dedicación permitieron que lograra esto.

Se agradece a CONICYT-PHCA/Magíster Nacional/2016-22160729 por apoyo financiero

Contents

List of Tables

List of Figures

Chapter 1

Introduction

The use of solar energy has raised awareness through the time not only as an alternative energy generation, but as an important resource that could contribute at the energetic matrix of the country. Nowadays, government foresees an increase of policies that support the renewable potential, as is expressed in the following paragraph from the official book of the Ministry of Energy, Chile [1].

"It is an objective of the Energy Policy take up this vocation, implementing the necessary conditions for renewable energy constituting 60% in 2035, and at least 70% of electricity generation by 2050 [...] From the achievements 2035, Chile will become an exporter of technology and services for the solar industry [...] this gives us the opportunity and the privilege of developing a global leadership in solar generation."

In Chile, participation of renewable energies that vary in electrics systems, such as solar and wind power, depend on their costs and the flexibility of the system to which these are incorporated. Hence, the resources from public and private will be allocated to capacity building of the actors, communities and organizations to create opportunities for local development issues such as energy efficiency, implementation of solar thermal systems and various socio-environmental technologies for the use of small-scale energy. In other hand, global investigation concerning solar cells lies improving its efficiency, durability and reduction of manufacturing costs. For this, type of material used is highlighted, promoting the study of encapsulant materials for the reliability and materials that will increase light trapping, as suggested publications awarded in [2–4]. Furthermore, the study of operating conditions and control mechanism of these variables in materials used in the industry is reflected in cooling systems, among others, [5–7].

The new types of solar cells, such as thin film, dye sensitized, organic and multi-junction are increasingly being used [8, 9]. The behaviour of these solar cells in dynamic regime differs from the one of the monocrystalline or polycrystalline solar cells. It led to create methods to analyze its dynamic response, characterizing the DC parameters cells from the variation of the capacitance applying reverse and forward bias. It is common to evaluate equivalent circuits from a proper fitting, generally containing diodes to model the PN junction.

Among the studied subject there is thermal runaway, which is a positive energy feedback that increased a local temperature, diminishing the efficiency due to the different magnitude currents caused, and the reliability on account of the accelerated material degradation. A mechanical characterization of the electron-hole pairs in the PN junction would determine stability criteria to avoid this unwanted effect, leading to control in a lossless way the operational conditions of the solar cell.

1.1 Objectives

1.1.1 General Objective

Perform an electro-thermal stability analysis of a semiconductor PN junction solar cell.

1.1.2 Specific Objectives

- Determine temporal eigenvalues of a linearized hydrodynamic model applied to a GaAs PN junction solar cell.
- Perform a convergence analysis of the numerical method used.
- Determine stability operation conditions by applying sensibility analysis, varying device parameters such as length and doping, as well as boundary conditions and non-dimensional parameters in the model.
- Determine relations between surface and junction temperature of device.

1.2 Methodology

- Simplify the one-dimensional two temperature hydrodynamic model for the GaAs PN junction to obtain a differential equation system of a transient state of a zero order variables.
- Uncouple space and time dimension and reduce the ODE order system, presenting it in a matrix form.
- Obtain numerically temporal eigenvalues using the steady state of zero order response.
- Study the convergence of the solution fixing operation conditions, changing the numerical method of ODE resolution.
- Select a range of oscillation of non-dimensional parameters to obtain the strictly positive eigenvalues and determine its behaviour.
- Use realistic lattice boundary conditions and study the incidence in the model, checking its verisimilitude.

Chapter 2

Background

In this chapter essential knowledge to understand the physics behind the solar cell behaviour and device construction criteria is presented. For this, it begins with semiconductor microstructure that explains and supports the equations used to model the phenomenon; then, macrostructure of solar cells that briefly explains the purpose of its layers; after that, gallium arsenide approach is justified; hence and finally, hydrodynamic and thermal stability with its consequence thermal runaway phenomenon are shown to explain the cause of its development in this Thesis.

2.1 Semiconductor Physics

2.1.1 Semiconductor Microstructure

Semiconductor materials used in solid state devices are crystalline materials composed by elements in group IV, combinations of groups III and V or II and VI of the Periodic Table. Most commonly used materials are Silicon (Si) or Germanium (Ge) from group IV, Gallium Arsenide (GaAs) or Indium Arsenide (InAs) from groups III-V and Cadmium Telluride (CdTe) from groups II-VI. Silicon (Si) is one of the most studied elements due to its abundance on the Earth's crust, production cost and behaviour at room temperature($300[K]$); hence Silicon technology is far the most advanced among all semiconductors technology. However, compound semiconductors have different properties that can be suitable in specific applications, such as solar cells. The combinations of elements that can be used imply a variety of electrical and mechanical properties such as conductivity, light absorption or generation. Table 2.1 shows the portion of the Periodic Table related to semiconductors. Material proprieties are influenced by crystalline cell orientation and defects like impurities, doping or free bonds, and lattice mismatch. The amount of unlinked bounds changes the way that light is absorbed and charge carriers are generated; selecting the type and quantity of certain impurity allows the tuning of the amount of charge carriers in the device, and lattice mismatches limit the compatibility between materials. That implies there is a limit in the construction of optimal designs.

Table 2.1: Portion of periodic table related to semiconductors [10].

Period	Column II	III	IV	V	VI
2		B Boron	C Carbon	N Nitrogen	O Oxygen
3	Mg Magnesium	Al Aluminium	Si Silicon	P Phosphorus	S Sulfur
4	Zn Zinc	Ga Galium	Ge Germanium	As Arsenic	Se Selenium
5	Cd Cadmium	In Indium	Sn Tin	Sb Antimony	Te Tellurium
6	Hg Mercury		Pb Lead		

The studied semiconductor materials are single crystals; that is, the atoms are arranged in a three dimensional periodic arrangement called *lattice*. Thermal vibrations associated with the atom are centered about a single and fixed position where it lies. For a given semiconductor, there is a unit cell that is representative of the entire lattice; it can be generated by repeating the unit cell throughout the crystal. This primitive unit cell is called as Bravais lattice and it is defined taking in account that any lattice point can be obtained by traslation and represents every crystalline material. There are 14 basic lattices, as can be seen in Figure 2.1.

All semiconductor materials have only cubic and hexagonal structures. These crystalline cubic forms can be composed by a single specie of atoms or a combination of different elements, classifying the semiconductors in elemental or compound, respectively. First case contains elements from the fourth column of the periodic table, such as Si, Ge or C and is also called a diamond structure. Second case contains elements from III and V or II and VI and each one of atoms has it own lattices, such as GaAs, AlAs and CdS; it is also called Zinc Blende structure. Others semiconductors have hexagonal closed pack like BN, AlN, GaN and SiC. In the particular case of GaAs, crystal is composed of two sublattices, each face centered cubic (fcc) and offset with respect to each other by half diagonal of the fcc cube, as can be seen in Figure 2.2.

Band Structure

To explain the Band Theory, a single atom whit its set of discrete energy levels for theirs electrons is considered. Electrons occupy quantum states with quantum numbers n, l, m and s, denoting the energy level, orbital and s, sublevel and spin of the electrons, respectively. If there are N identical atoms brought together in a very close proximity as in a crystal, the outer electron could do a spatial overlap in their orbitals, which means two of these electrons could trade place occupying a new spatial extended energy states. Since the Pauli Exclusion Principle can only be satisfied if these electrons occupy a set of distinct, spatially extended energy levels, the atomic orbital splits into an energy band containing a set of electron states having a set of closely spaced energy levels.

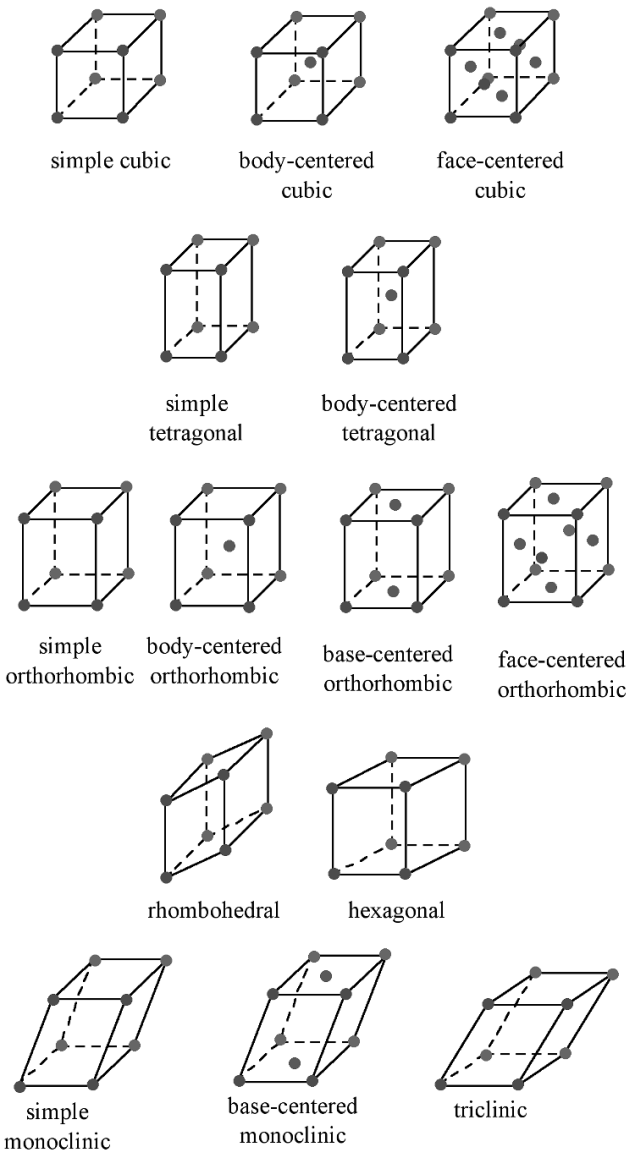

Figure 2.1: Bravais lattices [11].

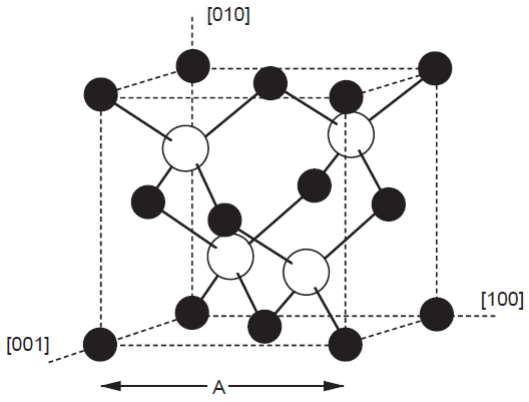

Figure 2.2: Conventional unit cube for GaAs [12].

These discrete energy levels are found by resolving Schrödinger equation for bounded electrons, which describes the temporal evolution of a particle. Considering a periodic potential from the periodic structure implies a difference in the allowed energies for electrons. These energy levels depend strongly on the distance between particles, known as dilatation, which is affected by lattice temperature.

As there are available energy levels, the prohibited ones generate a band of an energy gap and energy states are located above and below it. Over it, conduction band is found; on the contrary, there is the valence band.

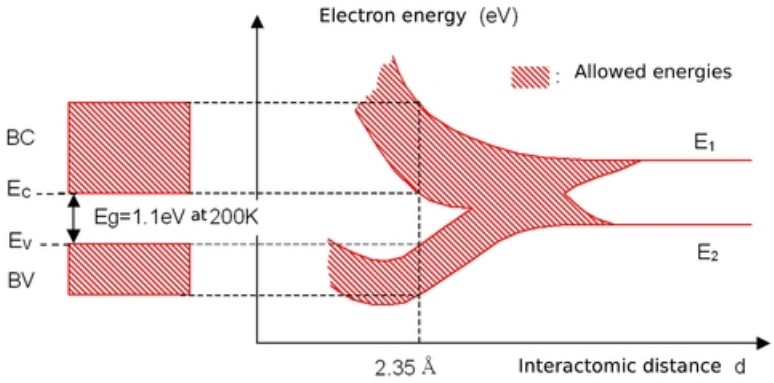

Figure 2.3: Energy bands in Silicon crystal with a diamond lattice structure [10].

In theory, at 0[K], valence band is complete and conduction band is empty; hence the material behaves as a perfect insulator. As temperature heightens, energy is introduced in the system so electrons in valence band can break bonds and carry charge to the conduction band. The space left by the moving electron induces others to move in the opposite direction if an electric field is applied, which equivalent to a positively charged pseudo-particle named as *hole*. Carriers representation is shown in Figure 2.4.

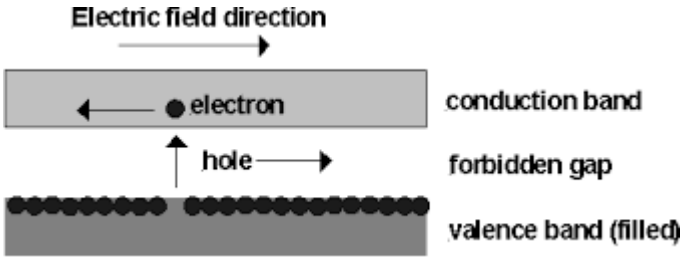

Figure 2.4: Representation of electron and holes [10].

Effective Mass

The energy diagram of a free electron in function of its momentum has a parabolic form. In a semiconductor crystal, an electron in the conduction band is similar to a free electron in being relatively free to move about in the crystal; however, because of the periodic potential of the nuclei, the basic equation of energy can no longer be valid. It is necessary to adjust the mass of the electron to match the basic expression, defining the effective mass. It is analogue to holes. Eq. (2.1) defines the effective mass of a conduction electron, in which m_n represents electron effective mass; E, energy; and ρ, momentum.

$$m_n = (\frac{\partial^2 E}{\partial \rho^2})^{-1} \tag{2.1}$$

Figure 2.5 shows a simplified energy-momentum relationship of a two basic types semiconductor. It is indirect if there is the necessity of changing the momentum of the electron to do a transition from the valence band to the conduction band, as Si (Figure 2.5a); case contrary it is direct semiconductor, as GaAs (Figure 2.5b). The upper parabola represents the conduction band, while the lower one is the valence band. The spacing at $p = 0$ between these two parabolas is the bandgap E_g, shown previously in Figure 2.3.

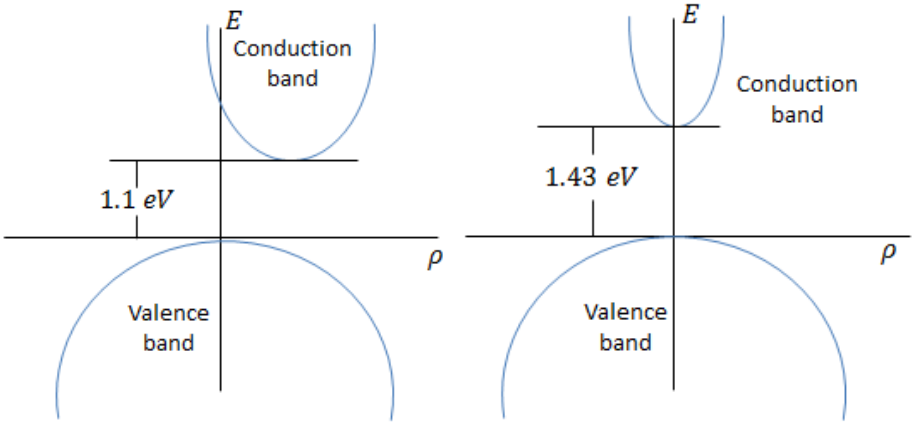

(a) Si (b) GaAs

Figure 2.5: Schematic energy-momentum diagram for Si and GaAs [13].

The actual energy-momentum relationships for a semiconductor such as GaAs and Si are much more complex and they are three dimensional, as is presented in the two-dimensional diagram of Figure 2.6. For diamond or zinc blende lattice, the maximum in the valence band and minimum in the conduction band occur at $p = 0$ or along one of these two directions; the first case is the most common, and it means that effective mass is constant and the electron motion is independent of crystal direction. Second case is the contrary.

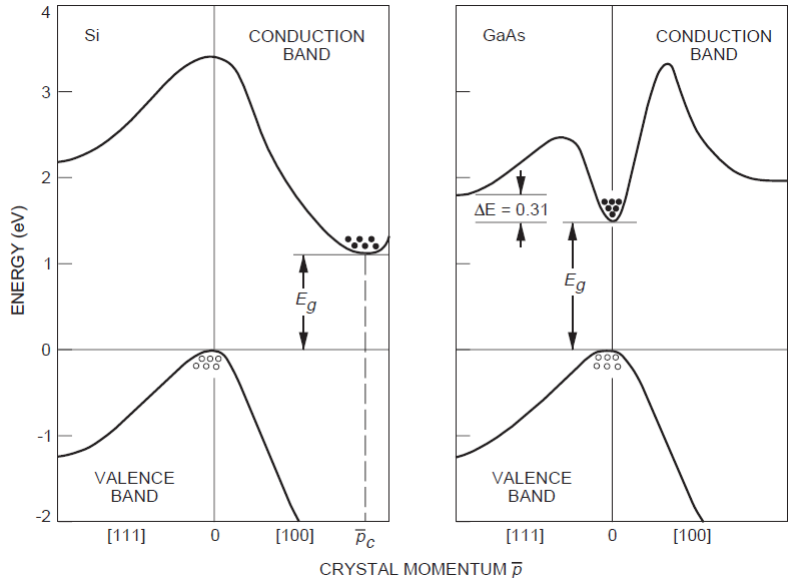

Figure 2.6: Actual bidimensional energy-momentum diagram for GaAs and Si [12]

Intrinsic Carrier Concentration

An intrinsic semiconductor is one that contains relatively small amounts of impurities compared with the thermally generated electrons and holes. In a steady-state condition at a given temperature without any external excitations, electron density (i.e, number of electrons per unit volume) is given by the product of the density of states, that is, the density of allowed energy states per energy range and unit volume, and by the probability of occupying that energy range. This last is given by the Fermi-Dirac distribution function, and depends on the Fermi level that is the energy at which the occupation probability by an electron is exactly one-half. The Fermi distribution for different temperatures is illustrated in Figure 2.7.

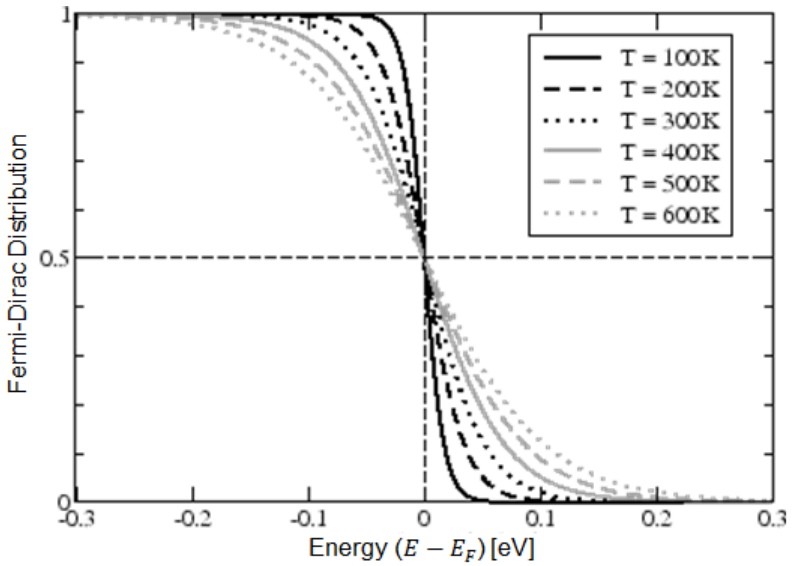

Figure 2.7: Fermi distribution function for various temperatures [10].

For an intrinsic semiconductor, the density of electrons n in the conduction band is equal to the density of holes p in the valence band, that is, $n = p = \eta_\mathrm{i}$ where η_i is the intrinsic carrier density. More general, matching Fermi levels for carriers, the Law of Mass Action $n \cdot p = \eta_\mathrm{i}^2$ is obtained.

Donors and Acceptors

When a semiconductor is doped with impurities, the semiconductor becomes extrinsic and impurity energy levels are introduced. It can be achieved by replacing an atom whit a different number of valence electrons. If there is an extra electron, is said that it is *donated* to the conduction band and semiconductor becomes n-type because of the addition of the negative charge carrier (N_D). By the contrary, if an additional electron is *accepted*, holes are created in the valence band, making a p-type semiconductor, with positive concentration (N_A).

By doping, semiconductors have different quantities of each carrier. The more abundant charge carriers are the majority carriers; the less abundant are the minority carriers.Under most conditions, the doping of the semiconductor is several orders of magnitude greater than the intrinsic carrier concentration, such that the number of majority carriers is approximately equal to the doping. Hence, applying the approximation and the Law of Mass Action, carriers concentration in p-type and n-type can be expressed as in Eqs. (2.2b) :

$$n - type : n_0 = N_D, \quad p_0 = \eta_\mathrm{i}^2/N_D, \tag{2.2a}$$

$$p - type : p_0 = N_A, \quad n_0 = \eta_\mathrm{i}^2/N_A \tag{2.2b}$$

2.1.2 Carrier Transport Phenomena

There are many transport processes, including drift, diffusion, recombination, generation, thermionic emission, tunneling, among others. It is considered the motion of charge carriers under the influence of an electric field and a carrier concentration gradient, which are predominant.

Drift Process

The thermal motion of an individual electron can be visualized as a succession of random scattering from collisions with lattice atoms, impurity atoms, and other scattering centers. Net displacement of an electron is zero over a sufficiently long period of time. The average distance between collisions is called the mean free path, and the average time between collisions is called the mean free time, τ_c.

When a small electric field is applied, an additional velocity component will be superimposed upon the thermal motion of electrons; it is called drift velocity. This is proportional to electric field by a factor which depends on the mean free time and effective mass, named mobility

μ_n, in units of $[cm^2 \cdot V^{-1} \cdot s^{-1}]$. Most important scattering mechanisms are about lattice and impurity. Lattice scattering results from thermal vibrations (also called phonons), so it increases with temperature; those movements disturb the periodic potential and allow energy to be transferred between the carriers and the lattice. The probability of impurity scattering depends on the total concentration of ionized impurities and becomes less significant at higher temperatures.

Diffusion Process

If there is a spatial variation of carrier concentration, these tend to move in an opposite direction of concentration gradient, generating a random thermal motion. This is called the diffusion current and it is proportional to the spatial derivative of the electron density. The current is positive and flows in the opposite direction of the electrons.

Generation and Recombination Processes

Carrier generation is a break-up of covalent bond to form electron and hole pairs, by releasing an electron from the valence band to the conduction band. Otherwise, recombination is the opposite process that restores the equilibrium condition. The most common processes for solar cells are light absorption for generation and Shockley-Read-Hall for recombination.

Light Absorption Photons incident on the surface of a semiconductor will be either reflected from the top surface, will be absorbed in the material or, failing either of the above two processes, will be transmitted through the material. For photovoltaic devices, reflection and transmission are typically considered loss mechanisms as photons which are not absorbed do not generate power. If the photon is absorbed it has the possibility of exciting an electron from the valence band to the conduction band. A key factor in determining if a photon is absorbed or transmitted is the energy of the photon. Therefore, only if the photon has enough energy the electron will be excited into the conduction band from the valence band. In many photovoltaic applications, the number of majority carriers in an illuminated semiconductor does not alter significantly; otherwise, minority carriers can be approximate by the light generated carriers.

There are three basic types of recombination in the bulk of a single-crystal semiconductor depending what involves the change of momentum and energy; for example, photons, electrons or phonons. These are radiative recombination, Auger recombination and Shockley-Read-Hall recombination.

Radiative Recombination It is also called band-to-band or direct recombination, usually dominates in direct-bandgap semiconductors, such as GaAs. In this, an electron from the conduction band directly combines with a hole in the valence band and releases a photon. The probability of electrons and holes will recombine directly is high, because the bottom

of the conduction band and the top of the valence band have the same momentum and no additional one is required for the transition across the bandgap. The rate of the direct recombination, R_{th}, is expected to be proportional to the number of electrons available in the conduction band and the number of holes available in the valence band.

Most commonly, when the semiconductor is indirect as in Silicon solar cells, indirect recombination predominates. In this, transition is via localized energy states in the forbidden energy gap called recombination centers.

Auger Recombination An electron and a hole recombine, but rather than emitting the energy as heat or as a photon, the energy and momentum is transferred to a third carrier, an electron in the conduction band. This electron then thermalizes back down to the conduction band edge. Auger recombination is most important at high carrier concentrations caused by heavy doping or high level injection under concentrated sunlight. In silicon-based solar cells, Auger recombination limits the lifetime and ultimate efficiency. The more heavily doped the material is, shorter the Auger recombination lifetime is.

Shockley-Read-Hall Recombination Recombination through defects levels, also called Shockley-Read-Hall or SRH recombination, does not occur in perfectly pure, undefected material. SRH recombination is a two-step process. An electron (or hole) is trapped by an energy state in the forbidden region which is introduced through defects in the crystal lattice. These defects can either be unintentionally introduced or deliberately added to the material, for example in doping the material; and if a hole (or an electron) moves up to the same energy state before the electron is thermally re-emitted into the conduction band, then it recombines. The rate at which a carrier moves into the energy level in the forbidden gap depends on the distance of the introduced energy level from either of the band edges.

2.2 PN junction

Joining n-type material with p-type material causes excess electrons in the n-type material to diffuse to the p-type side and excess holes from the p-type material to diffuse to the n-type side [10]. Movement of electrons to the p-type side exposes positive ion cores in the n-type side while movement of holes to the n-type side exposes negative ion cores in the p-type side, resulting in an electron field at the junction and forming the depletion region (See Figure 2.8). An electric field E forms between the positive ion cores in the n-type material and negative ion cores in the p-type material. This region is called the "depletion region" since the electric field quickly sweeps free carriers out, hence the region is depleted of free carriers. A "built in" potential V_{bi} due to electric field that is formed at the junction.

A PN junction can operate under forward and reverse bias. Forward bias occurs when a voltage is applied across the device such that the electric field formed by the PN junction is decreased. It eases carrier diffusion across the depletion region, and leads to increased diffusion current. In the presence of an external circuit that continually provides majority carriers, recombination increases which constantly depletes the influx of carriers into the solar cell. This increases diffusion and ultimately increases current across the depletion region. Reverse bias occurs when a voltage is applied across the solar cell such that the electric field formed by the PN junction is increased and consequently, diffusion current decreases.

Semiconductor devices have three modes of operation:

- Thermal Equilibrium: There are not external inputs such as light or applied voltage. The currents balance each other out so there is no net current within the device.
- Steady State: There are external inputs such as light or applied voltage, but the conditions do not change with time. Devices typically operate in steady state and are either in forward or reverse bias.
- Transient: Usually present in solar cells, it occurs if the applied voltage changes rapidly. There will be a short delay before the solar cell responds.

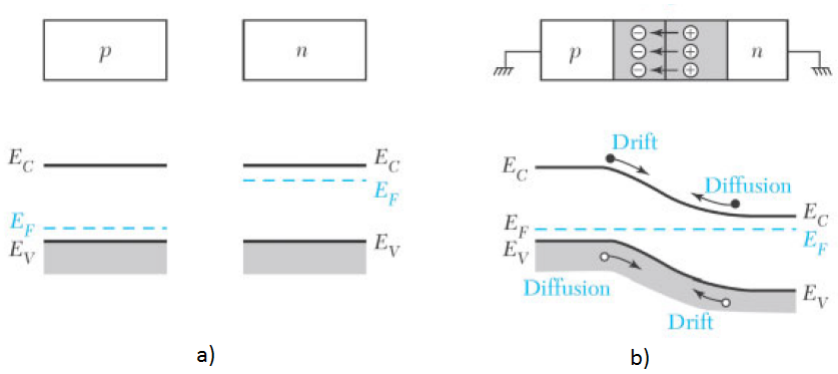

Figure 2.8: a)Uniformly doped p-type and n-type semiconductors.b)Electric field in the depletion region and the energy band diagram of a PN junction in thermal equilibrium [10].

2.3 Photovoltaic Solar Cell

A solar cell is a dispositive that produces photovoltaic (PV) electricity [10] [14]. Radiation of the Sun enters the semiconductor PN junction reaches the depletion region of the solar cell generates electron-hole pairs, which are able to flow through an external circuit and provide electrical power. The solar cell functions as a forward biased PN junction; however, current flow occurs in the opposite direction to that shown in Figure 2.9.

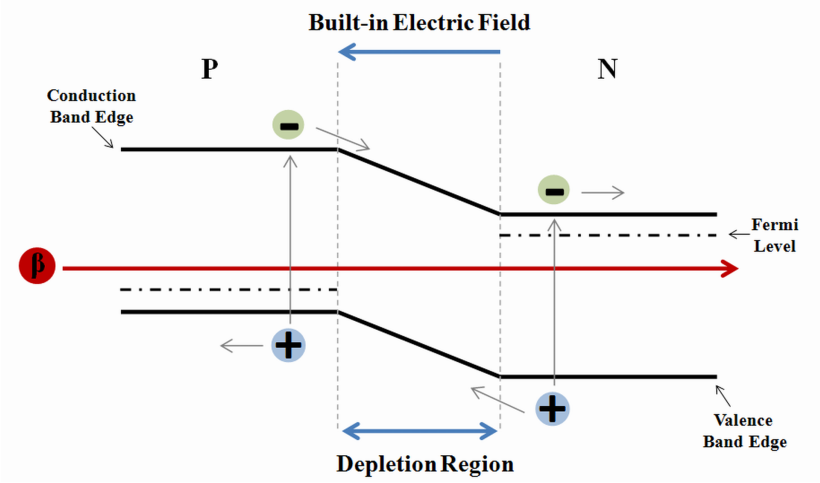

Figure 2.9: Band diagram of solar cell.Generated electron-hole pairs drift across the depletion region [14].

The generated minority carriers will drift across the depletion region and enter the n- and p-regions as majority carries as shown. It is also possible for electron-hole pairs to be generated within about one diffusion length or either side of depletion regions and through diffusion to reach the depletion region, where drift will again allow these carriers to cross to the opposite side. It is import to avoid recombination because it produces heat generation and doesn't contribute the electron flow.

If the PN junction is illuminated in the junction region then the reverse current increases substantially due to the electron-hole pairs that are optically generated. Without optical generation, the available electrons and holes that comprise reverse saturation current are thermally generated minority carries, which are low in concentration.

The optically generated current is larger than diffusion current and it continues to dominate current flow until stronger forward bias conditions are present. The current-voltage (I-V) characteristic of solar cells is shown in Figure 2.10, where there is the appropriate operating point for a solar cell in which current flows out the positive terminal (p-side), though the external circuit and then, into the negative terminal(n-side).

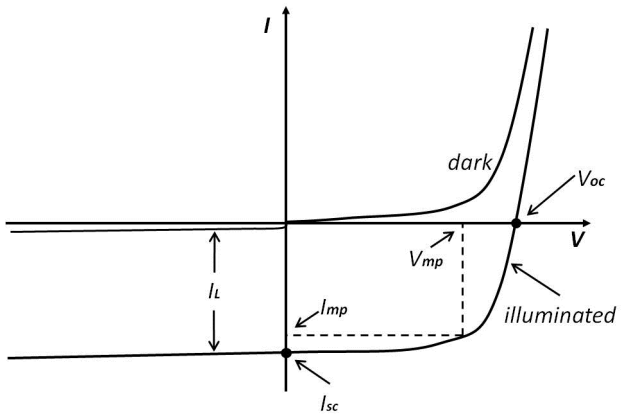

Figure 2.10: I-V Characteristic of solar cell [14].

From the I-V curve in Figure above, the following parameters can be identified: Short-circuit current (I_{SC}), open-circuit voltage (V_{OC}) and the ones that form the fill factor (FF).

I_{SC} is the current through the solar cell when the voltage across the solar cell is zero, i.e, when the solar cell is short circuited. V_{OC} is the maximum voltage available from a solar cell and this occurs at zero current and corresponds to the amount of forward bias on the solar cell due to the bias of the solar cell junction with the light-generated current. The short-circuit current and the open-circuit voltage are the maximum current and voltage respectively from a solar cell; however, at these points solar cell power is zero. FF contribute to determine the maximum power from a solar cell and is defined as the ratio of the maximum power (ponderation of maximum power points I_{mp} and V_{mp}) to the product of I_{SC} and V_{OC}.

2.3.1 Design

Solar cell structure is composed generally by six layers, including the semiconductor, as it is shown in Figure 2.11.

- Encapsulate: it is made of glass or other clear material, such clear plastic, and seals the cell from the external environment.
- Contact Grid: It is made of a good conductor, such as a metal, and it serves as a collector of electrons, decreasing the number of photons reaching the semiconductor surface, allowing more photons to penetrate.
- Antireflective Coating (AR Coating): Through a combination of a favorable refractive index and thickness, this layer serves to guide light into the solar cell.
- N-Type Semiconductor or Negative doping layer of semiconductor: Photon's energy transfers to the valence electron, allowing it to escape its orbit, leaving a hole. In other words, photoelectric effect happens.
- P-Type Semiconductor or Positive doping layer: In there, freed electrons attempt to unite with holes providing current.
- Back Contact: usually made out of a metal, covers the entire back surface of the solar cell and acts as a conductor.

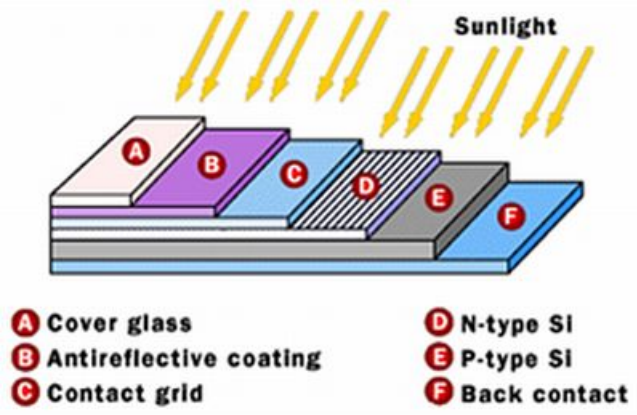

Figure 2.11: Schematic diagram of solar cell layers [15].

In order for light to reach the junction area of the PN junction, it should be close to the surface of semiconductor and be large enough to capture the desired radiation. Highly doped thin region simultaneously serves as a front electrode with high lateral conductivity and one side of PN junction, normally, n-side due to its electron mobility that allows higher conductivity. A metal grid is deposited on this layer and forms an ohmic contact to n+ material that blocks sunlight. Areas exposed to sunlight are coated with an anti reflection layer.

2.4 Properties of Gallium Arsenide

Gallium arsenide (GaAs) is a III-V compound semiconductor composed of the element gallium (Ga) from column III and the element arsenic (As) from column V of the periodic table of the elements [12]. GaAs was first created by Goldschmidt and reported in 1929, but the first reported electronic properties of III-V compounds as semiconductors did not appear until 1952. In 1970, the first GaAs heterostructure solar cells were created by the team led by Zhores Alferov in the USSR. In the early 1980s, the efficiency of the best GaAs solar cells surpassed that of conventional, crystalline silicon-based solar cells. In the 1990s GaAs solar cells took over from silicon as the cell type most commonly used for photovoltaic arrays for satellite applications. Later, dual- and triple-junction solar cells based on GaAs with germanium and indium gallium phosphide layers were developed as the basis of a triple-junction solar cell, which held a record efficiency of over 32% and can operate also with light as concentrated as 2.000[$suns$]. GaAs-based devices hold the world record for the highest-efficiency single-junction solar cell at 28.8%. This high efficiency is attributed to the extreme high quality GaAs epitaxial growth, surface passivation by the AlGaAs, and the promotion of photon recycling by the thin film design.

As a solar cell, it presents many benefits in compare to Silicon cells.

- For undoped GaAs, the energy bandgap is 1.42[eV] at room temperature,allowing higher operating temperatures.
- GaAs devices requires only a few microns thick to absorb sunlight, due to its high absorptivity. Commonly used crystalline silicon requires a layer 100 microns or more thick to accomplish the same effect.
- GaAs is highly resistant to radiation damage and it has high efficiency.
- GaAs has a thermal conductivity of 0.55[$W \cdot cm^{-1\circ}C^{-1}$], which is about one-third that of silicon and one-tenth that of copper. As a consequence, the power handling capacity and therefore the packing density of a GaAs integrated circuit is limited by the thermal resistance of the substrate.
- The mobility of GaAs is about double than Si at typical field strengths. Devices can work at significantly higher frequencies than Si.

A cell with a GaAs base can have several layers of slightly different compositions, allowing more precision in controlling generation and collection of electrons and holes. In other hand, silicon cells have been limited to variations in the level of doping. For example, one of the most common GaAs cell structures has a very thin window layer made of aluminum gallium arsenide, which allows electrons and holes to be created close to the electric field at the junction.

Never the less, it has a high cost that limits its application to concentrator systems, meanly.

Researchers are exploring several approaches to reduce the cost of GaAs devices. These include placing GaAs cells on cheaper substrates; growing GaAs cells on a removable, reusable GaAs substrate; and making GaAs thin films, similar to those made of copper indium diselenide and cadmium telluride.

2.5 Hydrodynamic Stability

Hydrodynamic stability concerns the stability and instability of motions of fluids [16]. The concept of stability of a state is "when... a small variation of present state will alter only by an infinitely small quantity the state at some future time, the condition of the system, whether at rest or in motion, is said to be stable; but when an infinitely small variation in the present state may bring about a finite difference in the state of the system in a finite time, the condition of the system is said unstable" − Maxwell.

In case of fluids, instability refers at the state where exists a chaotic three-dimensional vorticity field with a broad spectrum of small temporal and spatial scales. This is called turbulence. Reynolds demonstrated that when velocity is slow, the flow describes a straight line through the tube, generating the laminar flow. Whether the Reynolds number is over a critic value, the phenomenon becomes unstable, letting be the turbulence state, with the appearance of flashes succeeded each other rapidly.

Stability in mechanical or electrical systems can be studied by using mathematical tools due to their few degrees of freedom. In other hand, continuous media in which the basic equations take the form of nonlinear partial differential equations, the number of degrees of freedom is infinite. That implies the use of simplifications as linearization approximations and extensions of the theory developed with discrete systems.

The major contributions to the study of hydrodynamic stability can be found in the theoretical papers of Helmholtz (1821-1894), combined with efforts of Reynolds (1842-1912), Kelvin (1824-1907) and Rayleigh (1842-1919), among others. This last is considered the founder of the theory of hydrodynamic stability, who between 1878 and 1917 published a great number of papers on this subject. Around 1907 there were the first intuitions about the existence of a critical Reynolds number to explain the problem of turbulence. In addition to the works of Prandtl (1875-1953), the first confirmation of linear theory by experiments was done by Taylor (1886-1975) in his work on vortices between concentric rotating cylinders. Lin (1916-) improved the mathematical procedures and laid the foundations for a general expansion of stability analysis. At that time the stability of Poiseuille flows had become a particularly controversial issue and Lin put it in order by his newer and more general analysis. The results of Lin were found to be correct by using a digital computer. Experimental results of Schubauer and Skramstad helped clarify that the critical Reynolds number marked only the threshold of sinuous motion and not that of turbulence. At that point, experimental results and theory agreed as far as eigenfunctions and eigenvalues were concerned. Around 1955, three main categories of manifestations of instability in a continuous medium were formulated: first, oscillations in parallel flows, channel flows and boundary layers; second, boundary layers along curved walls and third, Benard cells and convective instabilities, cases where the mean flow is zero. Basic flow is defined by the set of fields that need to be specified at each point and time, for instance velocity and temperature. From the physical point of view, we want to know if the basic flow can be observed or not. If a small disturbance is introduced, this may either die away, persists as a disturbance of similar magnitude or grows so much that the basic flow becomes a different flow pattern. Stability problems can be found in many fields such as mechanics, electronics, aeronautical engineering, economics. [17]

2.6 Hot Spot in PV Solar Cells

Solar cell stability is an important factor in determining device lifespan, return of investment, pricing and warranty policies. Stability is often studied under harsher conditions than working cells are exposed into the field, so that 30 years of field stress can be inferred with 20 days of laboratory study, through increased concentrations of light, higher temperatures or greater humidity (accelerated life testing, ALT). Established experimental work on device degradation has found that temperature is an important parameter, accelerating it exponentially [18]. Moreover, without cell degradation by temperature, solar cells may have a lifetime greater than 100 years [19].

Increase of solar cell junction temperature can negatively affect output power and energy conversion efficiency due to a decrease of the open circuit voltage. This temperature depends on the packaging of solar cells and the environmental factors such as ambient temperature and wind characteristics [20–22].

Any temperature fluctuation in a local area of the film structure can increase the electrical conduction and cause a shutting pathway or hot spot [23]. Hot spot profile depends on where it is located and current densities, as can bee seen in Figure 2.12. Temperature is higher at the center of the device and reduces lower values at the edges. Also, the difference in temperature of hotter point and its surroundings is in the order of $10[K]$.

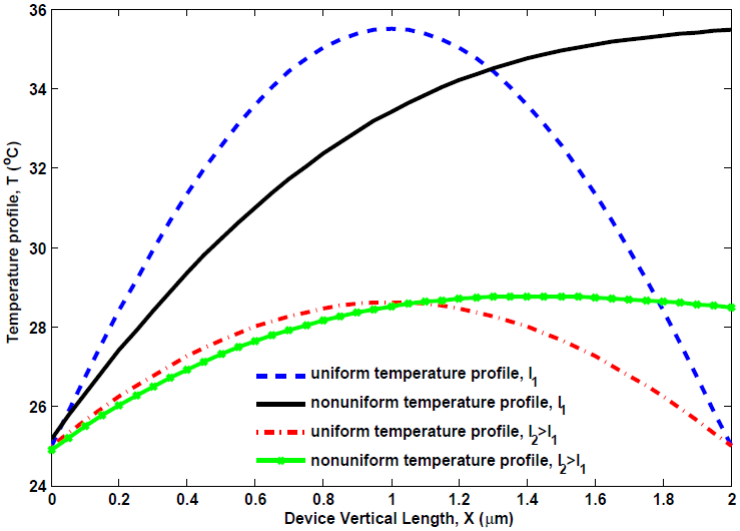

Figure 2.12: Hot spot temperature profile, TCO layer [23].

The temperature variation in the structure is usually reversible before physically impacting the atomic structure. This non-uniform characteristic of a PV device can be produced meanly due to its material structure or light absorption profile. First case refers to crystalline defects or composed structures heterogeneity. In the second case, radiation patrons that evolve during time or variations in the whether such as the passing of a cloud produce it [24]. This condition means variations between local PV parameters in different areas of a module or in variations between the parameters of nominally identical solar cells cut from the same module. An example of measurable consequence is that hot spots are typically located close

to module bus bars, which can be consider as a defect in the device [25]. Another one is that nominally identical cells may degrade differently.

As PV devices are thermally insulated and have a low lattice thermal conduction, the fluctuation in electric flow in the semiconductor layer triggers a variation in the temperature profile, well known in large are PV modules. This variation results in spots of high transversal conduction (i.e in a parallel plane to the layer width), allowing a local heat generation that may develop in an unstable temperature increase.

It usually concentrates its effects in a specific zone of the device, where a hot spot is generated. The stability of this point determines the magnitude of the degradation process; if it is stable, its temperature decreases until it reaches the equilibrium with the surrounds, damaging the zone slowly. Case contrary, but less frequent, the temperature increases exponentially leading to the runaway phenomenon.

The thermal runaway phenomenon corresponds to an uncontrolled response of energy generated by its own system when the temperature surpasses a critical value, usually with catastrophic consequences. Even if its application in PV is relatively new, alluding the work of Karpov in the last decade, it is a well know process in other scientific areas meanly by exothermic chemical reactions, such as in electrical engineering (current hogging), chemistry (temperature accelerated exothermic reactions) [26, 27], astrophysics (nova explosion due to runaway nuclear fusion) [28], among others.

In photovoltaic solar cells, the thermal runaway phenomenon causes problems with PV reliability, diminishing its lifespan and efficiency. This develops a current crush effect due to inherent non-uniform junction temperature [29].

Experimentally, temperature profile of PV solar cells can be observed with infrared camera mapping (IR), hence the temporal evolution of hot spots and its location in the frontal plane of the device can be registered. Another mapping techniques which also reveal lateral non-uniformities are optical beam induced current (OBIC), electron beam induced current (EBIC), surface photo-voltage (SPV) mapping, photoluminescence (PL) mapping, and some others [30, 31].

Analytically, typical junction models are usually based on diodes configurations, where the equation system includes the Ohm's Law, Kirchoff current and voltage laws, saturation current and a heat transfer equation, which usually contains a light absorption, Joule dissipation, Newton cooling law and a conductive heat transfer terms at least [9, 25, 29, 32].

Diode current I_D is given by temperature dependent Shockley Equation, Eq.(2.3):

$$I_D = I_0 \left(\mathrm{e}xp(\frac{qV}{nK_BT}) - 1\right) \tag{2.3a}$$

$$I_0 = I_{00}\, \mathrm{e}xp(\frac{-E_g}{nKT}) \tag{2.3b}$$

Where E_g represents band gap energy; n, the ideality factor; k_B, Boltzmann's constant; T, junction temperature;I_0, reverse saturation current;I_{00}, a constant; q, electron charge; and the voltages.

Heat equation can be written as:

$$C\frac{\mathrm{d}T}{\mathrm{d}t} = H + IV + \chi\Delta T - \alpha\Delta T - \sigma\Delta T^4 \tag{2.4}$$

where the C corresponds to a constant flux; H, to Joule dissipation; χ, to convection; α, to conduction; and σ, to radiation.

PN junction modelled as equivalent circuit with diodes configurations usually includes current source simulating the sun illumination and resistances, thermal and electrical, as can be seen in Figure 2.13

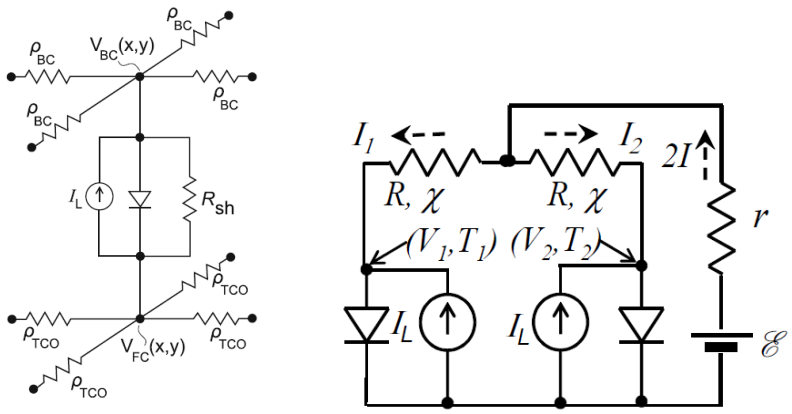

(a) two diodes [32] (b) One diode [25]

Figure 2.13: Equivalent circuit of PN junction.

Vasko et al. [25] made a study in thin film PV modules, specifically in a triple junction based on a-Si:H. It revealed that even when radiation is uniformly distributed in the module making a uniform temperature profile at the beginning, its distribution became less homogeneous in the course of heating and hot spots usually developed in the proximity of bus bars, as can be seen in Figure 2.14.

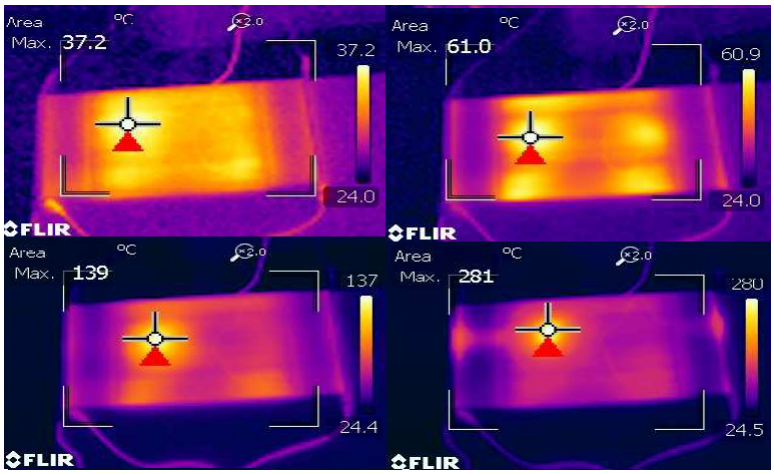

Figure 2.14: IR mapping triple junction a-Si:H [25]

Hot spots formation takes place when the forward current exceeds a certain critical value, in this case approximately $15[A]$. In addition, it was experimentally demonstrated that hot spots are sensitive to convective air currents. Temporal evolution of hot spot temperature behaves exponentially, which triggers the phenomenon of runaway instability, where the spot gets hotter and simultaneously shrinks in its linear dimensions (See Figure 2.15); the temperature of faraway regions simultaneously decreases as they dissipate smaller currents. Gorji [23] also demonstrates that an already created hot spot can redistribute the temperature profile of neighbour areas.

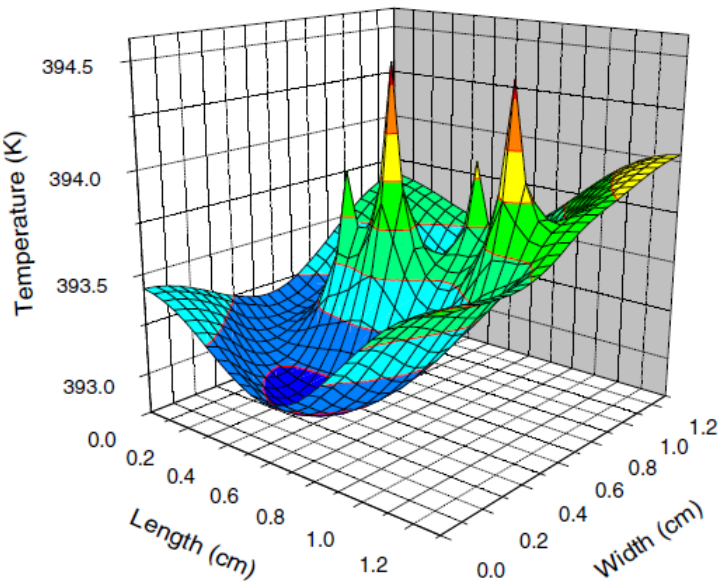

Figure 2.15: Temperature distribution over sample at $2[suns]$ [25].

It can be avoided in this case by increasing thermal conductivity by a factor, achievable in practice, which allows to the module reach a maximum temperature beyond the critical ($90[°C]$), as can be seen in Figure 2.16.

Karpov et al. [32] made a thermal stability analysis on thin film photovoltaic modules, released that PV can undergo zero threshold localized thermal runaway leading to thermal instabilities that affects negatively the device performance and reliability. Non uniform material degradation accelerates at hot spots, such that an initial hot spot may then degrade in a runaway mode under more and more stress as it becomes progressively shunting. Moreover, it can be unstable with respect to infinitesimally small fluctuations. They model the device as two diodes, with heat capacitances and resistors, applying a linear stability analysis over characteristics equations and then checking it by numerical modelling. This model also corroborates the fact that scaling some device properties, like increasing thermal insulation and decreasing thickness, runaway can be avoided.

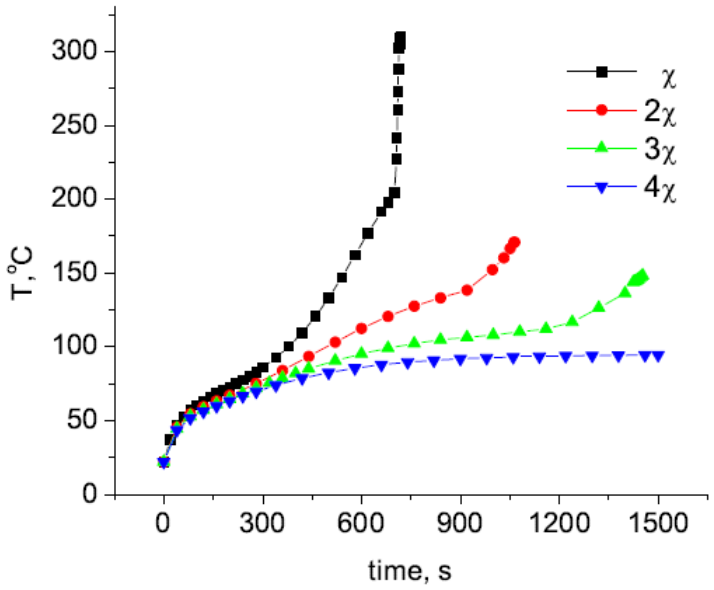

Figure 2.16: Simulated temporal temperature as a function of thermal conductivity χ [25].

Chapter 3

Model Description

From the hydrodynamic model of the PN junction presented by Osses [33] temporal eigenvalues of the transient component of the zero order perturbation will be found. Transport equations for electrons and holes model are deduced from the Boltzmann equations and semi-classical theory.

Reference system is defined as the spatial coordinate x^*, in the direction of the electron flow, and t^* as time. Current is driven through the device by a voltage difference, diffusion, generation and recombination processes between the two contacts at $x^* = 0.5L$, whit L as the total device longitude. The one-dimensional two-temperature hydrodynamic equations for electron and hole flow in a PN junction solar cell include:

- Gauss's law in Eqs. (3.1a) and (3.1b), which describe variation of electric potential as a function of charge distribution.
- Mass conservation equations for electrons and holes in Eqs. (3.1c) and (3.1d), which consider mass variation in a control volume (PN junction).
- Momentum conservation equations for electrons and holes in Eqs. (3.1e) and (3.1f), which includes effects of Lorentz force, pressure and collisions.
- Energy conservation equation for electrons and lattice in Eqs. (3.1g) and (3.1h), which consider effect of pressure for electrons and heat transfer by conduction and collision term for both electrons and lattice.

It is considered thermal equilibrium among electrons and holes. Therefore, the electron and hole temperature are imposed to be equals and constants throughout the device, T_c^*. The changes of kinetic energy of electrons due to their interactions with the lattice is described in Eq. (3.1g) and lattice thermal energy in Eq. (3.1h).

The system of equations is as follows:

$$\frac{\partial^2 V^*}{\partial x^{*2}} = -\frac{\mathrm{e}}{\epsilon_s}\left(p^* - n^* - N_A\right), \quad x^* < x_J^*, \tag{3.1a}$$

$$\frac{\partial^2 V^*}{\partial x^{*2}} = -\frac{\mathrm{e}}{\epsilon_s}\left(p^* - n^* + N_D\right), \quad x^* > x_J^*, \tag{3.1b}$$

$$\frac{\partial n^*}{\partial t^*} + \frac{\partial (u_{\mathrm{e}}^* n^*)}{\partial x^*} = (G_n^* - R_n^*), \tag{3.1c}$$

$$\frac{\partial p^*}{\partial t^*} + \frac{\partial (u_h^* p^*)}{\partial x^*} = (G_p^* - R_p^*), \tag{3.1d}$$

$$\frac{\partial u_{\mathrm{e}}^*}{\partial t^*} + u_{\mathrm{e}}^* \frac{\partial u_{\mathrm{e}}^*}{\partial x^*} = \frac{\mathrm{e}}{m_{\mathrm{e}}}\frac{\partial V^*}{\partial x^*} - \frac{k_B}{m_{\mathrm{e}} n^*}\frac{\partial (n^* T_c^*)}{\partial x^*} - \frac{u_{\mathrm{e}}^*}{\tau_{el}}, \tag{3.1e}$$

$$\frac{\partial u_h^*}{\partial t^*} + u_h^* \frac{\partial u_h^*}{\partial x^*} = -\frac{\mathrm{e}}{m_h}\frac{\partial V^*}{\partial x^*} - \frac{k_B}{m_h p^*}\frac{\partial (p^* T_c^*)}{\partial x^*} - \frac{u_h^*}{\tau_{hl}}, \tag{3.1f}$$

$$\frac{\partial T_c^*}{\partial t^*} + u_{\mathrm{e}}^* \frac{\partial T_c^*}{\partial x^*} = -\frac{2}{3} T_c^* \frac{\partial u_{\mathrm{e}}^*}{\partial x^*} + \frac{2}{3n^* k_B}\frac{\partial}{\partial x^*}\left(k_{\mathrm{e}}\frac{\partial T_c^*}{\partial x^*}\right) - \frac{T_c^* - T_L^*}{\tau_E} + \frac{m_{\mathrm{e}} u_{\mathrm{e}}^{*2}}{3k_B \tau_E} + \frac{2q_{heat}^*}{3n^* k_B}, \tag{3.1g}$$

$$C_L \frac{\partial T_L^*}{\partial t^*} = \frac{\partial}{\partial x^*}\left(k_L \frac{\partial T_L^*}{\partial x^*}\right) + \frac{3n^* k_B}{2}\left(\frac{T_c^* - T_L^*}{\tau_E}\right), \tag{3.1h}$$

where $V^*(x^*, t^*)$ is the electrostatic potential, $n^*(x^*, t^*)$ is the electron density, $p^*(x^*, t^*)$ is the hole density, $u_{\mathrm{e}}^*(x^*, t^*)$ is the x^*-component electron drift velocity, $u_h^*(x^*, t^*)$ is the x^*-component hole drift velocity and T_c^* is the electron and hole temperature, T_L^* is the lattice temperature and q_{heat}^* is an imposed heat per unit length in an unit area in which the current passes, which is absorbed from sunlight. The junction is defined at $x^* = x_J^*$. It is noteworthy that the symbol $*$ that accompany each variable represents its dimensional state.

By considering $T_C = constant$ in space, Eqs. (3.1g) and (3.1h) can be reduce to the following:

$$C_L \frac{\partial T_L^*}{\partial t^*} = \frac{\partial}{\partial x^*}\left(k_L \frac{\partial T_L^*}{\partial x^*}\right) + \frac{1}{2\tau_E} m_{\mathrm{e}} n^* u_{\mathrm{e}}^{*2} + q_{heat}^* - n^* k_B T_c^* \frac{\partial u_{\mathrm{e}}^*}{\partial x^*} \tag{3.2}$$

3.1 Physical parameters

The physical parameters are the electron charge, e, the permittivity of the semiconductor, ϵ_s, the donor concentration, N_D, the acceptor concentration, N_A, the effective electron mass, m_{e}, the effective hole mass, m_h, the Boltzmann constant, k_B, the generation rate for electrons, G_n^*, the generation rate for holes, G_p^*, the recombination rate for electrons, R_n^*, the recombination rate for holes, R_p^*, the momentum relaxation time for electrons, τ_{el}, the momentum relaxation time for holes, τ_{hl}, the energy relaxation time for electrons, τ_E, the lattice thermal conductivity k_L, and the heat capacity for lattice C_L. In this analysis we consider τ_{el}, τ_{hl}, τ_E, k_L, and C_L as constant values. In the next Table 3.1 there are values used considering a reference temperature of 300[K].

Table 3.1: Physical properties for GaAs [34]

Constant	Value
e	1.60218×10^{-19} [C]
ϵ_s	113.28×10^{-12} [C^2/(N m^2)]
k_B	1.38066×10^{-23} [J/K]
k_L	42.61 [W/(m K)]
N_D	1×10^{16} [m^{-3}]
N_A	1×10^{16} [m^{-3}]
m_e	6.01×10^{-32} [kg]
m_h	4.65×10^{-31} [kg]
C_L	8.73×10^{5} [J/(m^3 K)]
μ_{no}	0.45 [m^2/(V s)]
τ_p	2×10^{-12} [s]
τ_E	4.4×10^{-10} [s]

3.2 Assumptions

There is thermal equilibrium between electrons and holes. The charge carrier temperature distribution is imposed to be uniform in space and known throughout the device but it can be higher than the lattice and room temperatures, which can vary. There are two reasons for this condition. First, carrier temperature fluctuations may increase the recombination rate, reducing the PN junction performance [35, 36], and also, these fluctuations may modify the momentum and energy relaxation times more significantly throughout the device than fluctuations in the lattice temperature values [37]. Secondly, an operating condition determined by an imposed heat flux, q^*_{heat}, where the transport of hot electrons can be achieved and maintained through the device in order to reduce the lattice heating and consequently the recombination rates, improving the performance of the PN junction solar cell.

Respecting to lattice temperature, hot spot is considered already created and it influences lattice boundary conditions at initial time. Temporal evolution of hot spot depends on its stability; if the phenomenon is stable, it is related to long term degradation and otherwise, thermal runaway is developed.

Other considerations are:

- The semi-classical approximation is valid, which means wave motion is despised in carrier transport and the uncertainty of carrier momentum description is low. It is used Boltzmann equation.
- Negligible magnetic field.
- Carrier density is consider in the depletion region.
- Electric field does not change in time, just in space. There isn't reflection and movement is not ondulatory.
- Homogeneous material.
- Structure band is isotropic and parabolic, which implies there is an scalar effective

mass.

- There are not collisions between same carriers. Only carrier/lattice and electron/hole collisions are considered. Collisions are binaries and perfectly inelastics, generated from energy loss by generating phonons.
- Shockley-Read-Hall recombination processes (SRH) for electrons and holes, since this mechanism determines the effective carrier lifetime and prevail under a dopying density below $10^{18}[cm^3]$; otherwise, Auger process is dominant (R_{AU}). Therefore, recombination rates depend exponentially on the applied voltage through the PN junction.
- Generation by phonons absortion.
- Heavily doped regions near the ends, which lead to ohmic contacts.

3.3 Boundary Conditions

Boundary conditions are extracted from Osses analysis [33] and can be seen in Figure 3.1. As it is said, x^* is in the direction of the electron flow, from 0 to L as since p-side edge to the other extreme in the n-side, and t^* is time.

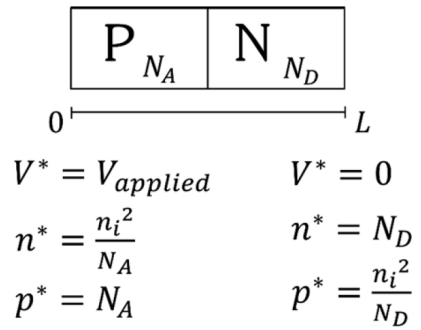

Figure 3.1: Device scheme with boundary conditions [33].

Voltage conditions refer that at zero bias, there isn't any total current density in both edges and there is an applied voltage only in p-side edge.

$$\frac{\mathrm{d}V^*}{\mathrm{d}x^*}(0,t^*) = 0, \tag{3.3a}$$

$$\frac{\mathrm{d}V^*}{\mathrm{d}x^*}(L,t^*) = 0, \tag{3.3b}$$

$$V^*(0,t^*) = V_{applied}, \tag{3.3c}$$

$$V^*(L,t^*) = 0. \tag{3.3d}$$

Carriers density are consider in equilibrium, meaning that boundary conditions are related to the intrinsic carrier concentration, n_{i} and impurities concentration, N_A and N_D.

$$n^*(0,t^*) = n_{\mathrm{i}}^2/N_A, \tag{3.4a}$$
$$n^*(L,t^*) = N_D, \tag{3.4b}$$
$$p^*(0,t^*) = N_A, \tag{3.4c}$$
$$p^*(L,t^*) = n_{\mathrm{i}}^2/N_D. \tag{3.4d}$$

The boundary conditions for the lattice temperature are a constant temperature through the dispositive in the beginning and a constant temperature in a fixed edge. The use of symmetric boundary conditions for the lattice temperature is supported by the fact that results from thermal modeling of photovoltaic solar cells show that the temperature of the semiconductor layer is mostly uniform along the normal axis [38].

$$T_L^*(0,t^*) = 330[K], \tag{3.5a}$$
$$T_L^*(L,t^*) = 330[K]. \tag{3.5b}$$

3.4 Non-dimensional Form

It is considered a non-dimensional form, using the reference parameters to cancel the dimension of variables. These reference parameters are V_0 voltage, N_0 doping density, L longitude of the device, t_0 time, U velocity, T_0 temperature and q_0 heat flux, defined as $q_0 = m_{\mathrm{e}} N_0 U^2/\tau_{el}$.

Non-dimensional variables are $V = V^*/V_0$, $n = n^*/N_0$, $p = p^*/N_0$, $x = x^*/L$, $u_{\mathrm{e}} = u_{\mathrm{e}}^*/U$, $u_h = u_h^*/U$, $T = T^*/T_0$ and $t = t^*/t_0$.

Replacing variables, a new set of equations is obtained.

$$\frac{\partial^2 V}{\partial x^2} = -\alpha\left(p - n - \frac{N_A}{N_0}\right), \quad x < x_J, \tag{3.6a}$$
$$\frac{\partial^2 V}{\partial x^2} = -\alpha\left(p - n + \frac{N_D}{N_0}\right), \quad x > x_J, \tag{3.6b}$$
$$\frac{\partial n}{\partial t} + \frac{\partial (u_{\mathrm{e}} n)}{\partial x} = (G_n - R_n), \tag{3.6c}$$
$$\frac{\partial p}{\partial t} + \frac{\partial (u_h p)}{\partial x} = (G_p - R_p), \tag{3.6d}$$
$$R_{\mathrm{e}}\left[\frac{\partial u_{\mathrm{e}}}{\partial t} + u_{\mathrm{e}}\frac{\partial u_{\mathrm{e}}}{\partial x}\right] = \frac{\partial V}{\partial x} - \frac{\beta}{n}\frac{\partial n}{\partial x} - u_{\mathrm{e}}, \tag{3.6e}$$
$$R_{\mathrm{e}}\left[\frac{\partial u_h}{\partial t} + u_h\frac{\partial u_h}{\partial x}\right] = -m_r\left[\frac{\partial V}{\partial x} + \frac{\beta}{p}\frac{\partial p}{\partial x}\right] - \gamma u_h, \tag{3.6f}$$
$$\psi_1\frac{\partial T_L}{\partial t} = \psi_2\frac{\partial^2 T_L}{\partial x^2} + \frac{1}{2}\nu n {u_{\mathrm{e}}}^2 + q_{heat} - \beta n\frac{\partial u_{\mathrm{e}}}{\partial x}. \tag{3.6g}$$

Non-dimensional groups used are $\alpha = \mathrm{e}L^2 N_0/V_0\epsilon_s$, $\gamma = \tau_{\mathrm{el}}/\tau_{hl}$, $m_r = m_{\mathrm{e}}/m_h$, $\beta = k_B T_c^*/\mathrm{e}V_0$, $\nu = \tau_{\mathrm{el}}/\tau_E$, $\psi_1 = \tau_{\mathrm{el}} C_L T_0/m_{\mathrm{e}} N_0 L U$, $\psi_2 = \tau_{\mathrm{el}} k_L T_0/m_{\mathrm{e}} N_0 L^2 U^2$, $R_{\mathrm{e}} = U^2 m_{\mathrm{e}}/\mathrm{e}V_0$, $G_n - R_n = (G_n^* - R_n^*)L/N_0 U$, $G_p - R_p = (G_p^* - R_p^*)L/N_0 U$, $t_0 = L/U$, $U = \mathrm{e}V_0\tau_{\mathrm{el}}/m_{\mathrm{e}}L$ and $R_{\mathrm{e}} = U\tau_{\mathrm{el}}/L$.

α is the available charge in the junction and its movement capacity. It is the ratio between charge per area unit $Q/A = \mathrm{e}NoL$ and the electric displacement $D = \epsilon_s V_0/L$. Increasing its value implies that carrier density variations involve a higher electric field variation, as is indicated in Eq. (3.6a) y Eq. (3.6b).

R_e is the Reynolds number for electrons due to the use of a hydrodynamic model, considering U as the maximum average electron velocity and kinematic viscosity as $nu_\mathrm{e} = L^2/\tau_{el}$. This last means that increasing the number of collisions between electrons and lattice implies higher thermal energy dissipation by the external electric field and consequently a lower gain in group velocity. Reynolds number also can be written as $R_\mathrm{e} = l_\mathrm{e}/L$, assuming l_e as the length free path defined as $l_\mathrm{e} = U\tau_{el}$. This definition corresponds to the Knudsen number for the electron cloud, which point out relative disorder grade of the system.

Relative mass m_r is the ratio between electron and hole mass. Knowing that hole mass represent a valence electron mass, m_r is equivalent to the relative inertia between conduction and valence electrons.

γ is the ratio between the momentum relaxation time of electron and hole. Otherwise, ν is the ratio between the momentum and energy relaxation time of electron.

β is the ratio between thermal energy of carriers and electric potential energy. A higher value implies a predominance of diffusive phenomena.

ψ_1 and ψ_2 are the ratio between the heat capacity and heat conduction of the lattice with a reference heat flux, respectively.

Chapter 4

Resolution Method

The aim of this chapter is to explain the methodology used to obtain the eigenvalues of the equation system. For this, perturbation method is applied to find zero order regular perturbation system. Then, the solution considered is divided in two terms: steady state component depending only in space and a transient response that varies in time and space. The last one determines system stability of the front of a small perturbation. Such method is used due to the non-linearity of the problem and the hardness to converge of the other numerical methods.

The followed steps and sections where they can be found are:

3.4 Find non-dimension form
4.2 Apply asymptotically perturbation series
4.3 Propose a separated variables solution
4.3 Reduce the o.d.e order.
4.3.2 Resolve o.d.e with numerical methods
4.3.3 Find the transfer matrix
4.3.3 Apply boundary conditions
5 Find eigenvalues

These are explained at following, preceding by a brief explanation of perturbation theory bases.

4.1 Perturbation Theory

Differential equations can be solved in closed form using solutions based on advanced theory, approximation by numerical analysis or approximation by formulas. The last includes the perturbation theory, that has an advantage of having an approximate formula for the solution of an equation and is possible to recognize the effects of the parameters in the solution better than the numerical approach.

In perturbation theory, the problem is simplified to a solvable equation. Then, the solution is the obtainable base form plus a perturbation, which usually takes the form of a series in base of a perturbation parameter "ϵ", which needs to be sufficiently small to give a good approximation. This solution only asymptotically converge to the one that responds to the target problem.

Several symbols are used in discussing approximations to functions and they serve to understand the associated error magnitude. The most commonly used are $\cong, o, O$ and O_S. The symbol $\cong$ used as $y(x;\epsilon) \cong \hat{y}(x;\epsilon)$ means that the function $\hat{y}$ is proposed as an approximation to y, nothing is implied about the validity of the approximation. A gauge function is a positive monotone function $\delta(\epsilon)$ defined in some interval $0 < \epsilon < \epsilon_0$ of interest for a particular problem; the most common gauge functions are defined for all $\epsilon > 0$. "Monotone" means that a gauge function must be increasing or decreasing through its domain. Gauge functions are used to measure the size of other function. The following are the most important definitions.

Assuming the following limit Lim exists, o, O and O_S can be defined as $Lim := limit_{(\epsilon\to 0+)} \frac{|f(\epsilon)|}{\delta(\epsilon)}$

$$f(\epsilon) = o(\delta(\epsilon)) \qquad if \quad Lim = 0, \tag{4.1a}$$
$$f(\epsilon) = O(\delta(\epsilon)) \qquad if \quad Lim < \infty, \tag{4.1b}$$
$$f(\epsilon) = O_S(\delta(\epsilon)) \qquad if \quad 0 < Lim < \infty. \tag{4.1c}$$

For the application in the error term, the next definition is established.

Definition: The function $f(x,\epsilon)$ satisfies the condition $f(x,\epsilon) = O(\delta(\epsilon))$ uniformly for x in the interval $a \leq x \leq b$ if and only if there exist constants c and ϵ_1 such that $|f(x,\epsilon)| \leq c\delta(\epsilon)$ for all x in $a \leq x \leq b$ and for all ϵ in $0 < \epsilon \leq \epsilon_1$.

Once these symbols are defined, it will be explained what kind of differential equations can be solved and how. If a problem looks like a solvable one and it can be separated as:

$$Ly + \epsilon Ny = 0, \tag{4.2}$$

where L and N are functions of differentials; y and ϵ are the unknown quantity and the perturbation parameter, respectively; $Ly = 0$ is the solvable equation and $\epsilon Ny = 0$ is the perturbation one. Its proposed solutions can be approximated as an asymptotic series

$$y(x;p;\epsilon) = \sum_{n=0}^{k} y_n(x;p)\delta_n(\epsilon) + o(\delta_k(\epsilon)). \tag{4.3}$$

In the particular case of an initial value problem with the form:

$$a\ddot{y} + b\dot{y} + cy = \epsilon f(t, y, \dot{y}, \epsilon), \tag{4.4a}$$
$$y(0) = \alpha, \tag{4.4b}$$
$$\dot{y}(0) = \beta. \tag{4.4c}$$

That exists for all $0 \leq t \leq T$, $|\epsilon| < \epsilon_0$, $\alpha \in A$ and $\beta \in B$. The solution can be defined by the following theorem.

Theorem: Let f be defined for all t in a compact interval $0 \leq t \leq T$, for all y and $\dot{y}$, and for all ϵ near zero. Let f have a continuous partial derivates of all order $\leq r$. Let compact intervals A and B be specified for α and β. Then there exists $\epsilon_0 > 0$ such that a solution.

$$y = \phi(t; \alpha; \beta; \epsilon). \tag{4.5}$$

Furthermore this solution is unique and ϕ is as smooth as f; that is, it has continuous partial derivates of all orders $\leq r$ with respect to all of its arguments t, α, β and ϵ.

It follows immediately from last theorem and Taylor's theorem that for any $k \leq r-1$, ϕ has an asymptotic approximation of the form.

$$\phi(t, \alpha, \beta, \epsilon) = \sum_{n=0}^{k} \phi_n(t; \alpha; \beta)\epsilon^n + O(\epsilon^{k+1}), \tag{4.6}$$

uniformly for $0 \leq t \leq T$ and for α, β in compact subsets.

4.2 Disturbed System

It is considered the physical properties for GaAs shown in Table 3.1. The values of the non-dimensional parameters have to be restricted to satisfy the built-in potential and the boundary conditions. The average time among collisions is small, and as a consequence, it is expected to have a small distance between two collisions for an electron in the flow. This implies that the Reynolds number is small, $R_\mathrm{e} < 1$, and it can be used as a perturbation parameter 'ϵ' in asymptotic perturbation series [34] for the dependent variables in Eqs. (3.6).

A symmetric PN junction in the dark and under light (constant net-generation rate), with $x_J = 0.5$ and $N_D = N_A$, was considered. Thus, the asymptotic perturbation series for the dependent variables are

$$V(x,t) = V_0(x,t) + \epsilon V_1(x,t) + O(\epsilon^2), \tag{4.7a}$$
$$n(x,t) = n_0(x,t) + \epsilon n_1(x,t) + O(\epsilon^2), \tag{4.7b}$$
$$p(x,t) = p_0(x,t) + \epsilon p_1(x,t) + O(\epsilon^2), \tag{4.7c}$$
$$u_\mathrm{e}(x,t) = u_{\mathrm{e}0}(x,t) + \epsilon u_{\mathrm{e}1}(x,t) + O(\epsilon^2), \tag{4.7d}$$
$$u_h(x,t) = u_{h0}(x,t) + \epsilon u_{h1}(x,t) + O(\epsilon^2), \tag{4.7e}$$
$$T_L(x,t) = T_{L0}(x,t) + \epsilon T_{L1}(x,t) + O(\epsilon^2). \tag{4.7f}$$

These consider an error of order ϵ^2, which implies only one perturbed term. To obtain a first order system replaced Eqs. (4.7) into the equation system Eqs. (3.6); then, factorize by the powers of ϵ and identify the order system related to its corresponding power. Terms with power over one are considered inside the error. At following, zero and first order is presented.

4.2.1 Zero order system

Equation system related to zero order is presented at following.

$$\frac{\partial^2 V_0(x,t)}{\partial x^2} = -\alpha\left(p_0(x,t) - n_0(x,t) - \frac{N_A}{N_0}\right), \quad x < x_J, \tag{4.8a}$$

$$\frac{\partial^2 V_0(x,t)}{\partial x^2} = -\alpha\left(p_0(x,t) - n_0(x,t) + \frac{N_D}{N_0}\right), \quad x > x_J, \tag{4.8b}$$

$$\frac{\partial n_0(x,t)}{\partial t} + \frac{\partial(u_{e0}(x,t)n_0(x,t))}{\partial x} = (G_n - R_n), \tag{4.8c}$$

$$\frac{\partial p_0(x,t)}{\partial t} + \frac{\partial(u_{h0}(x,t)p_0(x,t))}{\partial x} = (G_p - R_p), \tag{4.8d}$$

$$\frac{\partial V_0(x,t)}{\partial x} n_0(x,t) - \beta\frac{\partial n_0(x,t)}{\partial x} - u_{e0}(x,t) = 0, \tag{4.8e}$$

$$-m_r\left[\frac{\partial V_0(x,t)}{\partial x} p_0(x,t) + \beta\frac{\partial p_0(x,t)}{\partial x}\right] - \gamma u_{h0} p_0(x,t) = 0, \tag{4.8f}$$

$$\psi_1\frac{\partial T_{L0}(x,t)}{\partial t} = \psi_2\frac{\partial^2 T_{L0}(x,t)}{\partial x^2} + \frac{1}{2}\nu n_0(x,t){u_{e0}}^2(x,t) + q_{heat} - \beta n_0(x,t)\frac{\partial u_{e0}(x,t)}{\partial x}. \tag{4.8g}$$

4.2.2 First Order System

Equation system related to first order is presented due to its similarity to low flow of zero order system; however, it is not solved. It is noteworthy that in this system, all variables depend on both dimensions and there are constants terms to the perturbation; that means there are terms constituted only by zero order variables.

$$\frac{\partial^2 V_1(x,t)}{\partial x^2} = -\alpha\left(p_1(x,t) - n_1(x,t)\right), \tag{4.9a}$$

$$\frac{\partial n_1(x,t)}{\partial t} + u_{e0}(x,t)\frac{\partial n_1(x,t)}{\partial x} + n_0(x,t)\frac{\partial u_{e1}(x,t)}{\partial x} + u_{e1}(x,t)\frac{\partial n_0(x,t)}{\partial x} + n_1(x,t)\frac{\partial u_{e0}(x,t)}{\partial x} = 0, \tag{4.9b}$$

$$\frac{\partial p_1(x,t)}{\partial t} + u_{h0}(x,t)\frac{\partial p_1(x,t)}{\partial x} + p_0(x,t)\frac{\partial u_{h1}(x,t)}{\partial x} + u_{h1}(x,t)\frac{\partial p_0(x,t)}{\mathrm{d}x} + p_1(x,t)\frac{\partial u_{h0}(x,t)}{\partial x} = 0, \tag{4.9c}$$

$$\begin{aligned} u_{e0}(x,t)n_0(x,t)\frac{\partial u_{e0}(x,t)}{\partial x} = {} & n_0(x,t)\frac{\partial V_1(x,t)}{\partial x} - \beta T_1(x,t)\frac{\partial n_1(x,t)}{\partial x} + n_1(x,t)\frac{\partial V_0(x,t)}{\mathrm{d}x} \\ & - n_0(x,t)u_{e1}(x,t) - n_1(x,t)u_{e0}(x,t), \end{aligned} \tag{4.9d}$$

$$\begin{aligned} -u_{h0}(x,t)p_0(x,t)\frac{\partial u_{h0}(x,t)}{\partial x} = {} & m_r p_0(x,t)\frac{\partial V_1(x,t)}{\partial x} + m_r\beta T_1(x,t)\frac{\partial p_1(x,t)}{\partial x} \\ & + m_r p_1(x,t)\frac{\partial V_0(x,t)}{\partial x} + \gamma p_0(x,t)u_{h0}(x,t) + \gamma p_1(x,t)u_{h0}(x,t), \end{aligned} \tag{4.9e}$$

$$\begin{aligned} \psi_1\frac{\partial T_{L1}(x,t)}{\partial t} = {} & \psi_2\frac{\partial^2 T_{L1}(x,t)}{\partial x^2} + \frac{1}{2}\nu n_1(x,t){u_{e0}}^2(x,t) + \nu n_0(x,t)u_{e0}(x,t)u_{e1}(x,t) \\ & - \beta n_1\frac{\partial u_{e0}(x,t)}{\partial x} - \beta n_0(x,t)\frac{\partial u_{e1}(x,t)}{\partial x}. \end{aligned} \tag{4.9f}$$

4.3 Linear stability analysis

Linear stability analysis determines what is the effect of an initial disturbance on a laminar flow. The system response can be expressed in two states: a steady and a transient one. The steady state solution depends only on space and can be considered as a base flow; the transient state solution can be considered as a perturbation of the system and it is defined as a small perturbation through a small parameter "δ", $|\delta| << 1$.

By replacing,

$$V_0(x,t) = \overline{V}(x) + \delta V'(x,t), \tag{4.10a}$$
$$n_0(x,t) = \overline{n}(x) + \delta n'(x,t), \tag{4.10b}$$
$$p_0(x,t) = \overline{p}(x) + \delta p'(x,t), \tag{4.10c}$$
$$u_{e0}(x,t) = \overline{u}_e(x) + \delta {u_e}'(x,t), \tag{4.10d}$$
$$u_{h0}(x,t) = \overline{u}_h(x) + \delta {u_h}'(x,t), \tag{4.10e}$$
$$T_{L0}(x,t) = \overline{T}_L(x) + \delta T'_L(x,t), \tag{4.10f}$$

in Eqs.(4.8), the following systems in Eqs.(4.11) and Eqs.(4.12) are obtained. In Eqs.(4.10), nomenclature $\overline{x}$ represents the steady flow and x', the transient response for any variable.

4.3.1 Steady-State System

This system has been solved by Osses [33], which numerical code was provided by C.Jara and J.Osses, and is used in the development of this Thesis. As explained in the Assumptions Section (3.2), $\overline{T}(x) = constant$. Each steady state variable is defined in an array of one thousand nodes and the relative error magnitude of these values is 10^{-13}.

$$\frac{\partial^2 \overline{V}(x)}{\partial x^2} = -\alpha \left(\overline{p}(x) - \overline{n}(x) - \frac{N_A}{N_0} \right), \quad x < x_J \tag{4.11a}$$
$$\frac{\partial^2 \overline{V}(x)}{\partial x^2} = -\alpha \left(\overline{p}(x) - \overline{n}(x) + \frac{N_D}{N_0} \right), \quad x > x_J \tag{4.11b}$$
$$\frac{\partial (\overline{u}_e(x)\overline{n}(x))}{\partial x} = (G_n - R_n), \tag{4.11c}$$
$$\frac{\partial (\overline{u}_h(x)\overline{p}(x))}{\partial x} = (G_p - R_p), \tag{4.11d}$$
$$\overline{n}(x)\frac{\partial \overline{V}(x)}{\partial x} - \beta \frac{\partial \overline{n}(x)}{\partial x} - \overline{n}(x)\overline{u}_e(x) = 0, \tag{4.11e}$$
$$m_r \left[\overline{p}(x)\frac{\partial \overline{V}(x)}{\partial x} + \beta \frac{\partial \overline{p}(x)}{\partial x} \right] + \overline{p}(x)\gamma \overline{u}_h(x) = 0, \tag{4.11f}$$
$$\psi_2 \frac{\partial^2 \overline{T}_L(x)}{\partial x^2} + \frac{1}{2}\nu \overline{n}(x)\overline{u}_e(x)^2 + q_{heat} - \beta \overline{n}(x)\frac{\partial \overline{u}_e(x)}{\partial x} = 0. \tag{4.11g}$$

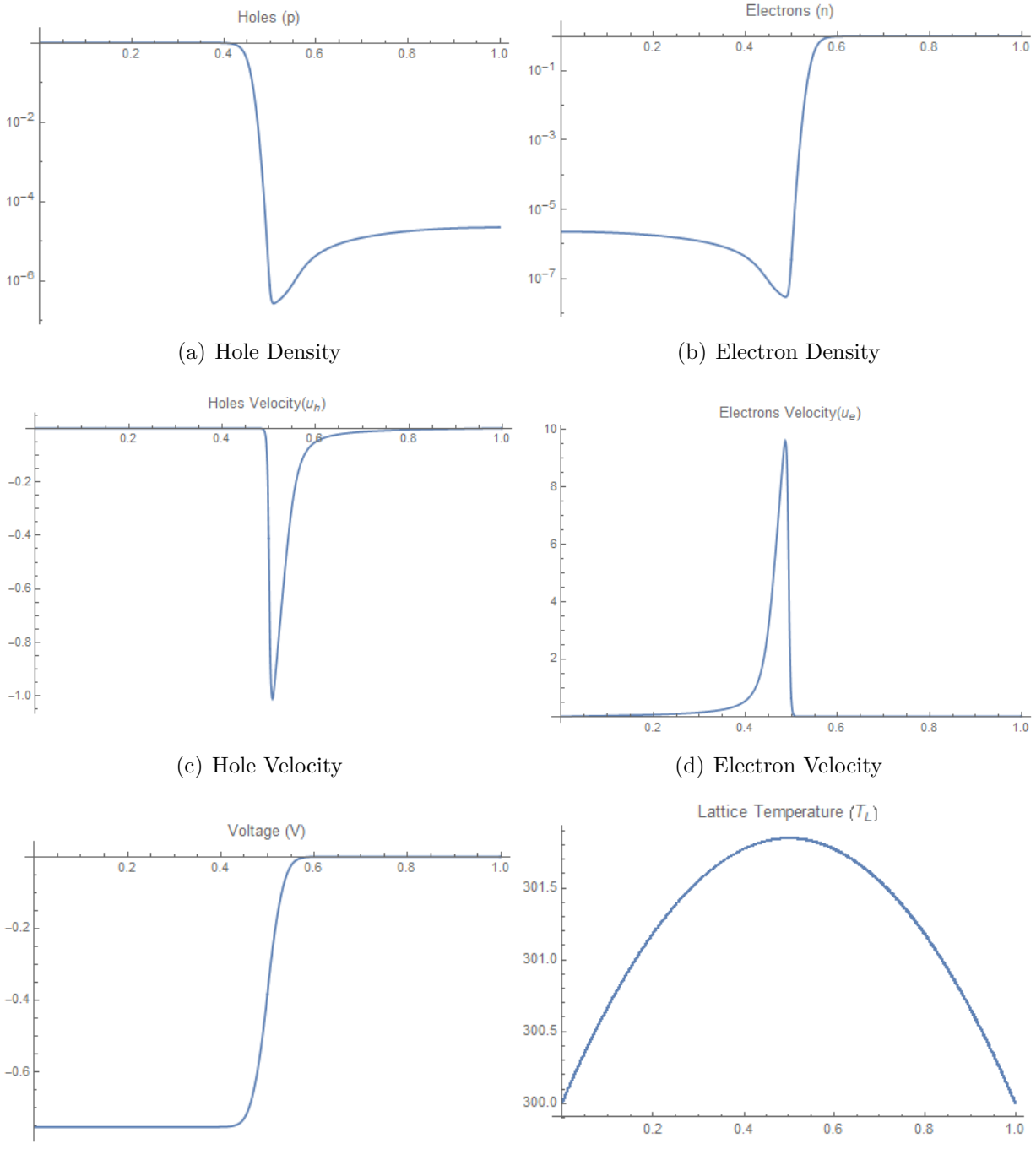

(a) Hole Density

(b) Electron Density

(c) Hole Velocity

(d) Electron Velocity

(e) Electric Potential

(f) Lattice Temperature

Figure 4.1: Steady-state variables distribution in space.

Graphs of the steady state response of zero order system thought space are displayed in Figure 4.1. These correspond to the particular case of thermal equilibrium, temperature of $330[K]$, an applied voltage of $0.4[V]$, a doping concentration of $10^{22}[m^{-3}]$ and a longitude of $4 \times 10^{-6}[m]$. The main code conditions of steady flow can be modified.

4.3.2 Transient-state System

Transient state system corresponds to equations extracted from zero order system without the pure steady state components and neglecting the contribution of terms with δ^2 or lower in order to linearize. Due to this, it can predict only the onset of instability.

$$\frac{\partial^2 V'(x,t)}{\partial x^2} + \alpha\left(p'(x,t) - n'(x,t)\right) = 0, \tag{4.12a}$$

$$\frac{\partial n'(x,t)}{\partial t} + \overline{u}_{\mathrm{e}}(x)\frac{\partial n'(x,t)}{\partial x} + \overline{n}(x)\frac{\partial {u_{\mathrm{e}}}'(x,t)}{\partial x} + {u_{\mathrm{e}}}'(x,t)\frac{\mathrm{d}\overline{n}(x)}{\mathrm{d}x} + n'(x,t)\frac{\mathrm{d}\overline{u}_{\mathrm{e}}(x)}{\mathrm{d}x} = 0, \tag{4.12b}$$

$$\frac{\partial p'(x,t)}{\partial t} + \overline{u}_{h}(x)\frac{\partial p'(x,t)}{\partial x} + \overline{p}(x)\frac{\partial {u_{h}}'(x,t)}{\partial x} + {u_{h}}'(x,t)\frac{\mathrm{d}\overline{p}(x)}{\mathrm{d}x} + p'(x,t)\frac{\mathrm{d}\overline{u}_{h}(x)}{\mathrm{d}x} = 0, \tag{4.12c}$$

$$\overline{n}(x)\frac{\partial V'(x,t)}{\partial x} - \beta\frac{\partial n'(x,t)}{\partial x} + n'(x,t)\frac{\mathrm{d}\overline{V}(x)}{\mathrm{d}x} - \overline{n}(x){u_{\mathrm{e}}}'(x,t) - n'(x,t)\overline{u}_{\mathrm{e}}(x) = 0, \tag{4.12d}$$

$$m_r\overline{p}(x)\frac{\partial V'(x,t)}{\partial x} + m_r\beta\frac{\partial p'(x,t)}{\partial x} + m_r p'(x,t)\frac{\mathrm{d}\overline{V}(x)}{\mathrm{d}x} + \gamma\overline{p}(x){u_{h}}'(x,t) + \gamma p'(x,t)\overline{u}_{h}(x) = 0, \tag{4.12e}$$

$$\begin{aligned}\psi_1\frac{\partial {T_L}'(x,t)}{\partial t} = \psi_2\frac{\partial^2 {T_L}'(x,t)}{\partial x^2} + \frac{1}{2}\nu n'(x,t){\overline{u}_{\mathrm{e}}}^2(x) + \nu\overline{n}(x)\overline{u}_{\mathrm{e}}(x){u_{\mathrm{e}}}'(x,t) - \beta n'\frac{\mathrm{d}\overline{u}_{\mathrm{e}}(x)}{\mathrm{d}x} \\ - \beta\overline{n}(x)\frac{\partial {u_{\mathrm{e}}}'(x,t)}{\partial x}.\end{aligned} \tag{4.12f}$$

Analyzing transient state of zero order response, first and second equation of system Eqs.(4.8) are the same hence it contribute in one equation. The lattice energy equation, Eq.(4.14f), is solved independently in the system of Eqs.(3.6), by using the solutions of $\overline{n}(x)$ and $\overline{u}_{\mathrm{e}}(x)$. As temporal terms in Eqs.(4.12) are defined by a first order derivative weighted and accompanied by parameters that depends only in space, it can be considered as constants for the temporal dimension. This kind of differential equation have an exponential solution, hence separated variables solutions is proposed as follows

$$\begin{Bmatrix} V' \\ n' \\ u'_{\mathrm{e}} \\ p' \\ u'_{h} \\ T'_{L} \end{Bmatrix} = \begin{Bmatrix} \widehat{V}(x) \\ \widehat{n}(x) \\ \widehat{u}_{\mathrm{e}}(x) \\ \widehat{p}(x) \\ \widehat{u}_{h}(x) \\ \widehat{T}_{L}(x) \end{Bmatrix} \mathrm{e}^{\omega t}, \tag{4.13}$$

where the eigenvalue ω and the amplitudes denoted by $\widehat{\ }$ are all complex. Thus, we get a

system of differential equations with variable coefficients:

$$\frac{\mathrm{d}^2\widehat{V}}{\mathrm{d}x^2} + \alpha\left(\widehat{p} - \widehat{n}\right) = 0, \tag{4.14a}$$

$$\omega\widehat{n} + \overline{u}_\mathrm{e}\frac{\mathrm{d}\widehat{n}}{\mathrm{d}x} + \overline{n}\frac{\mathrm{d}\widehat{u}_\mathrm{e}}{\mathrm{d}x} + \widehat{u}_\mathrm{e}\frac{\mathrm{d}\overline{n}}{\mathrm{d}x} + \widehat{n}\frac{\mathrm{d}\overline{u}_\mathrm{e}}{\mathrm{d}x} = 0, \tag{4.14b}$$

$$\omega\widehat{p} + \overline{u}_h\frac{\mathrm{d}\widehat{p}}{\mathrm{d}x} + \overline{p}\frac{\mathrm{d}\widehat{u}_h}{\mathrm{d}x} + \widehat{u}_h\frac{\mathrm{d}\overline{p}}{\mathrm{d}x} + \widehat{p}\frac{\mathrm{d}\overline{u}_h}{\mathrm{d}x} = 0, \tag{4.14c}$$

$$\overline{n}\frac{\mathrm{d}\widehat{V}}{\mathrm{d}x} - \beta\frac{\mathrm{d}\widehat{n}}{\mathrm{d}x} + \widehat{n}\frac{\mathrm{d}\overline{V}}{\mathrm{d}x} - \overline{n}\widehat{u}_\mathrm{e} - \widehat{n}\overline{u}_\mathrm{e} = 0 \tag{4.14d}$$

$$m_r\overline{p}\frac{\mathrm{d}\widehat{V}}{\mathrm{d}x} + \beta m_r\frac{\mathrm{d}\widehat{p}}{\mathrm{d}x} + m_r\widehat{p}\frac{\mathrm{d}\overline{V}}{\mathrm{d}x} + \gamma\overline{p}\widehat{u}_h + \gamma\widehat{p}\overline{u}_h = 0 \tag{4.14e}$$

$$\psi_1\omega\widehat{T}_L = \psi_2\frac{\mathrm{d}^2\widehat{T}_L}{\mathrm{d}x^2} + \frac{1}{2}\nu\widehat{n}\overline{u}_\mathrm{e}^2 + \nu\overline{n}\,\overline{u}_\mathrm{e}\widehat{u}_\mathrm{e} - \beta\widehat{n}\frac{\mathrm{d}\overline{u}_\mathrm{e}}{\mathrm{d}x} - \beta\overline{n}\frac{\mathrm{d}\widehat{u}_\mathrm{e}}{\mathrm{d}x}. \tag{4.14f}$$

A numerical method to solve a first order ODE is used, hence it is necessary to reduce the system order, defining two new variables with physical meaning:

$$\widehat{E} = -\frac{\partial\widehat{V}}{\partial x} \tag{4.15a}$$

$$\widehat{q}_L = \frac{\partial\widehat{T}_L}{\partial x} \tag{4.15b}$$

where E represents the electrical field and q_L, the heat transfer flux from the lattice.

To solve numerically the equation system, the basic form $y'(x) = f(y, x)$ is required. For this, it is organized in a matrix form, where the vector is defined "$\mathbf{Y}$" as an array of the parameters including the last added, considering their contribution to the equation system. Hence, it can be written as:

$$\mathbf{J}\frac{\mathrm{d}\mathbf{Y}}{\mathrm{d}x} = \mathbf{P}\mathbf{Y}, \tag{4.16}$$

or

$$\frac{\mathrm{d}\mathbf{Y}}{\mathrm{d}x} = [\mathbf{J}^{-1}\mathbf{P}]\mathbf{Y}, \tag{4.17}$$

where,

$$\mathbf{Y} = \left\{\begin{array}{c} \widehat{V} \\ \widehat{E} \\ \widehat{n} \\ \widehat{u}_\mathrm{e} \\ \widehat{p} \\ \widehat{u}_h \\ \widehat{T}_L \\ \widehat{q}_L \end{array}\right\}, \tag{4.18}$$

$$\mathbf{J} = \begin{bmatrix} 1 & 0 & 0 & 0 & 0 & 0 & 0 & 0 \\ 0 & 1 & 0 & 0 & 0 & 0 & 0 & 0 \\ 0 & 0 & \overline{u}_{\mathrm{e}} & \overline{n} & 0 & 0 & 0 & 0 \\ 0 & 0 & 0 & 0 & \overline{u}_h & \overline{p} & 0 & 0 \\ \overline{n} & 0 & -\beta & 0 & 0 & 0 & 0 & 0 \\ m_r\overline{p} & 0 & 0 & 0 & m_r\beta & 0 & 0 & 0 \\ 0 & 0 & 0 & 0 & 0 & 0 & 1 & 0 \\ 0 & 0 & 0 & -\beta\overline{n} & 0 & 0 & 0 & \psi_2 \end{bmatrix}, \tag{4.19}$$

$$\mathbf{P} = \begin{bmatrix} 0 & -1 & 0 & 0 & 0 & 0 & 0 & 0 \\ 0 & 0 & -\alpha & 0 & \alpha & 0 & 0 & 0 \\ 0 & 0 & -\omega - \frac{\mathrm{d}\overline{u}_{\mathrm{e}}}{\mathrm{d}x} & -\frac{\mathrm{d}\overline{n}}{\mathrm{d}x} & 0 & 0 & 0 & 0 \\ 0 & 0 & 0 & 0 & -\omega - \frac{\mathrm{d}\overline{u}_h}{\mathrm{d}x} & -\frac{\mathrm{d}\overline{p}}{\mathrm{d}x} & 0 & 0 \\ 0 & 0 & -\frac{\mathrm{d}\overline{V}}{\mathrm{d}x} + \overline{u}_{\mathrm{e}} & \overline{n} & 0 & 0 & 0 & 0 \\ 0 & 0 & 0 & 0 & -\frac{\mathrm{d}\overline{V}}{\mathrm{d}x} - m_r\gamma\overline{u}_h & -m_r\gamma\overline{p} & 0 & 0 \\ 0 & 0 & 0 & 0 & 0 & 0 & 0 & 1 \\ 0 & 0 & -\frac{1}{2}\nu{\overline{u}_{\mathrm{e}}}^2 + \beta\frac{\mathrm{d}\overline{u}_{\mathrm{e}}}{\mathrm{d}x} & -\nu\overline{n}\overline{u}_{\mathrm{e}} & 0 & 0 & \omega\psi_1 & 0 \end{bmatrix}, \tag{4.20}$$

$\mathbf{J}^{-1}\mathbf{P}$ is a square matrix which depends on the eigenvalue in time ω and the position x.

4.3.3 Boundary Conditions

From the definition of the perturbation:

$$y(x,0) = y_0(x,0) + \epsilon y_1(x,0) + O(\epsilon^2). \tag{4.21}$$

Imposing the perturbation contribution neglected in borders, zero order response is:

$$y(x,0) = y_0(x,0) = \overline{y}(x) + \delta y'(x,0). \tag{4.22}$$

As the boundary conditions expressed to the target problem must be fulfilled at every time, they define the steady-state's. Hence, the transient conditions are defined null when they are explicit in the target problem and unknown in the contrary. This can be expressed as $\mathbf{Y}(0)$ at $x = 0$ and $\mathbf{Y}(1)$ at $x = 1$:

$$\mathbf{Y}(0) = \begin{Bmatrix} 0 \\ 0 \\ 0 \\ \widehat{u}_{\mathrm{e}}(0) \\ 0 \\ \widehat{u}_h(0) \\ 0 \\ \widehat{q}_L(0) \end{Bmatrix}, \quad \mathbf{Y}(1) = \begin{Bmatrix} 0 \\ 0 \\ 0 \\ \widehat{u}_{\mathrm{e}}(1) \\ 0 \\ \widehat{u}_h(1) \\ 0 \\ \widehat{q}_L(1) \end{Bmatrix}. \tag{4.23}$$

To simplify the numerical resolution by integrating the differential equation Eq.(4.17) from $x = 0$ to $x = 1$, auxiliaries initial conditions are used [34]. Multiples $\mathbf{Y}(0)$ are defined

as the orthonormal vectors e_i, where subscript i defined the position of the value 1 in the vector. Solving with these basic vectors, generates a new matrix **A** which defined the relation between the boundary conditions at $x = 0$ and $x = 1$ as the form:

$$\mathbf{Y}(1) = \mathbf{A}\mathbf{Y}(0). \tag{4.24}$$

This matrix **A** is entitled the transfer matrix and explicit the behaviour of the system. In this case, it depends only on the eigenvalues ω that are determined by the boundary conditions.

4.3.4 Integration Methods

Numerical methods are based on information about the target function by introducing points between two intermediate points [39].

The Cauchy problem, also known as initial value problem, describe the nature of the problem to solve and consist of finding the solution of and ODE given suitable initial conditions. In particular, denoting by I an interval of $\mathbb{R}$ containing the point x_0, Cauchy problem associate with a first order ODE reads:

Find a real-valued function $y \in C^1(I)$, such that:

$$y'(x) = f(x, y(x)), \qquad x \in I, \tag{4.25a}$$
$$y(x_0) = y_0. \tag{4.25b}$$

where $f(x, y(x))$ is a given real-valued function in the strip $S = I \times (-\infty, \infty)$, which is continuous with respect both variables.

Fixing $0 < X < \infty$, letting $I = (x_0, x_0 + X)$ be the integration interval and, correspondingly, for $h > 0$, let $x_n = x_0 + nh$, with $n \in \mathbb{N}$, be the sequence of discretization nodes of I into subintervals $I_n = [x_n, x_{n+1}]$. The width of h of such intervals is called the *discretization stepsize*. It is used the notation $y_j = y(x_j)$ and $f_j = f(x_j, u_j)$.

One-step Methods

A numerical method for the approximation problem in Eq.(4.25) is called *one-step* method if $\forall n \geq 0$, y_{n+1} depends only on y_n. Otherwise, the scheme is called a *multi-step* method.

Most commonly used one-step method are:

1. forward Euler method
$$y_{n+1} = y_n + hf_n. \tag{4.26}$$
2. backward Euler method
$$y_{n+1} = y_n + hf_{n+1}. \tag{4.27}$$

In both cases, y' is approximate through a finite difference: forward and backward. These are first order approximations of the first derivative of y with respect to h.

3. trapezoidal (or Crack-Nicolson) method

$$y_{n+1} = y_n + \frac{h}{2}[f_n + f_{n+1}]. \tag{4.28}$$

This method approximate the integration by the trapezoidal quadrature rule.

4. Heun method

$$y_{n+1} = y_n + \frac{h}{2}[f_n + f(x_{n+1}, y_n + hf_n)]. \tag{4.29}$$

It is derived from the previous one by replacing f_{n+1} with the forward Euler method.

Multi-steps Methods

In multi-step method are widely used due to its better accuracy. Simpler one came from the centered finite difference and is named as *midpoint method*:

$$y_{n+1} = y_{n-1} + 2hf_n \tag{4.30}$$

When solving a nonlinear Cauchy problem of the form in Eq.(4.25), at each step implicit schemes require dealing with this nonlinear equation. The *predictor-corrector methods* consist of two kinds of steps: The initial, "prediction" step, starts from a function fitted to the function-values and derivative-values at a preceding set of points to extrapolate this function's value at a subsequent, new point. The next, "corrector" step refines the initial approximation by using the predicted value of the function and another method to interpolate that unknown function's value at the same subsequent point. One of the most known method is Runge-Kutta Method.

Runge-Kutta Method

Runge Kutta method maintain the structure of one-step methods, and increase their accuracy at the price of an increase of functional evaluations at the each time level, thus sacrifying linearity. The second order solution at step x_{n+1} is obtained from:

$$y_{n+1} = y_n + \gamma_1 k_1 + \gamma_2 k_2, \tag{4.31}$$

where functions k_1 and k_2 are defined sequentially

$$k_1 = hf(x_n, y_n), \tag{4.32a}$$
$$k_2 = hf(x_n + \alpha h, y_n + \beta k_1), \tag{4.32b}$$

where α, β, γ_1 and γ_2 are constants to be determined. These ensure the highest order accuracy for the method. To establish this order, Taylor series expansion of $y(x_{n+1})$ is considered, determining the value of β, γ_1 and γ_2. Most commonly value used for the arbitrary constant α is $1/2$ leading to the following formula:

$$y_{n+1} = y_n + k_2, \tag{4.33a}$$
$$k_1 = hf(x_n, y_n), \tag{4.33b}$$
$$k_2 = hf(x_n + \frac{1}{2}h, y_n + \frac{1}{2}k_1). \tag{4.33c}$$

The order of the method, that means the order of the associated error, requires at least the same quantity of steps or stages. The maximum order when these values coincide is fourth, hence it is the most commonly used and an example of it is presented at following;

$$y_{n+1} = y_n + \frac{h}{6}(k_1 + 2k_2 + 2k_3 + k_4), \tag{4.34a}$$

$$k_1 = f(x_n, y_n), \tag{4.34b}$$

$$k_2 = f(x_n + \frac{1}{2}h, y_n + \frac{h}{2}k_1), \tag{4.34c}$$

$$k_3 = f(x_n + \frac{1}{2}h, y_n + \frac{h}{2}k_2), \tag{4.34d}$$

$$k_4 = f(x_{n+1}, y_n + hk_3). \tag{4.34e}$$

4.3.5 Temporal Eigenvalues

Once the transfer matrix $\mathbf{A}$ is determined, a non-trivial solution is required to be satisfied for the system of algebraic equations in terms of $\widehat{u}_{\mathrm{e}}(0)$, $\widehat{u}_h(0)$ and $\widehat{q}_L(0)$(see $\mathbf{Y}(0)$) that contains the boundary conditions at $x = 1$. This system is defined by the matrix $\mathbf{B}$, which rows are filled in with equations of voltage, electric field and lattice temperature, and its columns are filled in with the unknown variables related to velocities and transferred heat. The new problem to solve become $\mathbf{B} \cdot \mathbf{y} = 0$ or equivalently:

$$\begin{bmatrix} a_{41} & a_{61} & a_{81} \\ a_{42} & a_{62} & a_{82} \\ a_{47} & a_{67} & a_{87} \end{bmatrix} \begin{pmatrix} \widehat{u}_{\mathrm{e}}(0) \\ \widehat{u}_h(0) \\ \widehat{q}_L(0). \end{pmatrix} = \begin{pmatrix} 0 \\ 0 \\ 0 \end{pmatrix} \tag{4.35}$$

This leads to find the linearly independence of the new matrix $\mathbf{B}$ by finding the conditions to force the determinant of $\mathbf{B}$ be equal to zero, that means, finding the eigenvalues ω's that solve the equation system.

Chapter 5

Results

In this chapter results under different variables are shown. First, conditions about steady state code, quantity of nodes, kind of numerical method used, among others, are determined. Then, data process is defined in order to be able to assign a physical meaning. Finally, varying operating conditions as boundary lattice temperature and design criteria as longitude, positive eigenvalues are presented.

5.1 Validity of Results

As the results is sensitive to steady state and transient state codes, numerical conditions are defined with their relative error respect to an ideal, defined in each case. These are determined under a thermal equilibrium state at $300[K]$ and evaluated their real part due to they determine the instability. Quantity of ω's values depends on intermediary steps of iteration methods and quantity of nodes from the grid discretization from the transient steady state flow. This implies the number of result eigenvalues could be infinity, which can be explained as a degeneration of the solution, mathematically translated as multiple roots or same magnitude power.

5.1.1 Main Code Tolerance

It is necessary to determine the significant digits that influence the eigenvalue solution. Varying by an order of 10^{-1} since 10^{-8} until 10^{-20}. From Figures 5.1, it is shown that the real part of eigenvalues is constant through significant digits until 10^{-13}, from which its value changes abruptly to another and remains constant. Respect to a solution evaluated at infinity significant numbers, that is supposed to be equal to the one obtained at 10^{-20}, relative error decreases abruptly to zero in both cases minimum and maximum from the set of eigenvalues.

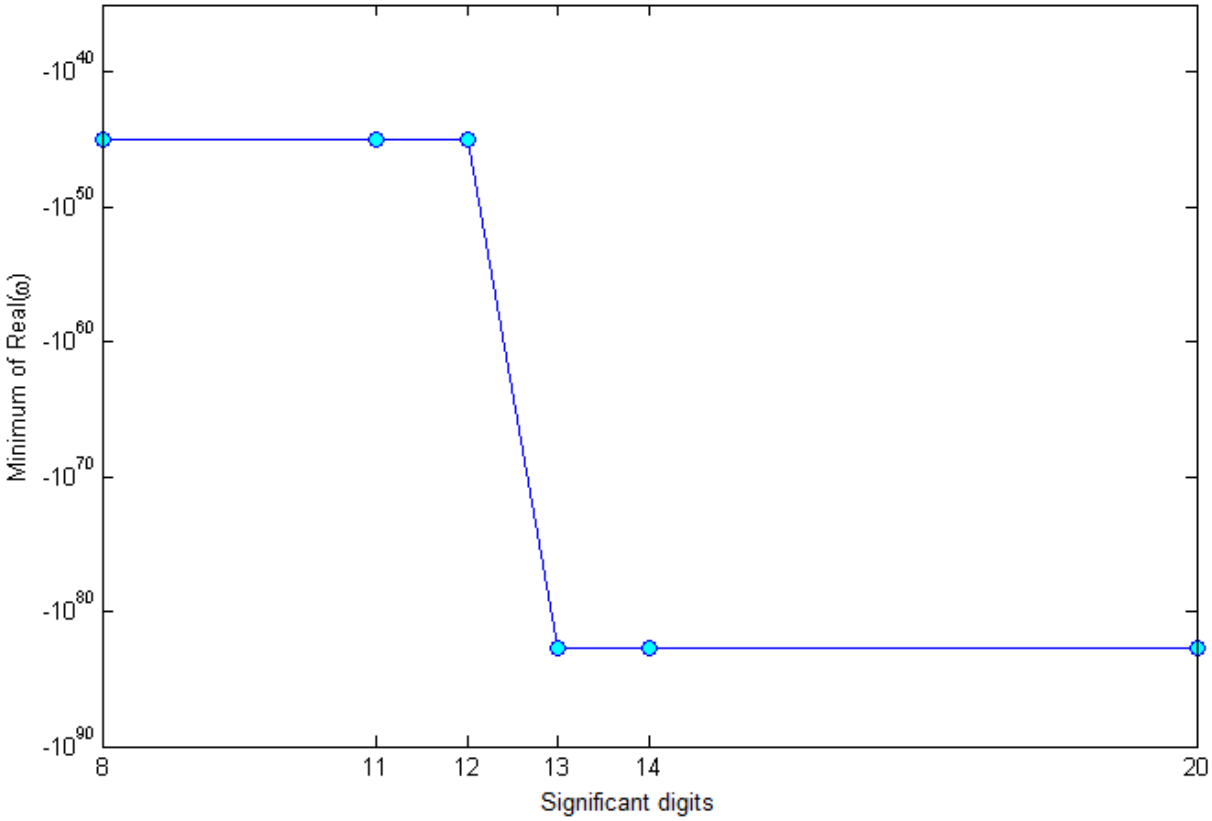

(a) Minimum of ω real component.

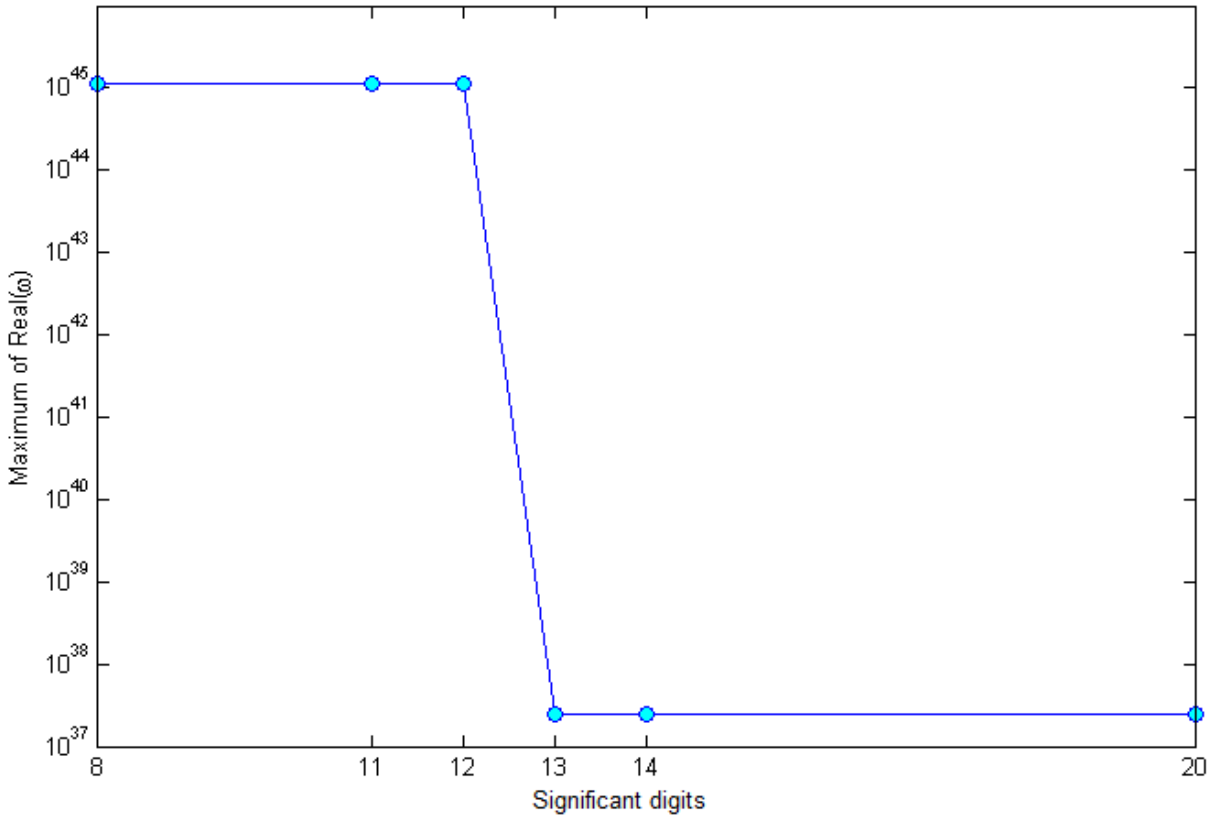

(b) Maximum of ω real component.

Figure 5.1: Significant digits in steady state code.

5.1.2 Transient-state Code Conditions

Imposing the tolerance in the main code as the critic value found, 10^{-13}, Runge Kutta method of different orders are compared varying the quantity of nodes used. In first case, an uncoupled system from heat transfer equation is shown, to compare lately with the complete system. Number of nodes used in second and fourth order Runge Kutta are compared in Figures 5.2 and 5.4. The abscissa axis expressed the quantity of nodes used in each iteration and the ordinate axis present all the strictly positive eigenvalues, but conjugated complex number are only expressed in one term.

Idealizing fourth order Runga Kutta method with 21 nodes, there are only 2 positive values with a maximum magnitude order over 10^{50} and a minimum below 10^{10}. By obtaining more values, the results contain a considerable proportion of zeros, indicating that the constant accompany the lower power of the polynomial decreases to zero. Numerical integration method inverses the matrix $[J^{-1}P]$ the same quantity of nodes numbers and powers it the same quantity of step of the method. Due to magnitude order of variables is negative (i.e, lower than one), values of terms of transfer matrix $\mathbf{A}$ diminish in each iteration.

In second Runge Kutta, Figure 5.2 shows that quantity of eigenvalues increases with the quantity of nodes. From the relative error in Figure 5.3, the minimum in each different quantity nodes cases is maintained below the ideal minimum and the maximum does not present a convergence, oscillating around a relative error of 10^{10}. For this reason this method can not be used.

Looking at Figure 5.4, in fourth order lower quantities of nodes (minor than 13) expressed acceptably the quantity of searched ω's but don't correspond in magnitude. Case contrary, higher quantities perform as a degenerated solution, that is, one state of energy with a corresponding magnitude has associated more than one value. Comparing results by the relative error presented in Figure 5.5, maximum value tends to an unitary error that keeps the magnitude order, same as the minimum value. Considering the relation between computational processing time and accuracy of the solution, the optimal case corresponds to the case with 11 nodes.

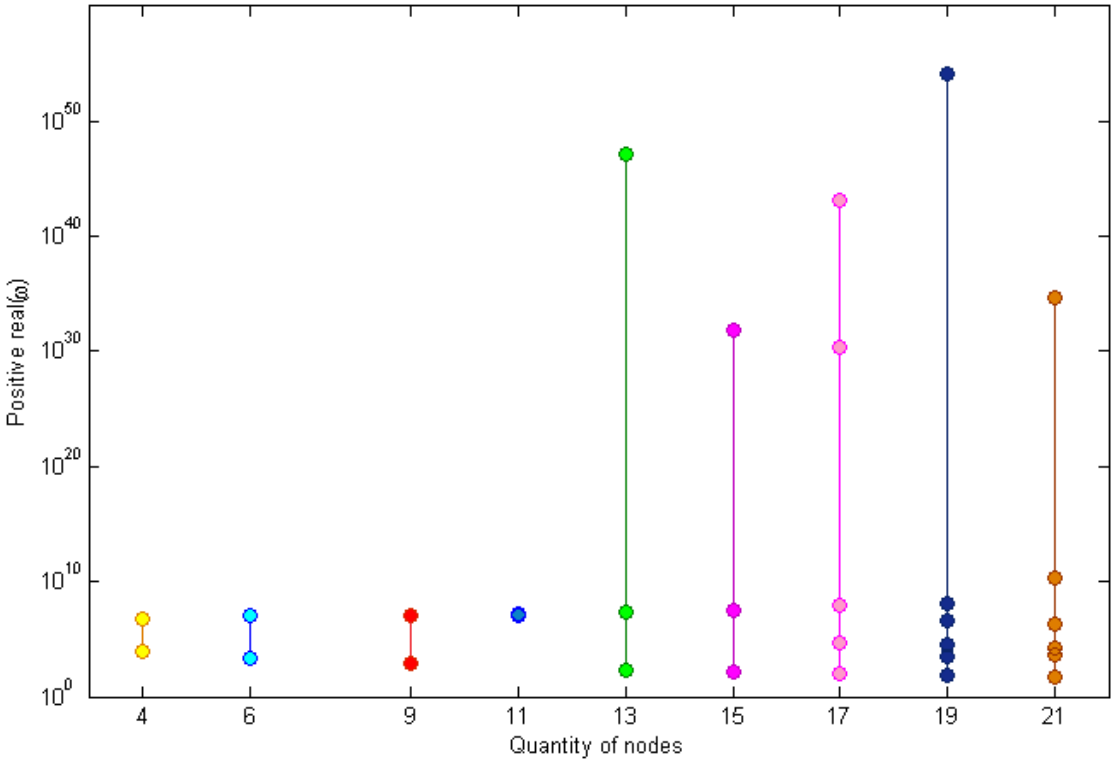

Figure 5.2: Positive eigenvalues from Runge Kutta 2nd order.

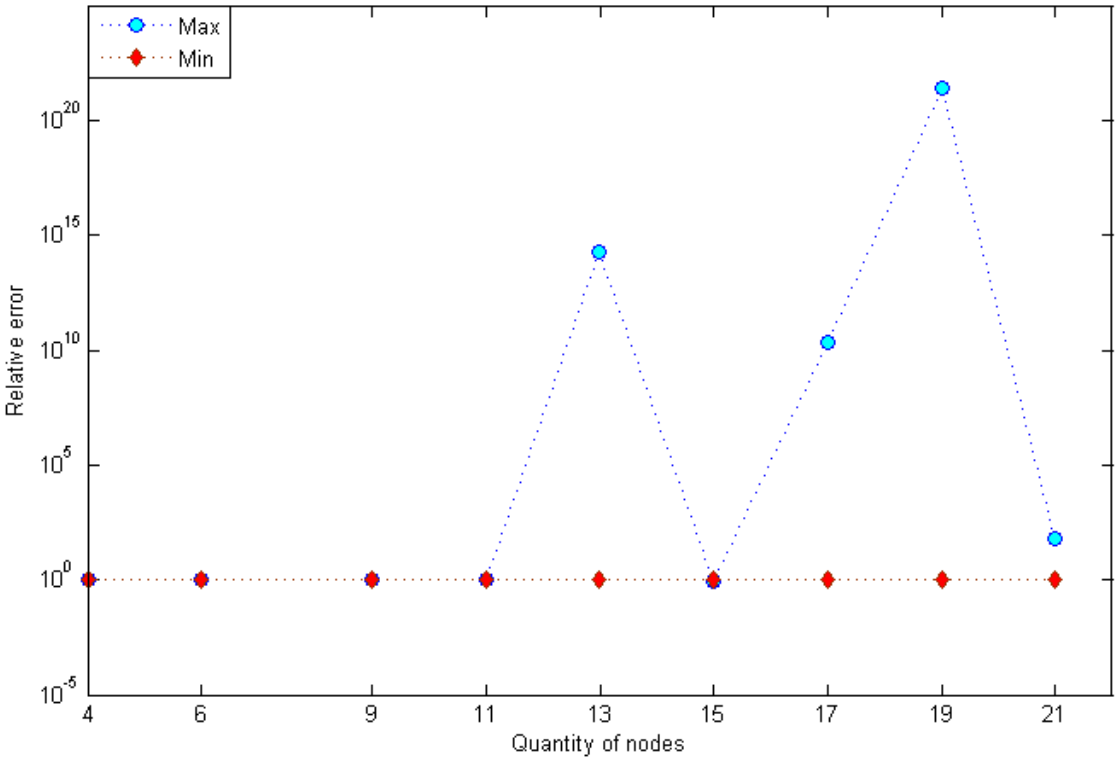

Figure 5.3: Relative error from Runge Kutta 2nd order.

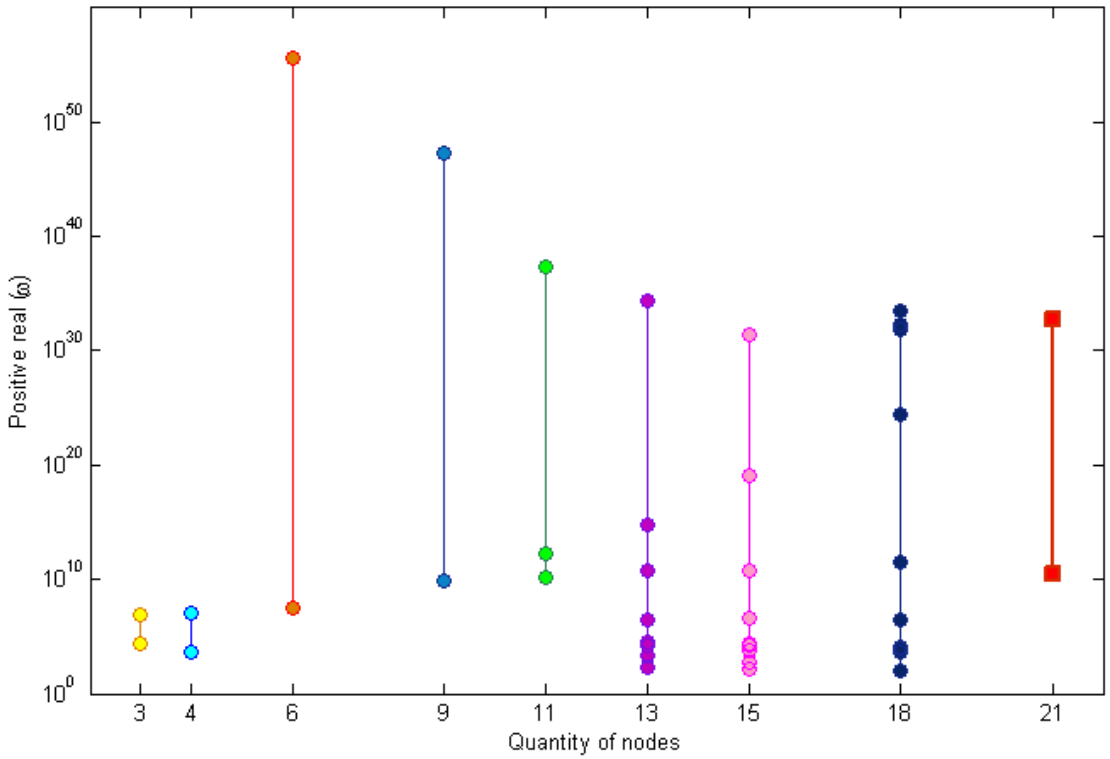

Figure 5.4: Positive eigenvalues from Runge Kutta 4th order.

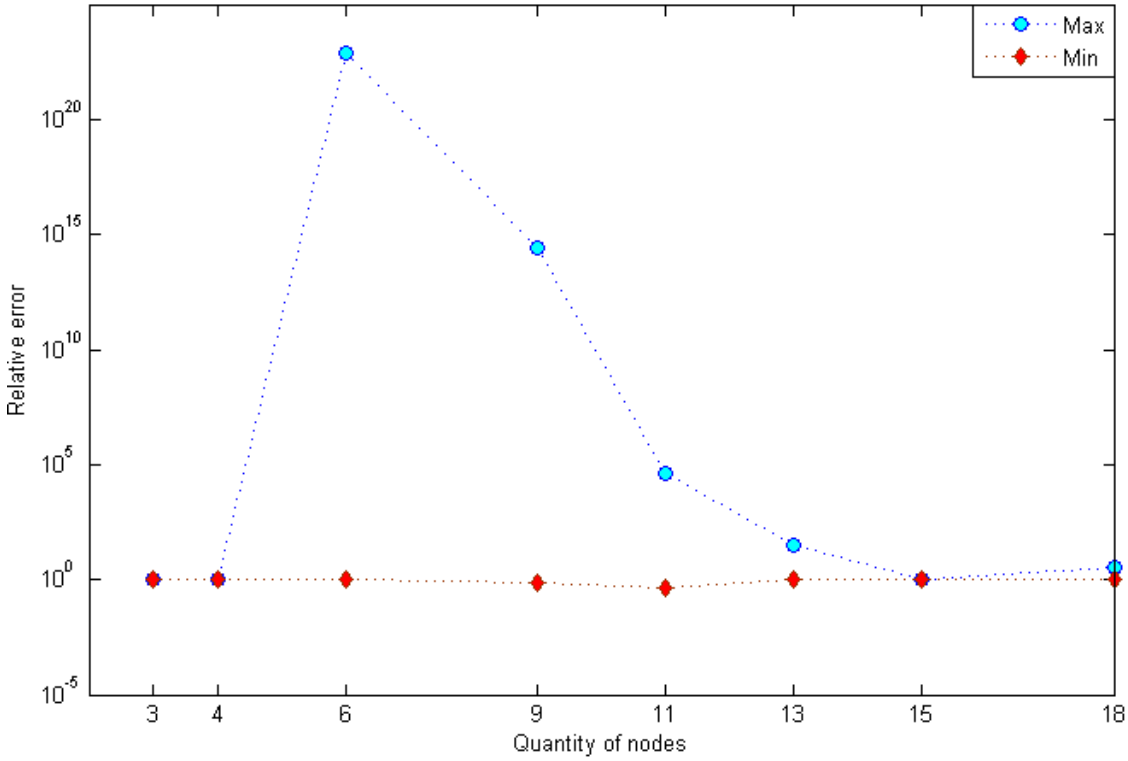

Figure 5.5: Relative error from Runge Kutta 4th order.

5.2 Data Processing

Solutions in general can be divided in complex and pure real solutions in which the real part (ω_R) of the eigenvalues represents unstable, growing exponentials in time. In case of complex values, the imaginary part (ω_I) correspond to oscillation frequency. As transient solutions are expressed in form $X(x)exp(\omega_R)cos(\omega_I + \phi)$, Figure **??** represents the incidence of temporal solution ω with an arbitrary amplitude in temporal representation.

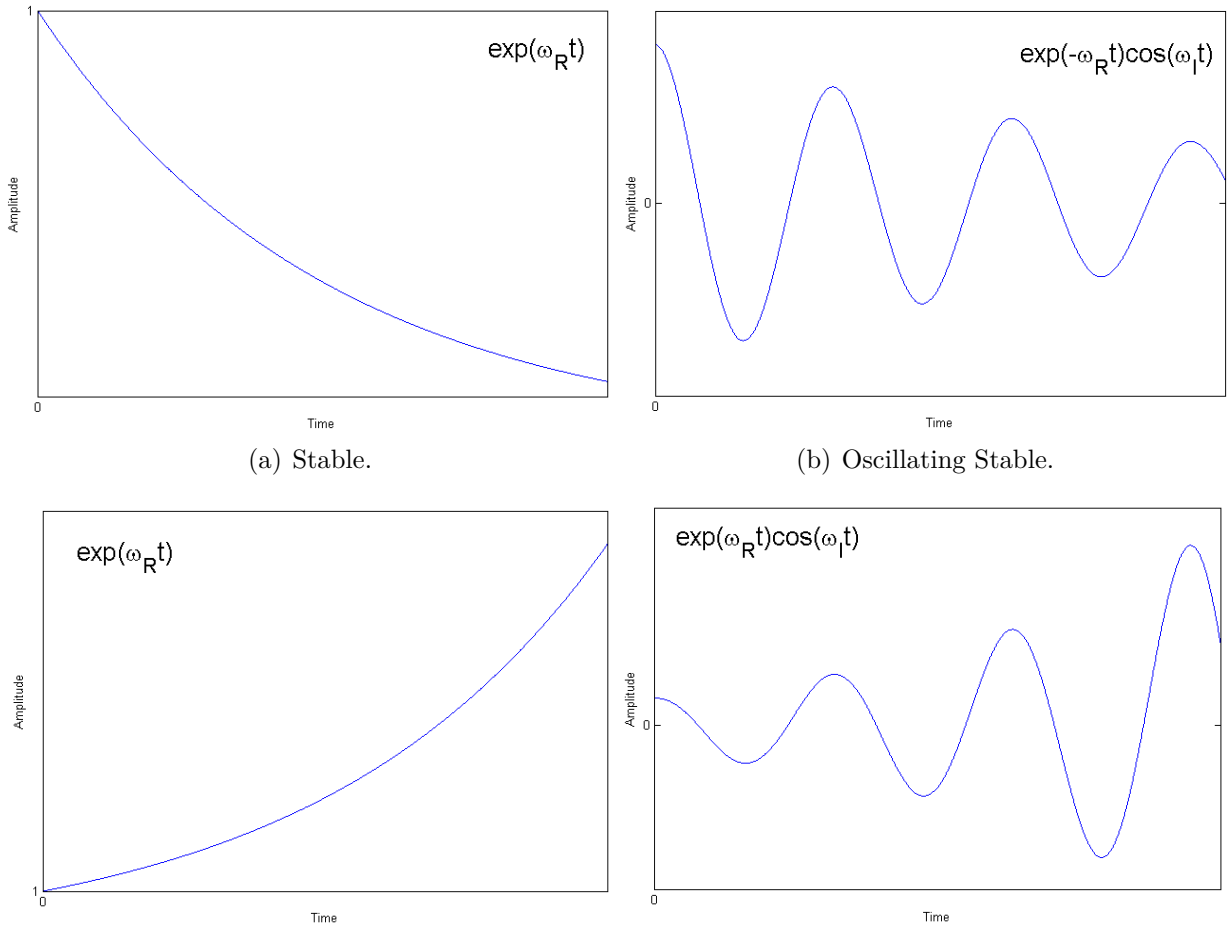

(a) Stable.

(b) Oscillating Stable.

(c) Unstable.

(d) Oscillating Unstable.

Figure 5.6: General transient response representation in time.

Stables solutions decreased its value to zero, allowing the system to answer as its steady state. In other hand, unstable solutions represents thermal runaway phenomenon, which leads to the quick degradation of device, rendering it useless and consequently without presenting the steady state.

5.2.1 Range of Allowed Eigenvalues

Various degradation mechanisms have been proposed in terms of atomic phenomenon [40], through there is no consensus in the field of what modes are presents in certain samples or if all possible modes are yet accounted for. In this Thesis, a range of allowed eigenvalues is proposed considering thermal inertia and a characteristic time of thermal runaway phenomenon.

Thermal inertia (I_{th}) is the material property to keep its temperature and is also known as thermal storage effect. It considers the degree of slowness with which the temperature of a body approaches that of its surroundings and the quantity of heat can be absorbed or lost. It depends on material's bulk thermal conductivity (k) and volumetric heat capacity, which is the product of density (ρ) and specific heat capacity (c), as can be seen in Eq. (5.1). For GaAs, $I_{th} = 8.647[Wm^{-2}K^{-1}\sqrt{s}]$, while for Si, $I_{th} = 15.668[Wm^{-2}K^{-1}\sqrt{s}]$ at room temperature $T_{room} = 300[K]$ and thermal equilibrium. As value for Si almost double GaAs, it is expected that GaAs allows lower times to increase its temperature.

$$I_{th} = \sqrt{k\rho c}. \tag{5.1}$$

As there is not experimental data of thermal evolution through time of solar cells based on GaAs junction, comparison will fall on experimental work of Vasko [25], who evaluated solar cells of a-Si:H triple junction. From an IR mapping, surface temperature is measured following a hot spot development under forced convective cooling. Hence, it is supposed that difference between surface and junction temperature is neglected.

Considering a mean thermal inertia of $\omega_{MTI} = 5.55 \times 10^{-4}$, calculated as the coefficient of exponential regression of experimental data [25], it could be stablish a range of allowed values with a meddle value equal to mean thermal inertial.

The range of allowed values represents limits in which thermal runaway occurs; solutions below lower limit are associated to times larger than phenomenon characteristic time and, in other hand, solutions over the upper limit implies times does not allowed considered the thermal inertia of device. To determine the range of calculated eigenvalues, it is necessary to considerate the non-dimensional constant t_0 to dimensionalize them.The parameter t_0 is a function of junction longitude L and temperatures T_C and T_L expressed as $t_0 = \frac{L^2}{\mathrm{v}_0 \cdot \mu_n}$,as can be seen in Figure 5.7.

Once eigenvalues become dimensional, they can be associated to a characteristic time, defined as necessary time to achieve $T(t_{\mathrm{end}}) = 600[K]$ from $T(t_{initial}) = 301[K]$, as can be seen in Eq.(5.2). These temperatures considering the steady state profile and transient state evolution, that means, it is supposed that in one part of the temperature profile of transient state solutions there is at least one point with a initial value of $1[K]$, which evolves to $300[K]$.

$$t(\omega^*) = ln(300)/\omega^* \tag{5.2}$$

Also, in order to compare to the reference eigenvalue ω_{MTI}, the calculated characteristic time is $t(\omega_{MTI}) = 18[min]$. Figures 5.8 and 5.9 represent a range of the calculated characteristic time as a function of eigenvalues; first, with a range equal to experimental data dispersion; and the second concentrates values closest to the reference.

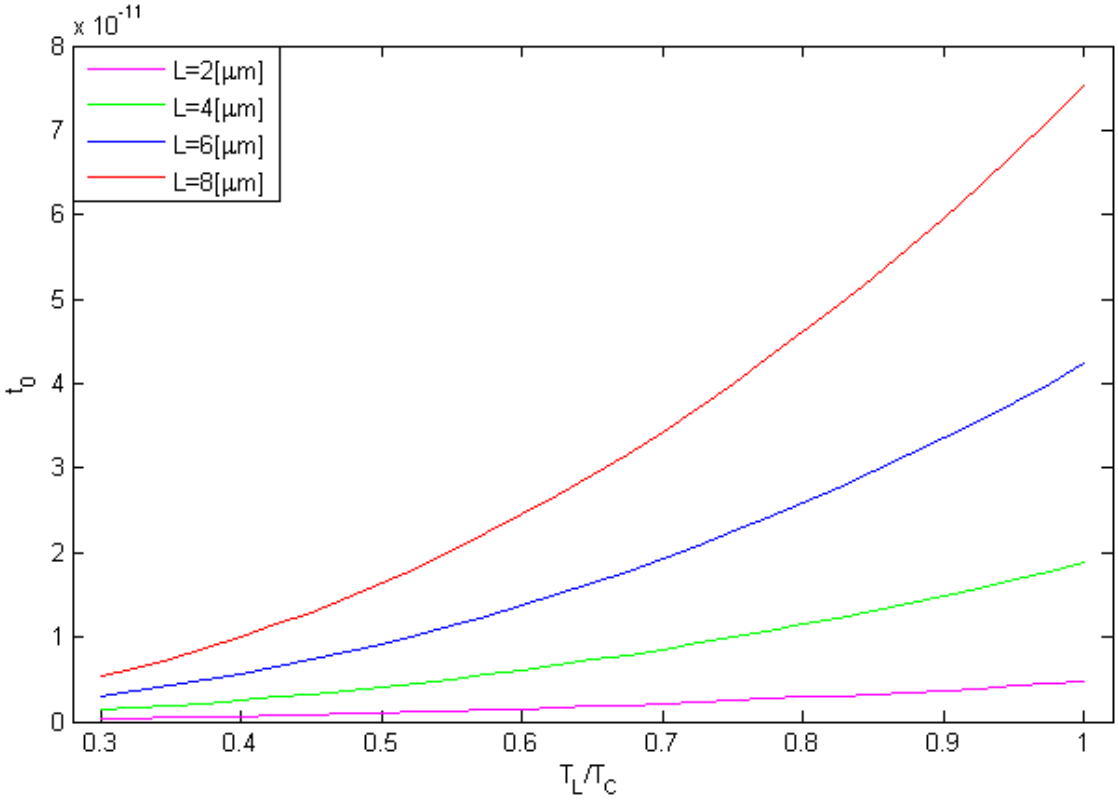

Figure 5.7: Reference time t_0.

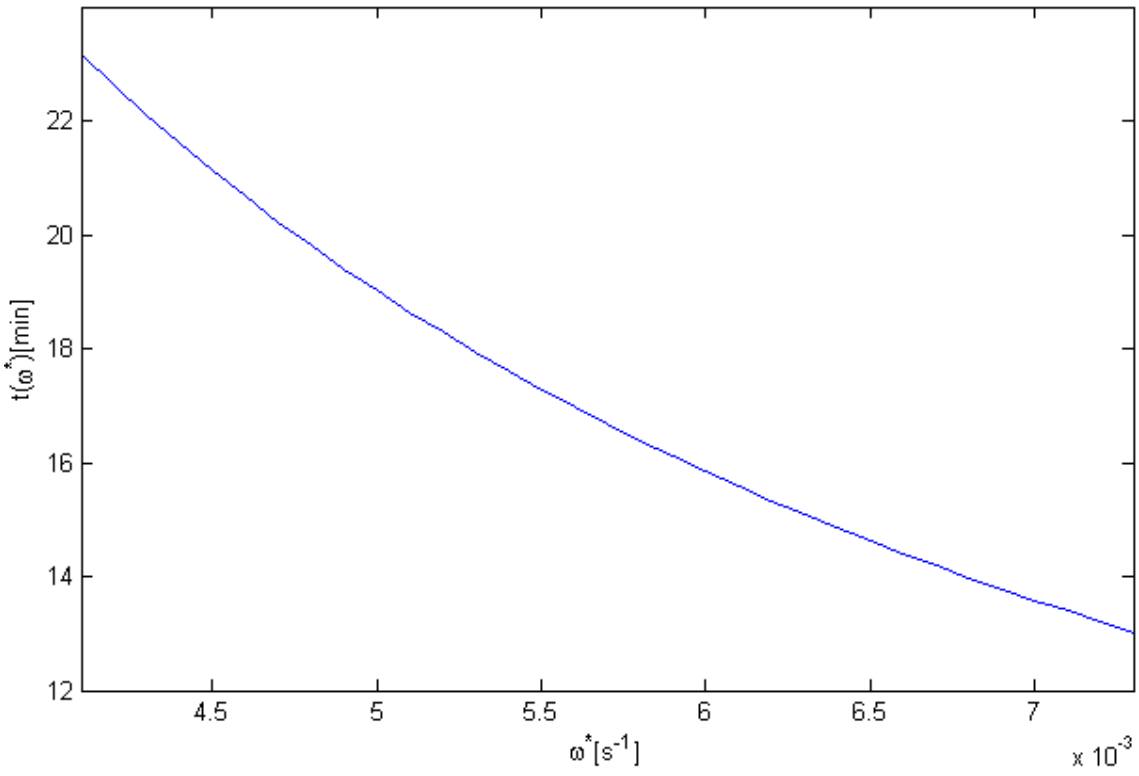

Figure 5.8: Allowed range of characteristic time.

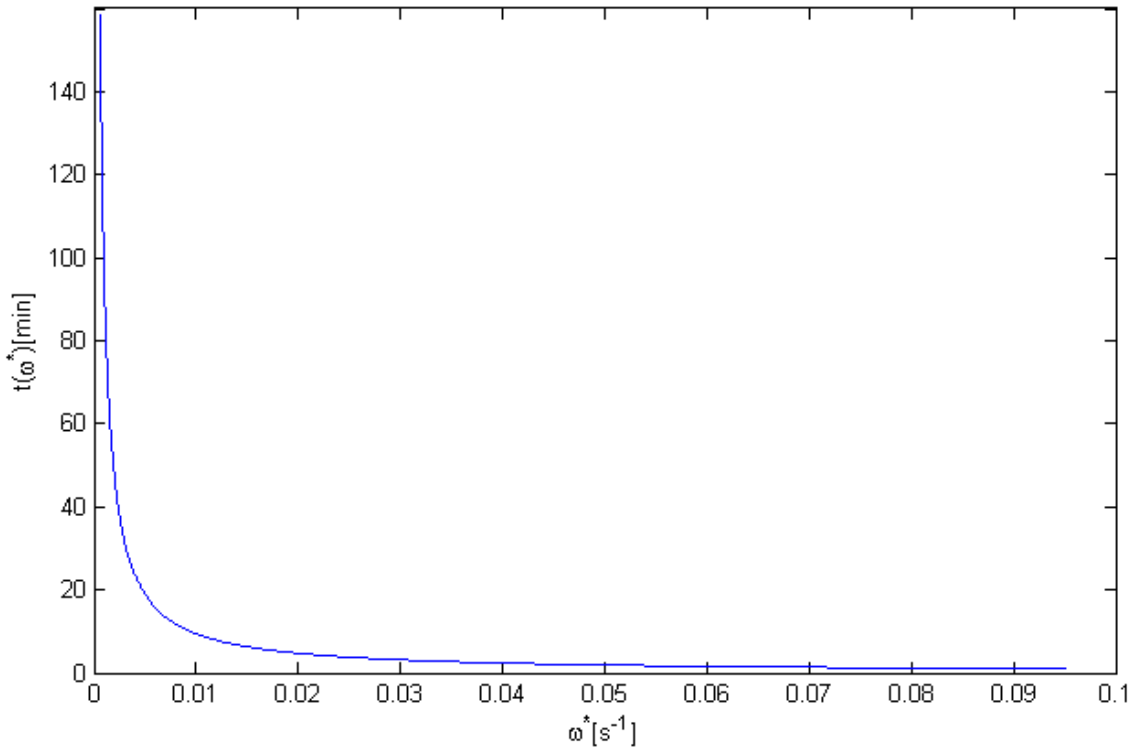

Figure 5.9: Allowed range of characteristic time-zoom.

5.3 Sensitivity Analysis

At following, a sensitivity analysis is applied to the system in order to determine device behaviour at front of changes in temperature, longitude and applied voltage. There are presented strictly positive solutions and then, data interpretation is presented as the previously defined characteristic time compared to the one generated by the experimental eigenvalue ω_{MTI}. The studied behaviour is focused in the allowed range; for this, zoom of each section is presented apart and its surrounding. The phenomenon will be stable if there any positive eigenvalues, but for analysis purpose there will be consider stable if a value leaves the allowed zone. In order to consider the complete scheme, total quantity of eigenvalues are presented in a base case of thermal equilibrium.

5.3.1 Solution at Thermal Equilibrium

Eigenvalues solutions at thermal equilibrium, with temperature of $300[K]$, longitude of $4 \times 10^{-6}[m]$ and an applied voltage of $0.4[V]$, are shown in Figures 5.10 and 5.11 considering both cases with-no and with heat transfer contribution, respectively.

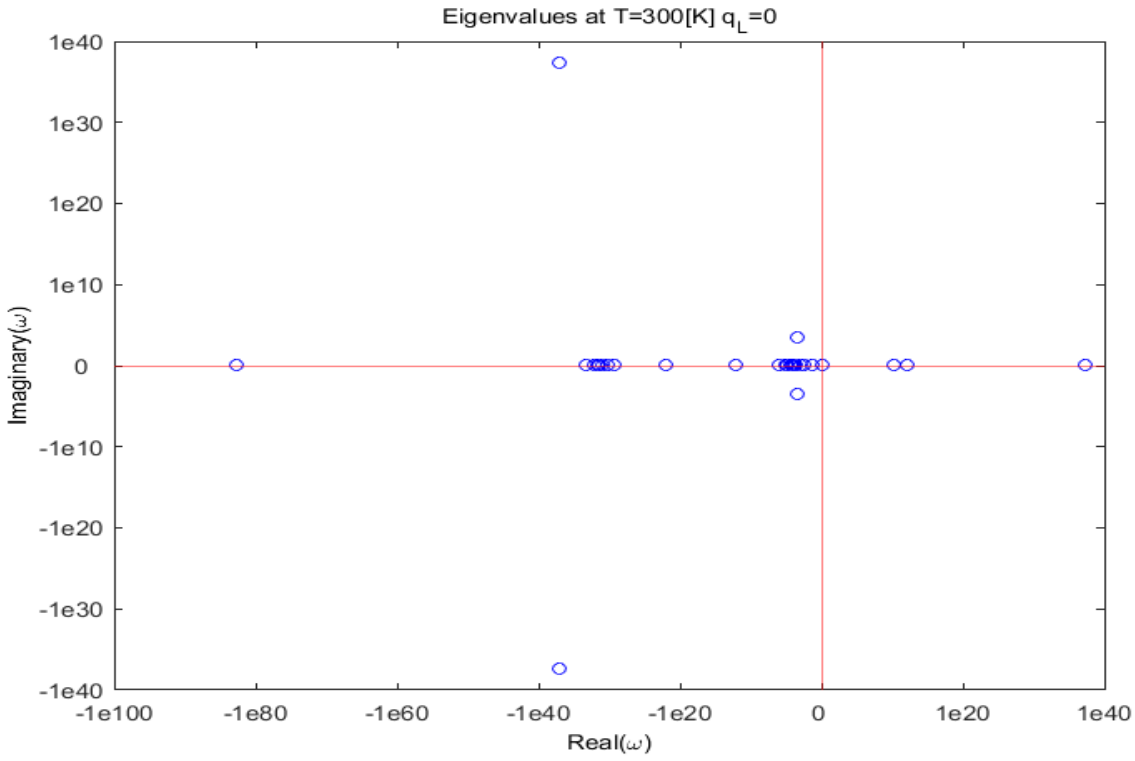

Figure 5.10: Eigenvalues at thermal equilibrium, $q_L = 0$.

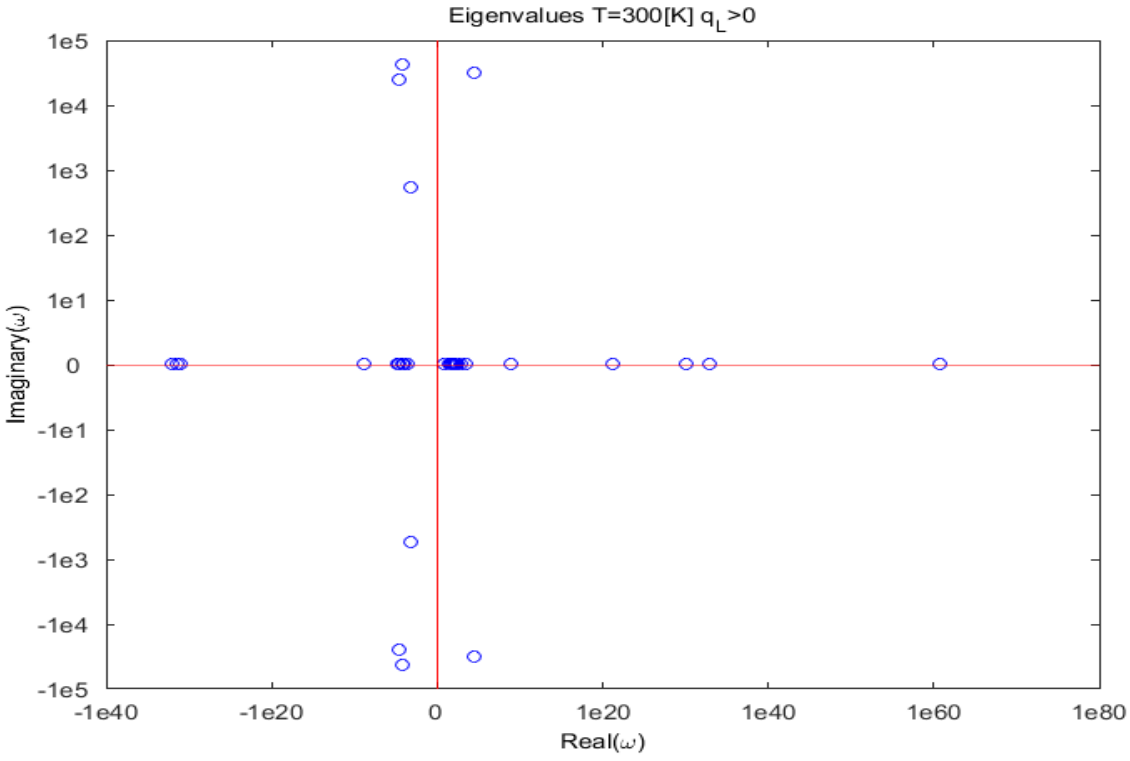

Figure 5.11: Eigenvalues at thermal equilibrium, $q_L > 0$.

With-no lattice temperature influence, solution is expressed in multiples eigenvalues with high magnitude, real part orders expressed from 10^{-100} until 10^{40} and imaginary part, from 10^{-40} to 10^{40}. Including energy equation contribution, graphs moves to the unstable zone at right, decreasing oscillating frequency. It can be interpreted as system without lattice temperature or $T_L = 0[K]$ has less probabilities of been unstable compared to the same system with a lattice temperature higher than zero. Also, in case of a positive lattice temperature, oscillating frequency (ω_I) of central values is higher than temporal evolution value (ω_R), representing a movement of carrier through the junction without a concrete direction, characteristic of turbulence phenomenon.

5.3.2 Variation in Temperature

As the model is two-temperature, three base cases are considered. First one, variation of lattice temperature and constant carrier temperature. Second one is the opposite of the first one and the last is a variation of both temperatures, considering the difference between them constant.

Lattice Temperature

Lattice temperature range is imposed with a lower value representing a room temperature of $300[K]$ and a maximum value of $550[K]$; this last is higher that used in accelerated degradation testing in order to considerate the difference between surface and junction temperature. Carrier temperature are considered $T_C = 650[K]$ in order to be never reach by lattice temperature and is constant to focus in the lattice temperature effect. Also, voltage and longitude are fixed in $V_{app} = 0.4[V], L = 4[\mu m]$.

Figure 5.12 represents eigenvalues results, concentrating the major quantity with a positive real lower than 10^5 and higher than 1; there are few values over that, that is, one for temperatures lower than $450[K]$ and two for the others. Respect to magnitude of the eigenvalues real part, $450[K]$ is the lattice temperature since the expansion of instability range becomes higher. As can be seen in Figure 5.13, most values led to high characteristic times, above $10^5[min]$, and they can be prevented considering forced cooling and by another regulation measures. There are also eigenvalues at low characteristic time, less than $10^{-5}[min]$ that can be considered instantaneous; hence, less probable due to thermal inertia. As there are not eigenvalues in the allowed zone until $450[K]$, Figure 5.14 shows that tendency of eigenvalues is increasing in time, so even if the phenomenon start at $450[K]$ it can be more controllable if temperature arises. $T_L = 450[K]$ is a temperature used in accelerated test that induces device degradation, so it is expected that an allowed eigenvalue is presented in that temperature. Also, at higher lattice temperature phenomenon stabilizes and can be linked to the decrease of device power [41].

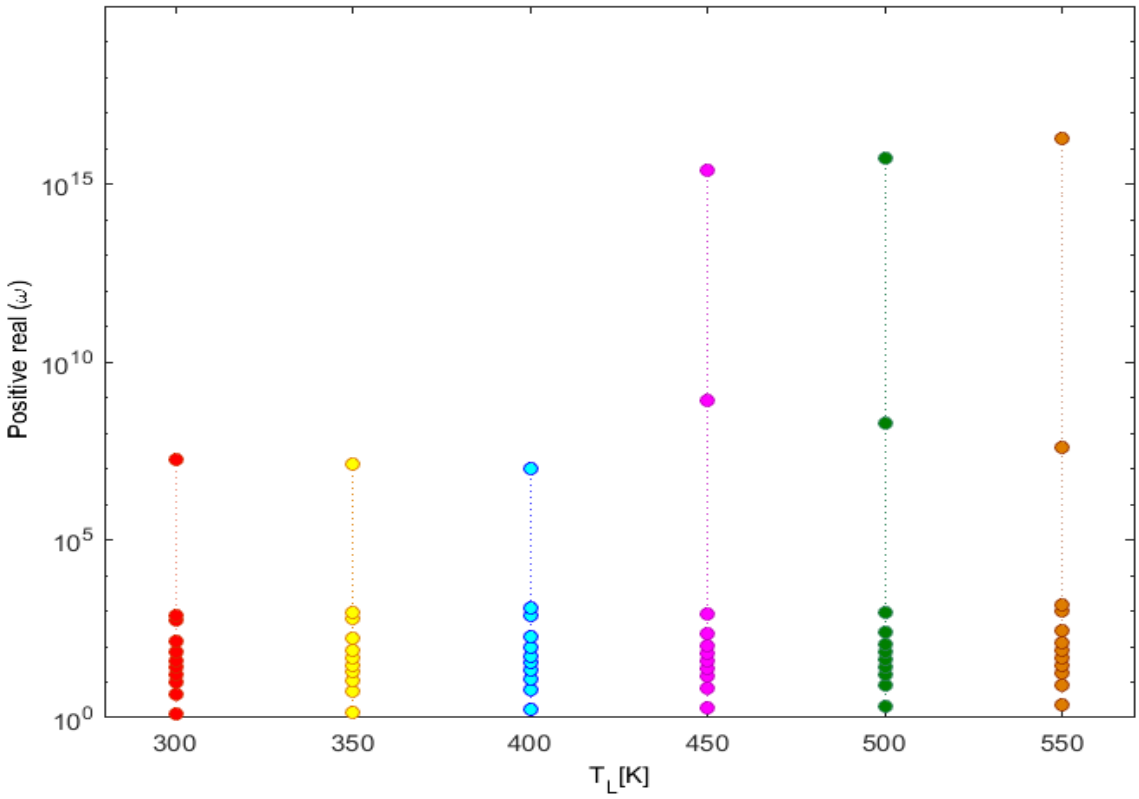

Figure 5.12: Positive eigenvalues at $T_C = 650[K], V_{app} = 0.4[V], L = 4[\mu m]$.

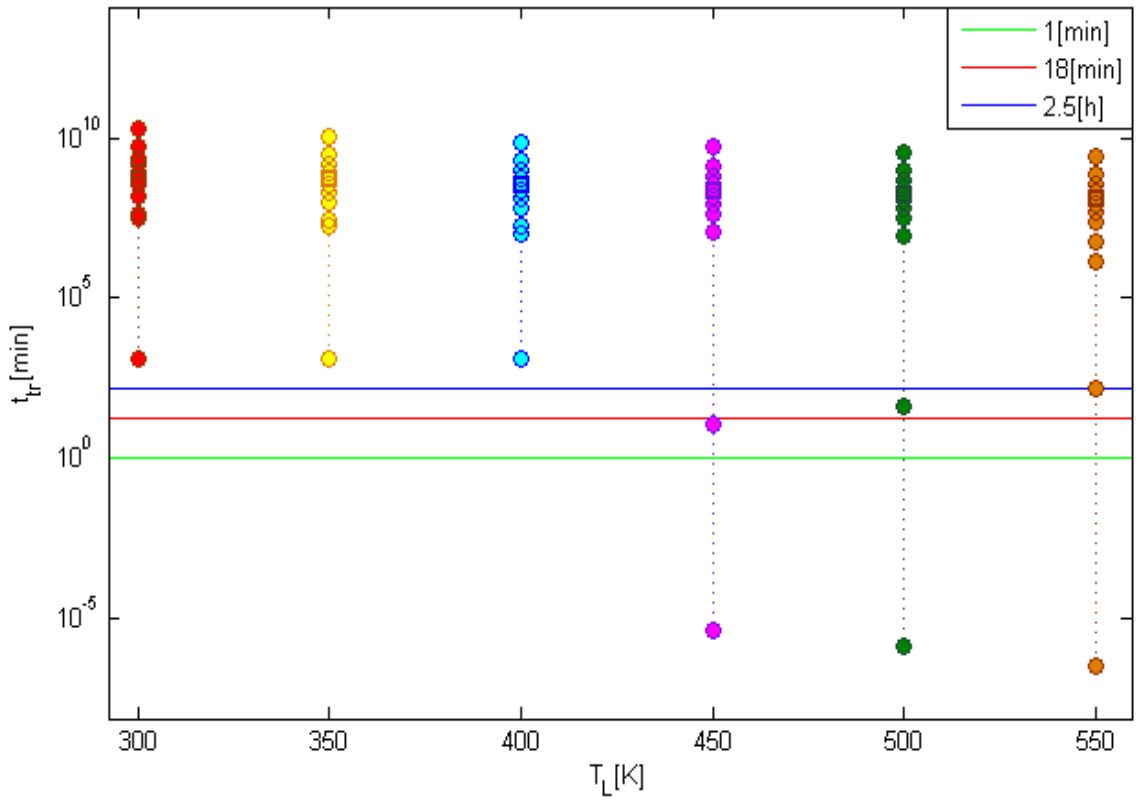

Figure 5.13: Characteristic time at $T_C = 650[K], V_{app} = 0.4[V], L = 4[\mu m]$.

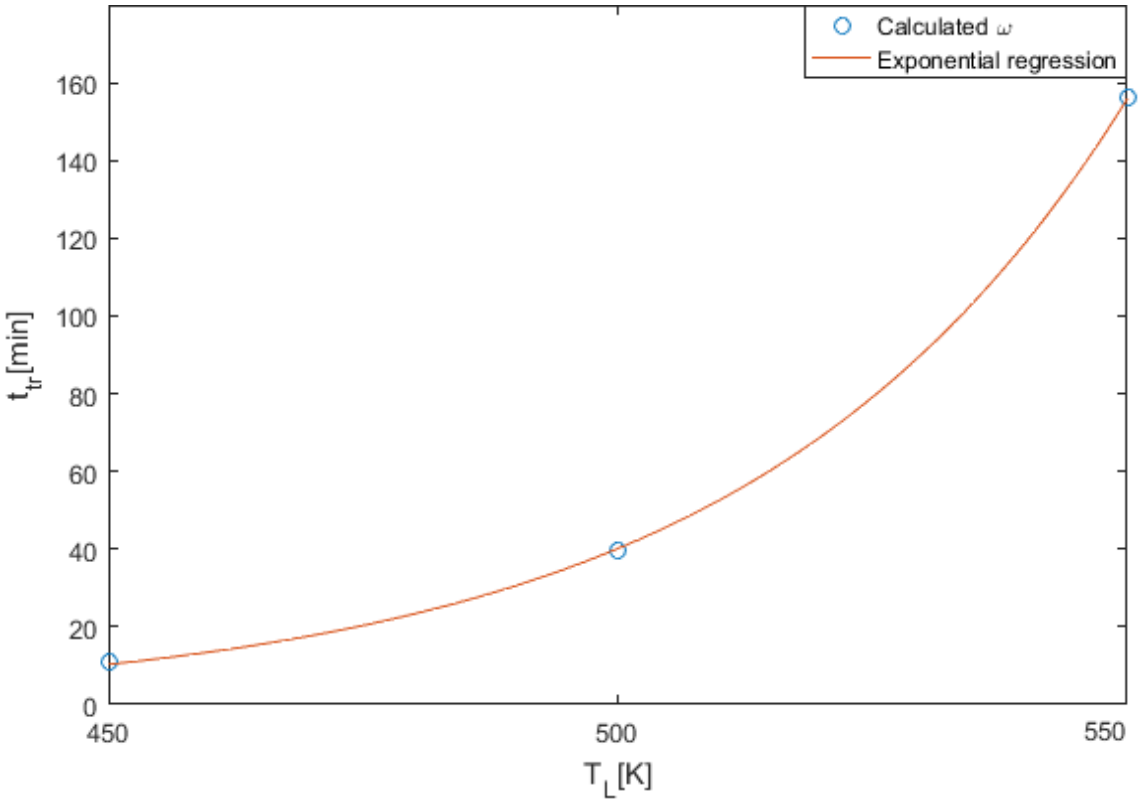

Figure 5.14: Allowed range at $T_C = 650[K], V_{app} = 0.4[V], L = 4[\mu m]$.

Carrier temperature

Carrier temperature start considering thermal equilibrium at $T = 300[K]$ and then increasing until $T_C = 800[K]$. Lattice temperature is fixed at $T_L = 300$, applied voltage at $V_{app} = 0.4[V]$ and longitude $L = 4[\mu m]$.

Figure 5.12 represents eigenvalues results showing that, in contrast with lattice temperature, carrier temperature increases the quantity of eigenvalues that are above the concentration range of $(1, 10^5)$, which coincides with the one presented for lattice temperature. There isn't a clear tendency in the maximum data, presenting a peak at $500[K]$. The minimum positive value, however, tends to decrease with the increase of carrier temperature. As can be seen in Figure 5.16, most values led to high characteristic times, above $10^5[min]$. There are also eigenvalues at low characteristic time, less than $10^{-5}[min]$, specially at thermal equilibrium. There is not a eigenvalue in the allowed zone at thermal equilibrium, but is so close so it is considered inside at the evidence that at that operating condition there is thermal runaway. Figure 5.17 shows that higher temperatures raise their characteristic time, making it more stable. Carrier with a temperature higher than the one of lattice is consider a hot carrier and it is proved that increases device efficiency by dimishing thermalization losses [41].

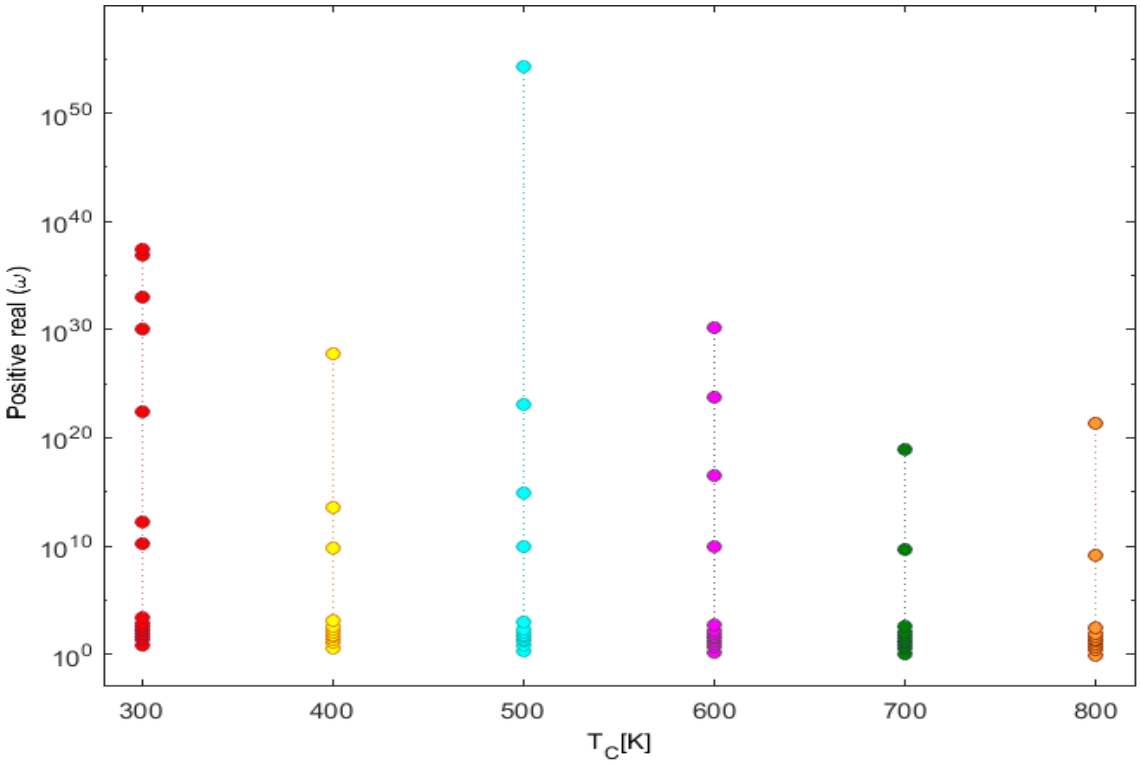

Figure 5.15: Positive eigenvalues at $T_L = 300[K], V_{app} = 0.4[V], L = 4[\mu m]$.

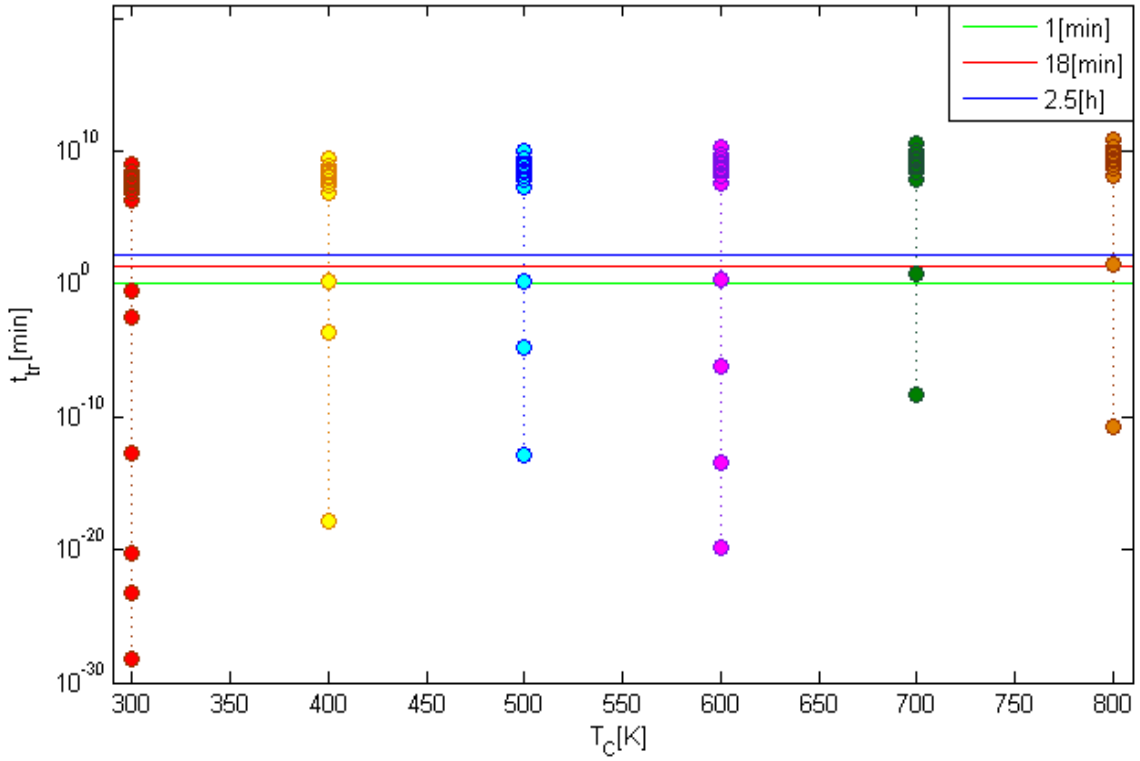

Figure 5.16: Characteristic times at $T_L = 300[K], V_{app} = 0.4[V], L = 4[\mu m]$.

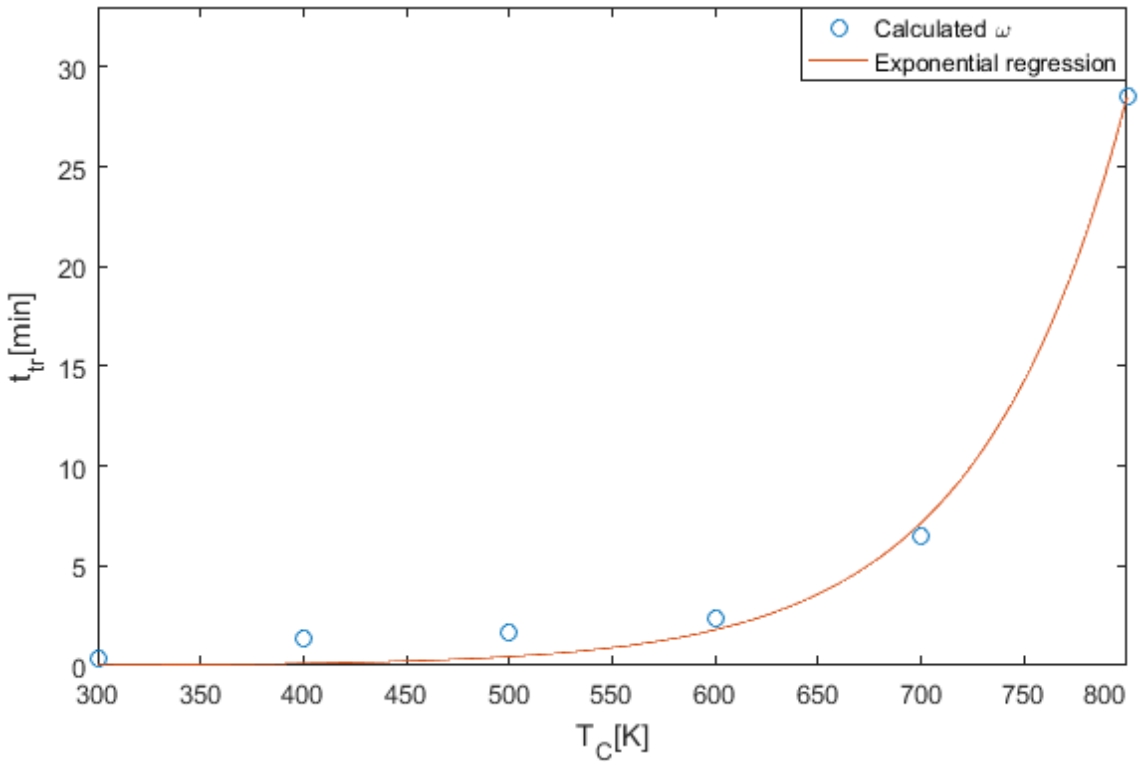

Figure 5.17: Allowed range at $T_L = 300[K], V_{app} = 0.4[V], L = 4[\mu m]$.

Constant Difference

To consider that an increase of lattice temperature leads to thermal runaway and an increase of carrier temperature stabilize it, a combined effect is studied by fixing a difference in temperature of $T_C - T_L = 150[K]$. Applied voltage is fixed at $V_{app} = 0.4[V]$ and longitude $L = 4[\mu m]$.

From Figure 5.18, quantity of eigenvalues decrease with the increase of temperature, carrier and lattice. The range of concentration is kept at any temperature configurations and the upper values tends to increase from $450[K]$. This leads to determine that lattice temperature is critical in the stability and carrier temperature could control the range of instability, decreasing the value of the solution. Figure 5.19 shows that only at $300[K]$ there is not any eigenvalue in the allowed range; the most close value presents a characteristic time higher than the upper limit. Lower values presents pseudo-spontaneous phenomenon, increasing the characteristic time from 10^{-60} until 10^{-10}, approximately. For lattice temperatures lower than $500[K]$, carrier temperature is lower than the used in the previous case (T_C constant). Figure 5.20 shows that at that range phenomenon is unstable, contrary to the one with $T_C = 650[K]$. To temperatures higher than $450[K]$, carrier temperature is higher too and phenomenon has a higher characteristic time, stabilizing the system even at high lattice temperatures. Also, projecting the analysis, it can be extracted that carrier temperature variation for a fixed lattice temperature behaves as contour lines, representing the same curve moving through characteristic time axis.

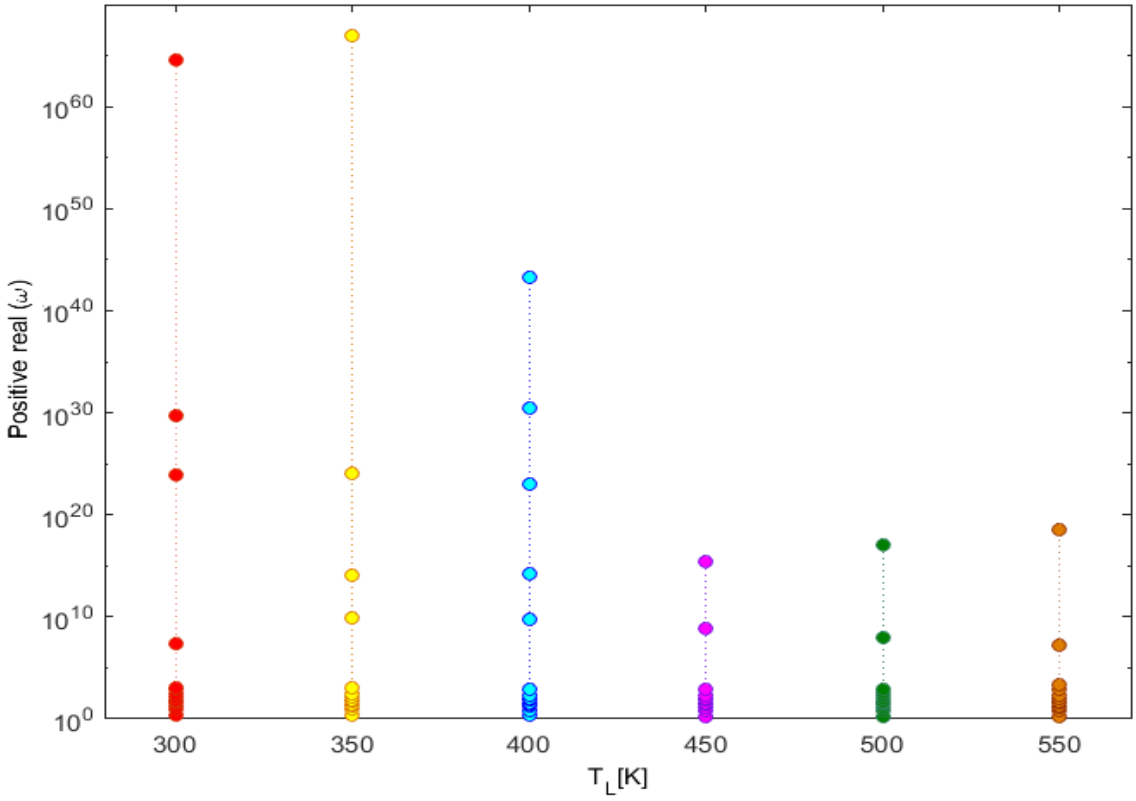

Figure 5.18: Positive eigenvalues at $T_C - T_L = 150[K], V_{app} = 0.4[V], L = 4[\mu m]$.

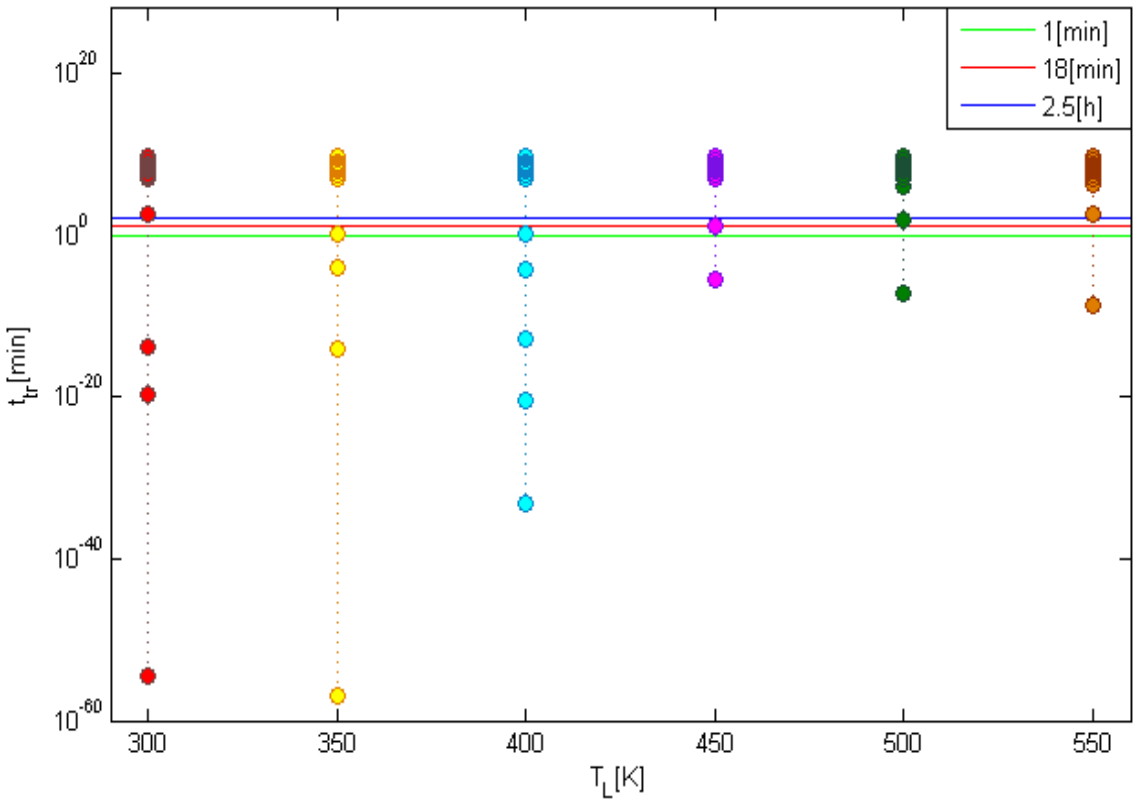

Figure 5.19: Characteristic time at $T_C - T_L = 150[K], V_{app} = 0.4[V], L = 4[\mu m]$.

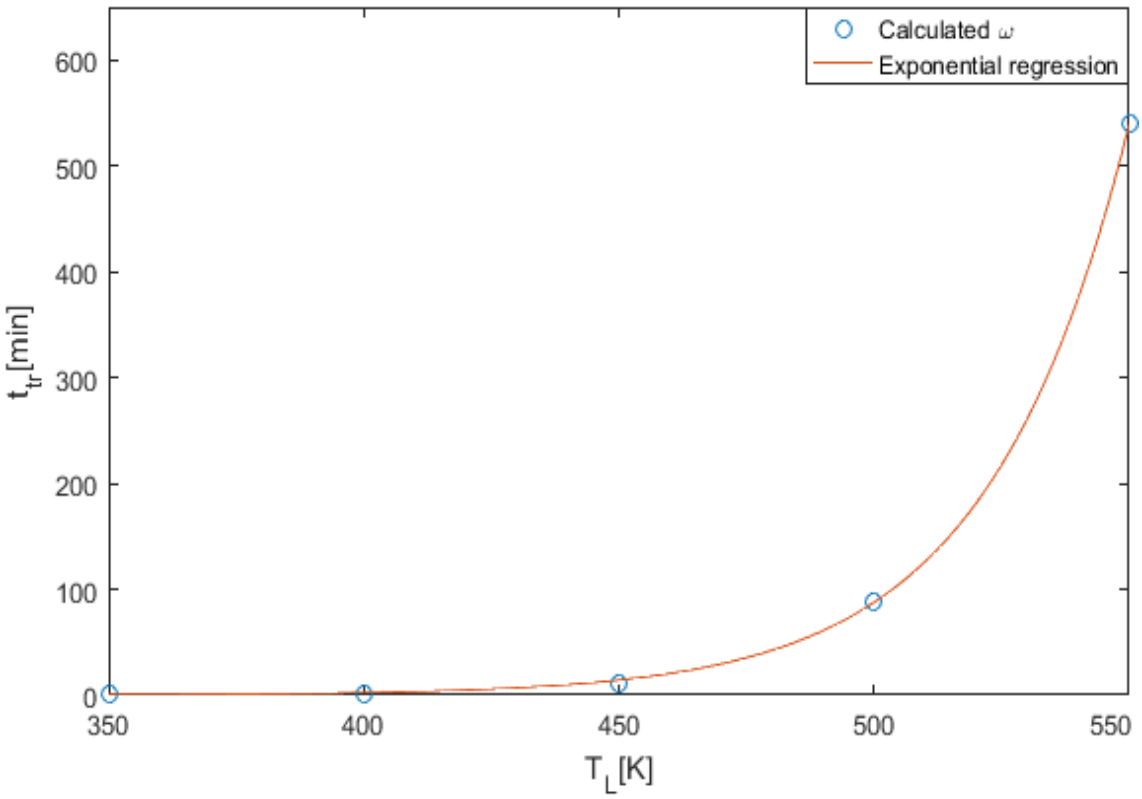

Figure 5.20: Allowed range at $T_C - T_L = 150[K], V_{app} = 0.4[V], L = 4[\mu m]$.

5.3.3 Variation in Longitude

Standard longitude is fixed in $4[\mu m]$ and the range proposed includes the half and the double part. Lattice temperature is fixed at $T_L = 300$, carrier temperature at $T_C = 450[K]$ and applied voltage at $V_{app} = 0.4[V]$.

Figure 5.21 represents the positive real eigenvalues solution. The concentration range determined before is kept too and the upper values change with longitude. The minimum value is approximately constant, while the center column tends to decrease, moving to the stability region. Figure 5.22 shows that in the case of a system "stable", with no values in the allowed range, changing longitude doesn't alter the stability. As a extrapolation from constant temperature difference analysis, is imposed that parameters behave as contour lines, so the analysis of stability of the allowed will be treated as it is could be reproduced in a unstable case. Figure 5.23 shows that decreasing longitude stabilizes the system, changing greatly the characteristic time varying from $4[\mu m]$ to $2[\mu m]$, and less important until $4[\mu m]$. It could be determine that there is a critical longitude that stabilizes the system, and over that system can change its time to $5[h]$ by decreasing to the half from $8[\mu m]$. As the recombination and generation rate does not depend in this model on longitude, net charge is not compromised. Also, the stability criteria fall on the capacity of absorbing and storage heat; hence, less mass (from less longitude) can keep less heat and avoid a greater increase of temperature in the system.

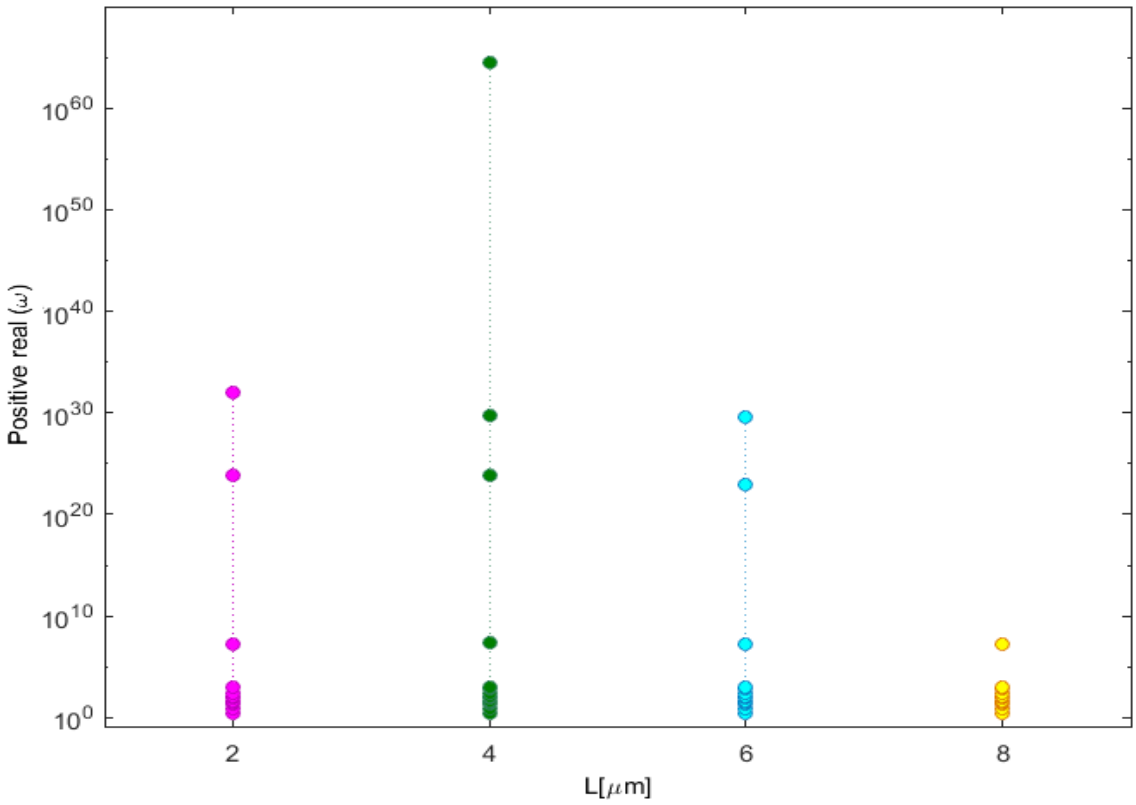

Figure 5.21: Positive eigenvalues at $T_L = 300[K], T_C = 450[K], V_{app} = 0.4[V]$.

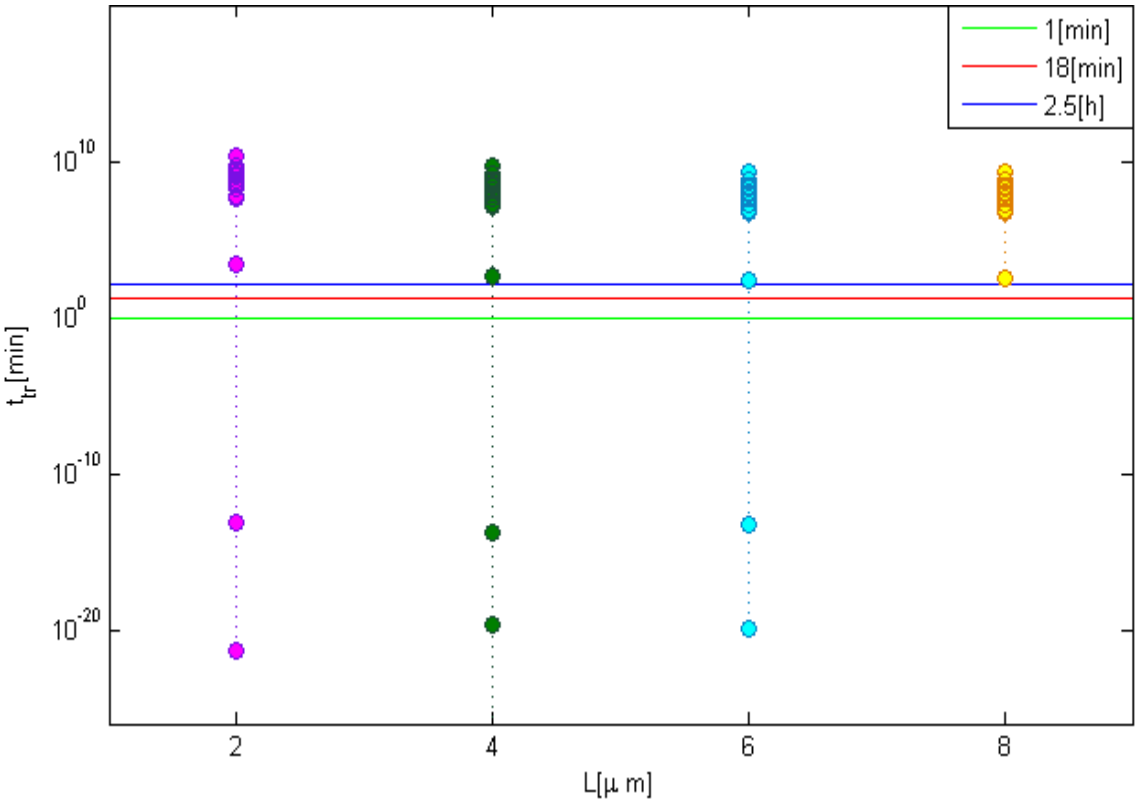

Figure 5.22: Characteristic time at $T_L = 300[K], T_C = 450[K], V_{app} = 0.4[V]$.

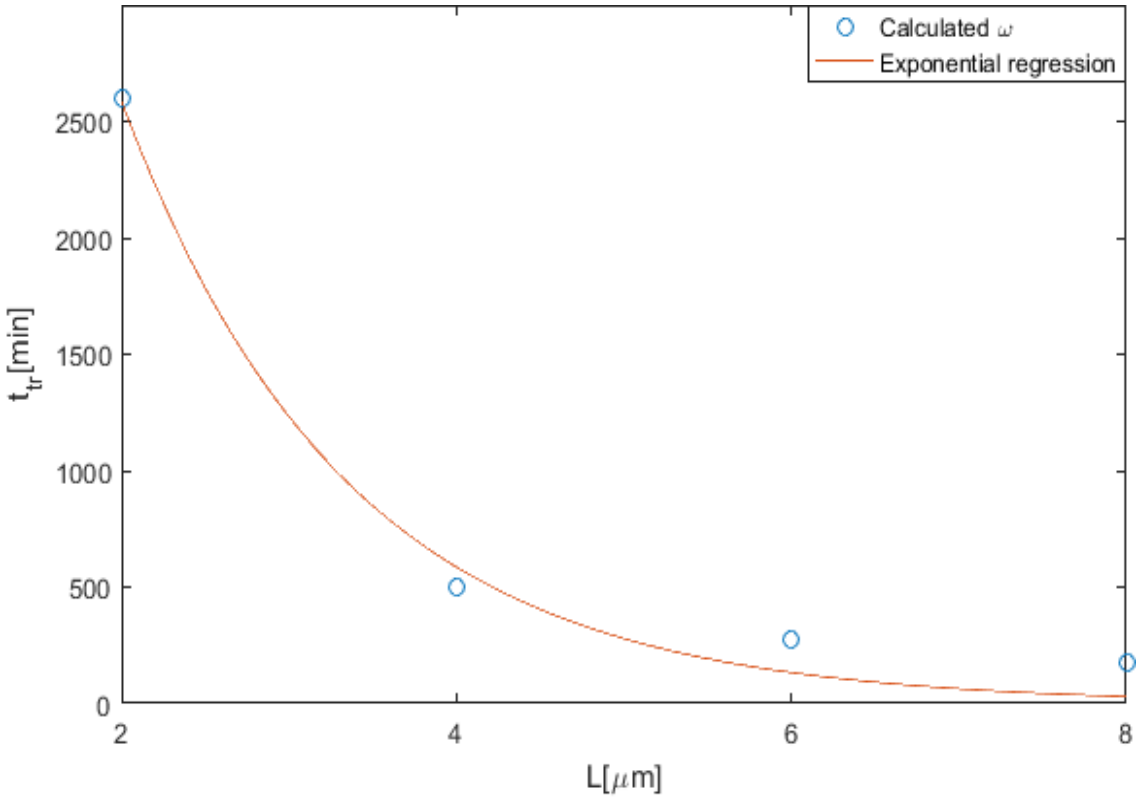

Figure 5.23: Allowed range at $T_L = 300[K], T_C = 450[K], V_{app} = 0.4[V]$.

5.3.4 Variation in applied voltage

Considering a minimum case of $0.4[V]$, applied voltage is study until $1[V]$. Lattice temperature is fixed at $T_L = 300$, carrier temperature at $T_C = 450[K]$ and longitude $L = 4[\mu m]$.

Figure 5.24 shows that the maximum value tends to decrease with the increase of applied voltage, getting near the negative zone. The range that concentrates value is the same at the previous cases and it doesn't change at varying the applied voltage. Figure 5.25 shows that most quantity of eigenvalue concentrates at high characteristic time,with a magnitude order of $10^{10}[min]$, approximately. Also, the are a few eigenvalues under the allowed zone that shows a increase tendency, suggesting a stabilization, but they disappear at $V_{app} = 0.8[V]$. Analogous as the previous case, the tendency analysis will be applied at the nearer values, with an order of 10^5. Figure 5.26 shows that the increase of applied voltage increase the characteristic time, stabilizing the system. Increasing the applied voltage arises total current density and, by accelerating electrons, the velocity in which heat is transported through the junction increases, leading to higher characteristic times.

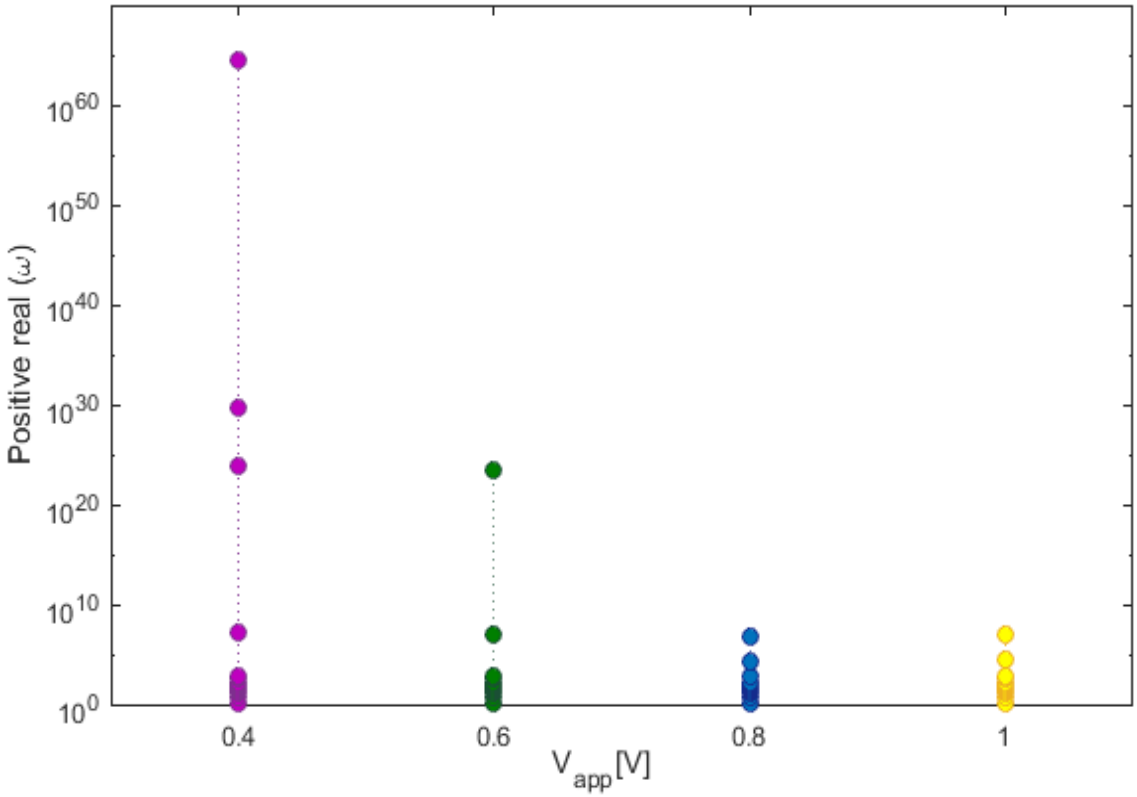

Figure 5.24: Positive eigenvalues at $T_L = 300[K], T_C = 450[K], L = 4[\mu m]$.

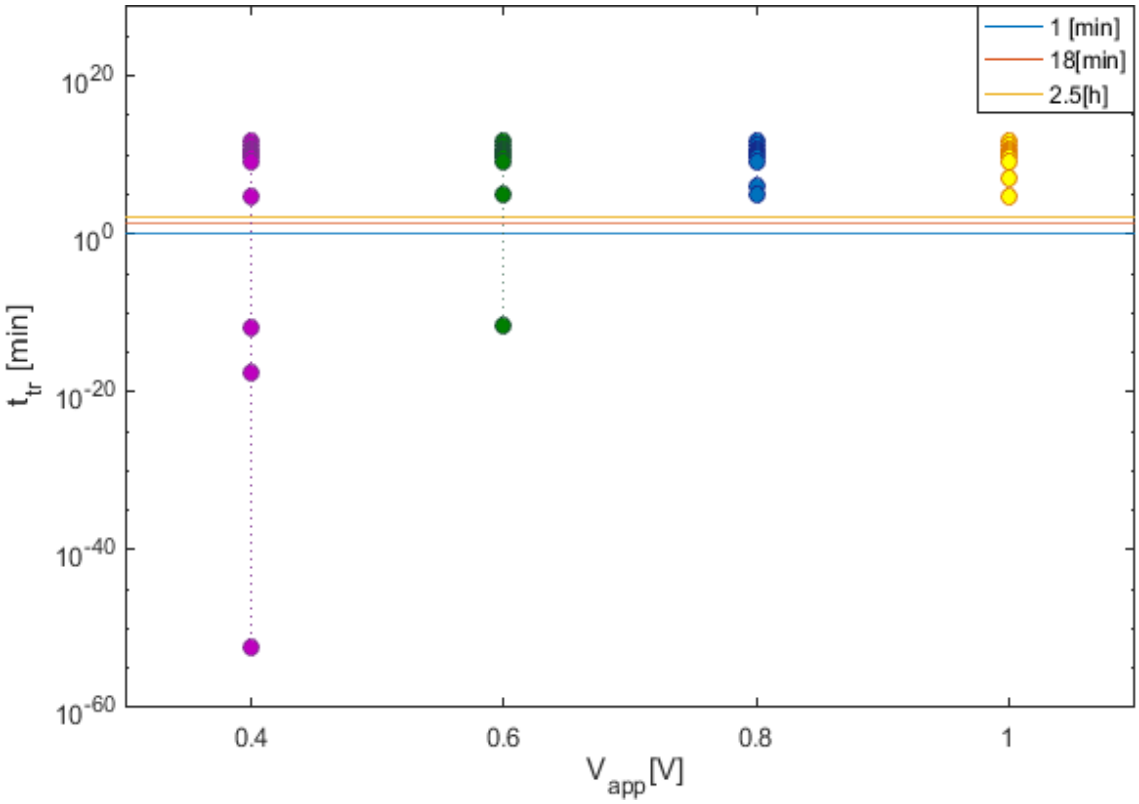

Figure 5.25: Characteristic time at $T_L = 300[K], T_C = 450[K], L = 4[\mu m]$.

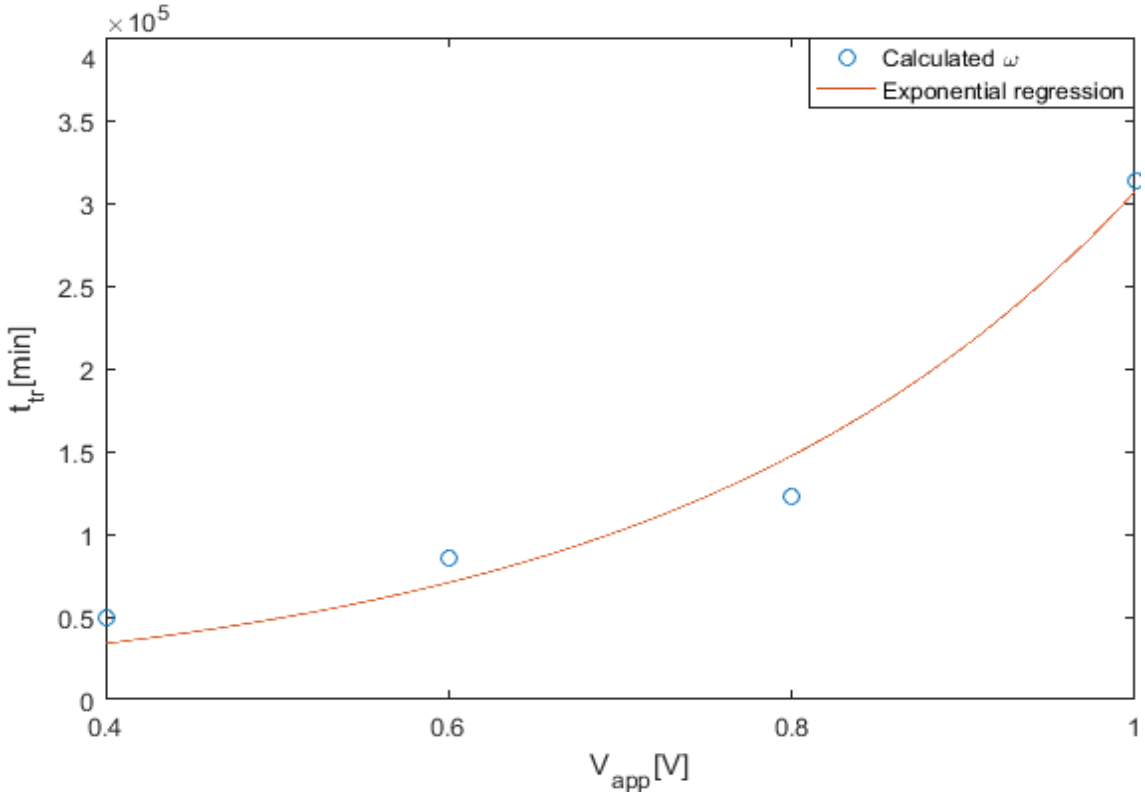

Figure 5.26: Allowed range at $T_L = 300[K], T_C = 450[K], L = 4[\mu m]$.

5.4 Surface Temperature

Thermal resistance is presented to stablish a relation between surface and junction temperature of device. This is a property, in this case of the encapsulant or package, that determines the temperature difference between the two reference points related to the delivered input power P, as can be seen in Eq. (5.3).

$$R = \frac{T_{junction} - T_{surface}}{P}. \tag{5.3}$$

Figure 5.27 presents experimental data of commercial Silicon solar cells, in which thermal resistance is compared to irradiation, showing that it depends inversely on it [22, 42].

As thermal resistance varies with irradiation, the difference between junction and surface temperature must increase too. In experimental works, a standard temperature difference in commercial Silicon solar cell at room temperature is measure considering cases with natural and forced cooling, as can be seen in Figure 5.28.

For the first case,Figure 5.28 a, surface temperature presents a minor increase with the irradiation power ($5[°C]$), while junction temperature almost $20[°C]$; maximum difference of $15[°C]$. This generates a decrease in efficiency that coincides with thermal runaway development. Under natural cooling, Figure 5.28 b, difference is significant, at orders of $45[°C]$.

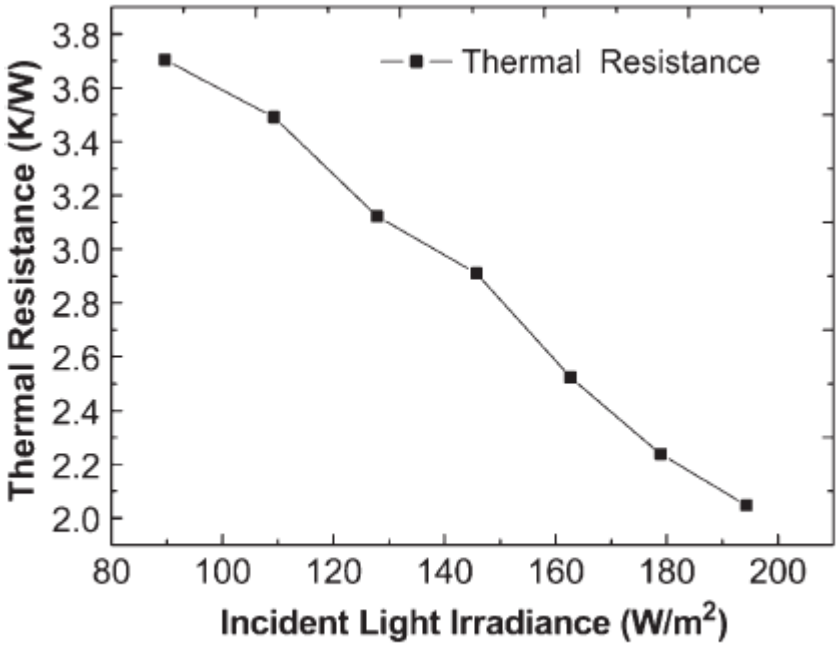

Figure 5.27: Thermal resistance at varying irradiation [42].

Considering that a hot spot temperature can reach 10[°C] over the surface temperature, difference between this surface point and junction temperature may be between 25[°C] to 55[°C]. It is also appreciable that junction temperature can increase without influence surface temperature greatly, that coincides with the lattice boundary conditions proposed. This effects is considered also for thin film, but it would be expected that range difference would be minor than the case of commercial cells.

Considering the following irradiation world map:

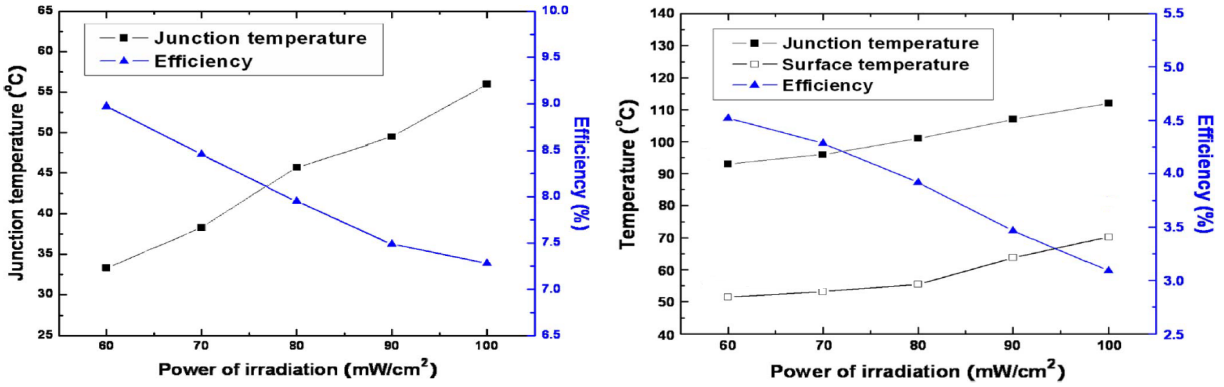

(a) Forced cooling.

(b) Natural cooling.

Figure 5.28: Temperature and efficiency varying irradiations [43].

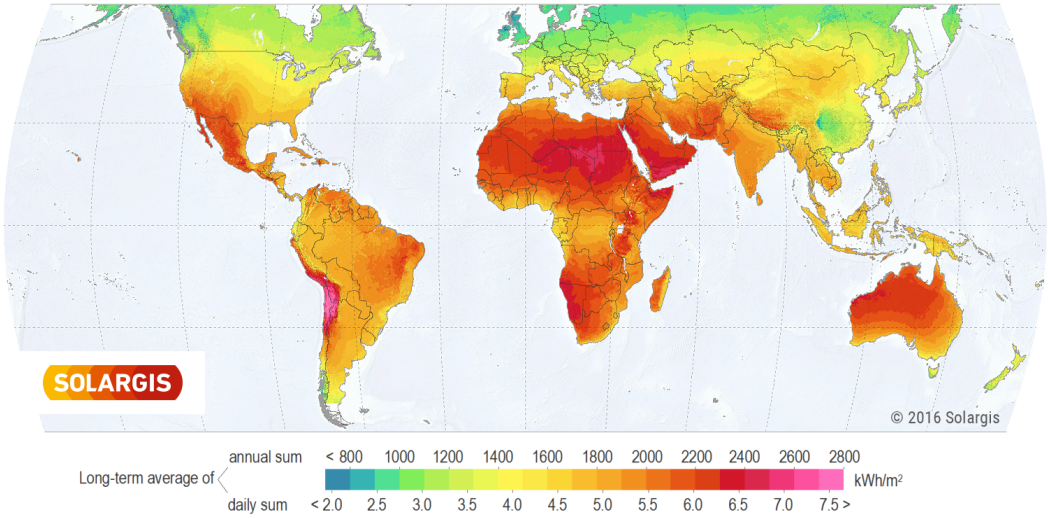

Figure 5.29: Global horizontal irradiation [44].

It is clear that a cell design for a sector with different irradiation changes its thermal behaviour, increasing the probability of developing thermal runaway at same operating conditions. It is recommendable to consider: during the design the stability sensitivity at varying longitude; and during the operation, the control of junction temperature or the use of forced cooling to reduce the difference between surface and junction temperature. If a hot spot is noticed and the thin film PV cell is using hot carrier technology, it could be stabilized increasing their temperature and, also, applied voltage can be changed .

Chapter 6

Conclusions and Future Work

In this Thesis a two-temperature 1-D hydrodynamic model is studied to determine thermal and electrical stability of PN junction solar cell. The model was previously solved for steady state condition at zero order at front a perturbation, which is used to found the solutions at a linearized transient state. Uncoupling time and space dimensions, temporal solution behaves as an exponential and the sign of real part of eigenvalues determines stability. As there is an infinite possible calculated eigenvalues, solution will be a probability; if there is at least one positive solution, the system can be unstable.

As there is not a consensus in which modes are allowed, it is proposed a characteristic time of thermal runaway that represents time to achieve a lattice temperature $600[K]$ from $300[K]$, considering a initial condition of $1[K]$ in some point of temperature profile. Allowed characteristic time range consider a experimental value as meddle; thermal inertia forbids instantaneous increases and slow times with magnitude of hours can be controlled, for example by cooling, and does not refers the thermal runaway phenomenon.

6.1 Conclusions

There are five cases simulated: varying temperature (lattice, carrier and both), longitude and applied voltage. In first case, varying temperature, there is considered one temperature variable and the other is fixed in a constant value, except for the last temperature case in where a constant difference is kept. Varying lattice temperature, thermal runaway start when lattice boundary achieve $450[K]$; an increase of carrier temperature, which represents hot carriers,stabilizes temporal behaviour; then, considering both cases, lattice temperature instability can be controlled by increasing temperature of hot carriers. Reducing the device length and increasing applied voltage gets the device significantly more stable. Influence depends on the cost of varying each variable in terms of how much stability system gains.

Respect to imaginary part of eigenvalue, oscillation frequency can be considered as turbulence, in which the chaotic movement is represented as a movement of carriers through the junction. It is only present for low eigenvalues, with real part less than 10^3, that corresponds

to high characteristic time and out of thermal runaway allowed range.

The presented model considers that junction boundary temperature doesn't evolve in time, hence the increase in temperature is in the middle of the junction, where the instability is develop. Changes in thermal resistance of encapsulant can avoid the phenomenon considering that its increase allows the system to never reach the critical junction temperature. Also, due to difference in temperature of surface and junction, cooling is imperative in order to control this critical condition. Forced cooling can present a difference in magnitude order of $10[K]$, so it is proposed to use when junction temperature can not be determined.

6.2 Future Work

Avoiding thermal runaway, solar cell properties can be maintain and lifespan can be prolonged. This work is an hypothetical case for academic studies, so conclusions are presented with qualitative nature, as tendencies and the existence of a critical value. For futures developments in the same line, there is proposed the following improvements in model.

- Carrier temperature variable in space and its relation to lattice temperature.
- Deeper studies in transient boundary conditions, considering the case with an initial lattice in order to determine surface temperature evolution.
- Test the model in an actual experimentally developed material, to compare cases with a more precise thermal inertia.
- Consider other layers in solar cell, to determine influence of thermal resistance in the model.
- Experimental study to determine allowed modes of degradation.
- Expand the model to more spatial dimensions, to capture the effect of redistribution of lattice temperature profile.
- Study long term degradation, considering multiples cycles and fatigue failure.

Bibliography

[1] Ministerio de Energía. *Energía 2050. Política energética de Chile*. Gobierno de Chile, 2015.

[2] Florian Pfeffer, Johannes Eisenlohr, Angelika Basch, Martin Hermle, Benjamin G Lee, and Jan Christoph Goldschmidt. Systematic analysis of diffuse rear reflectors for enhanced light trapping in silicon solar cells. *Solar Energy Materials and Solar Cells*, 152:80–86, 2016.

[3] Bita Farhadi and Mosayeb Naseri. A novel efficient double junction ingap/gaas solar cell using a thin carbon nano tube layer. *Optik-International Journal for Light and Electron Optics*, 127(15):6224–6231, 2016.

[4] Johannes Eisenlohr, Nico Tucher, Hubert Hauser, Martin Graf, Jan Benick, Benedikt Bläsi, Jan Christoph Goldschmidt, and Martin Hermle. Efficiency increase of crystalline silicon solar cells with nanoimprinted rear side gratings for enhanced light trapping. *Solar Energy Materials and Solar Cells*, 155:288–293, 2016.

[5] Sanjeev Jakhar, MS Soni, and Nikhil Gakkhar. Historical and recent development of concentrating photovoltaic cooling technologies. *Renewable and Sustainable Energy Reviews*, 60:41–59, 2016.

[6] Leonardo Micheli, Eduardo F Fernandez, Florencia Almonacid, Tapas K Mallick, and Greg P Smestad. Performance, limits and economic perspectives for passive cooling of high concentrator photovoltaics. *Solar Energy Materials and Solar Cells*, 153:164–178, 2016.

[7] Marco Beccali, Maurizio Cellura, Sonia Longo, and Francesco Guarino. Solar heating and cooling systems versus conventional systems assisted by photovoltaic: Application of a simplified lca tool. *Solar Energy Materials and Solar Cells*, 2016.

[8] DT Cotfas, PA Cotfas, and S Kaplanis. Methods and techniques to determine the dynamic parameters of solar cells: Review. *Renewable and Sustainable Energy Reviews*, 61:213–221, 2016.

[9] A Rezaee Jordehi. Parameter estimation of solar photovoltaic PV cell- a review. *Renewable and Sustainable Energy Reviews*, 61:354–371, 2016.

[10] Simon Min Sze. *Semiconductor Devices: Physics and Technology*. John Wiley & Sons, 2008.

[11] Said Ibrahim, Dina Ibrahim, and Guido Righini. *Structure of Solid, course Chemistry of Energy Storage Materials*. Minerva, 2014.

[12] Sammy Kayali, George Ponchak, and Roland Shaw. *GaAs MMIC Reliability Assurance Guideline for Space Applications*. California Institute of Technology, 1996.

[13] Chih-Tang Sah. *Fundamentals of Solid-state Electronics*. World Scientific, 1991.

[14] Adrian Kitai. *Principles of solar cells, LEDs and diodes: the role of the PN junction*. John Wiley & Sons, 2011.

[15] Shin-ichiro Sato, Takeshi Ohshima, and Mitsuru Imaizumi. Modeling of degradation behavior of InGaP/GaAs/Ge triple-junction space solar cell exposed to charged particles. *Journal of Applied Physics*, 105(4):044504, 2009.

[16] François Charru. *Hydrodynamic Instabilities*, volume 37. Cambridge University Press, 2011.

[17] Williams R Calderón Munoz. *Linear stability of electron-flow hydrodynamics in ungated semiconductors*. PhD thesis, University of Notre Dame, 2009.

[18] Jason F Hiltner and James R Sites. Stability of CdTe solar cells at elevated temperatures: bias, temperature, and Cu dependence. In *National center for photovoltaics (NCPV) 15th program review meeting*, volume 462, pages 170–175. AIP Publishing, 1999.

[19] Naba R Paudel, Kristopher A Wieland, Matthew Young, Sally Asher, and Alvin D Compaan. Stability of sub-micron-thick CdTe solar cells. *Progress in Photovoltaics: Research and Applications*, 22(1):107–114, 2014.

[20] David L King, Jay A Kratochvil, and William E Boyson. Temperature coefficients for pv modules and arrays: measurement methods, difficulties, and results. In *Photovoltaic Specialists Conference, 1997., Conference Record of the Twenty-Sixth IEEE*, pages 1183–1186. IEEE, 1997.

[21] Thomas Nordmann and Luzi Clavadetscher. Understanding temperature effects on PV system performance. In *Photovoltaic Energy Conversion, 2003. Proceedings of 3rd World Conference on*, volume 3, pages 2243–2246. IEEE, 2003.

[22] BJ Huang, PE Yang, YP Lin, BY Lin, HJ Chen, RC Lai, and JS Cheng. Solar cell junction temperature measurement of PV module. *Solar Energy*, 85(2):388–392, 2011.

[23] Nima E Gorji. Thermal runaway in thin film PV: temperature profile modeling. 2014.

[24] C Magarreiro, MC Brito, and PMM Soares. Assessment of diffuse radiation models for cloudy atmospheric conditions in the azores region. *Solar Energy*, 108:538–547, 2014.

[25] Anthony C Vasko, Aarohi Vijh, and Victor G Karpov. Hot spots spontaneously emerging in thin film photovoltaics. *Solar Energy*, 108:264–273, 2014.

[26] Celina Mikolajczak, Michael Kahn, Kevin White, and Richard Thomas Long. *Lithium-ion batteries hazard and use assessment*. Springer Science & Business Media, 2012.

[27] KT Wan, FA Cozzarelli, and DJ Inman. Thermal runaway due to strain-heating feedback. *AIAA journal*, 26(10):1263–1268, 1988.

[28] Jordi Casanova, Jordi José, Enrique García-Berro, Steven N Shore, and Alan C Calder. Kelvin-helmholtz instabilities as the source of inhomogeneous mixing in nova explosions. *Nature*, 478(7370):490–492, 2011.

[29] LL Liou and B Bayraktaroglu. Thermal stability analysis of AlGaAs/GaAs heterojunction bipolar transistors with multiple emitter fingers. *IEEE Transactions on Electron Devices*, 41(5):629–636, 1994.

[30] VG Karpov, AD Compaan, and Diana Shvydka. Random diode arrays and mesoscale physics of large-area semiconductor devices. *Physical Review B*, 69(4):045325, 2004.

[31] D. Shvydka V.G.Karpov. Understanding and mitigating effects of non-uniformities on reliability on thin film photovoltaic. *Reliability of Photovoltaic Cells, Modules, Components, and Systems II*, 7412:15, 2009.

[32] VG Karpov, A Vasko, and A Vijh. Hot spot runaway in thin film photovoltaics and related structures. *Applied Physics Letters*, 103(7):074105, 2013.

[33] Juan Osses-Márquez and Williams R Calderón-Muñoz. Thermal influence on charge carrier transport in solar cells based on GaAs PN junctions. *Journal of Applied Physics*, 116(15):154502, 2014.

[34] Williams R Calderón-Muñoz, Debdeep Jena, and Mihir Sen. Temperature influence on hydrodynamic instabilities in a one-dimensional electron flow in semiconductors. *Journal of applied physics*, 107(7):074504, 2010.

[35] IN Volovichev, GN Logvinov, O Yu Titov, and Yu G Gurevich. Recombination and lifetimes of charge carriers in semiconductors. *Journal of applied physics*, 95(8):4494–4496, 2004.

[36] Sara Shishehchi, Asghar Asgari, and Reza Kheradmand. The effect of temperature on the recombination rate of AlGaN/GaN light emitting diodes. *Optical and quantum electronics*, 41(7):525–530, 2009.

[37] Ansgar Jüngel, Maria Cristina Mariani, and Diego Rial. Local existence of solutions to the transient quantum hydrodynamic equations. *Mathematical Models and Methods in Applied Sciences*, 12(04):485–495, 2002.

[38] Jong Pil Kim, Ho Lim, Ju Hun Song, Young June Chang, and Chung Hwan Jeon. Numerical analysis on the thermal characteristics of photovoltaic module with ambient

temperature variation. *Solar Energy Materials and Solar Cells*, 95(1):404–407, 2011.

[39] Alfio Quarteroni, Riccardo Sacco, and Fausto Saleri. *Numerical mathematics*, volume 37. Springer Science & Business Media, 2010.

[40] Roussillon Karpov, Shvydka. Physical modes of thin film PV degradation. *Conference Record of the Thirty First IEEE*, pages 437–440, 2005.

[41] Williams R Calderón-Muñoz and Cristian Jara-Bravo. Hydrodynamic modeling of hot-carrier effects in a PN junction solar cell. *Acta Mechanica*, pages 1–14, 2016.

[42] Jihong Zhang, Yulin Gao, Yijun Lu, Lihong Zhu, Ziquan Guo, Guolong Chen, and Zhong Chen. Transient thermal resistance test of single-crystal-silicon solar cell. *IEEE Transactions on Electron Devices*, 59(9):2345–2349, 2012.

[43] Sun Ho Jang and Moo Whan Shin. Thermal characterization of junction in solar cell packages. *IEEE Electron Device Letters*, 31(7):743–745, 2010.

[44] SolarGIS. Free download of solar resource maps. urlhttp://solargis.com/, 2016.